

**INVESTIGATION OF THE CURRENT TRANSMISSION  
HYSTERESIS IN ELECTRON HOP FUNNELS**

by

Marcus Pearlman

A thesis

submitted in partial fulfillment

of the requirements for the degree of

Master of Science in Electrical Engineering

Boise State University

May 2012

© 2012

Marcus Pearlman

ALL RIGHTS RESERVED

BOISE STATE UNIVERSITY GRADUATE COLLEGE

**DEFENSE COMMITTEE AND FINAL READING APPROVALS**

of the thesis submitted by

Marcus Pearlman

Thesis Title: Investigation of the Current Transmission Hysteresis in Electron Hop  
Funnels

Date of Final Oral Examination: 13 May 2012

The following individuals read and discussed the thesis submitted by student Marcus Pearlman, and they evaluated his presentation and response to questions during the final oral examination. They found that the student passed the final oral examination.

Jim Browning, Ph.D.

Chair, Supervisory Committee

Wan Kuang, Ph.D.

Member, Supervisory Committee

Kris Campbell, Ph.D.

Member, Supervisory Committee

The final reading approval of the thesis was granted by Jim Browning, Ph.D., Chair, Supervisory Committee. The thesis was approved for the Graduate College by John R. Pelton, Ph.D., Dean of the Graduate College.

Dedicated to Thabby

## ACKNOWLEDGMENTS

Thank you to Tyler Rowe, who implemented much of the experimental setup and performed many of the experiments shown in this thesis. Thank you to Dr. Browning for being a great advisor. Thank you to Lael Matthews and Ed Henderson for their help with the experimental setup. Thank you to Charlie Lester for the initial starting point for the simulation work done in this thesis. Funding was provided by the U.S. Air Force Office of Scientific Research under Grant FA9550-08-1-0396.

## ABSTRACT

To integrate field emitter arrays (FEAs) into microwave vacuum electron devices, the use of insulating funnels, called electron hop funnels, is proposed. Electrons are emitted into the wide end of the funnel, and utilizing secondary electron emission to sustain current, the electrons "hop" up the funnel walls. Eventually the electrons exit the funnel as a denser and more uniform electron beam. To pull the electrons up the funnel, an electrode, called the hop electrode, is placed around the exit of the funnel to generate an electric field between the funnel exit and the electron source. The current transmitted through the device depends directly on the hop voltage, and experimental work has found that there is hysteresis in the transmitted current vs. the hop voltage (I-V characteristic). The shape of the I-V curve changes when the voltage is ramped up or down. To characterize and explain the hysteresis, a model of the hop funnel was simulated in the particle trajectory code LORENTZ 2E. The results of the simulations show that hysteresis is a fundamental characteristic of hop funnels. Experimental data does not directly match the simulation results but confirms the general trend found in the simulations.

# TABLE OF CONTENTS

<b>ACKNOWLEDGMENTS</b> .....	iv
<b>ABSTRACT</b> .....	v
<b>LIST OF TABLES</b> .....	ix
<b>LIST OF FIGURES</b> .....	x
<b>LIST OF ABBREVIATIONS</b> .....	xvii
<b>1 Introduction</b> .....	1
1.1 Overview .....	1
<b>2 Background</b> .....	4
2.1 Field Emission .....	4
2.2 Field Emitter Arrays .....	5
2.2.1 Ungated FEAs .....	6
2.2.2 Gated FEAs .....	6
2.2.3 Characteristics .....	9
2.2.4 Issues for FEAs .....	9
2.3 Electron Wall Interactions .....	11
2.3.1 Secondary Electron Emission .....	11
2.3.2 Backscattering .....	19

2.3.3	Other Interactions . . . . .	19
2.4	Electron Transport . . . . .	20
2.5	Hop Funnels . . . . .	21
2.6	Prior Work . . . . .	22
2.6.1	Hopping Transport Study . . . . .	24
2.6.2	Hop Funnels from Low Temperature Co-Fired Ceramic . . . . .	29
2.6.3	Transverse Energy Study . . . . .	36
2.6.4	Printable Field Emitter Display (pFED) . . . . .	36
<b>3</b>	<b>Experiment . . . . .</b>	<b>39</b>
3.1	Overview . . . . .	39
3.2	Experimental Setup . . . . .	39
3.2.1	Hop Funnel . . . . .	39
3.2.2	Field Emitter Arrays . . . . .	42
3.2.3	Mechanical Setup . . . . .	44
3.2.4	Measurement and Control Setup . . . . .	46
3.2.5	Procedure . . . . .	47
3.3	Experimental Results . . . . .	48
3.3.1	90° Hop Funnel Using Motorola Cathode . . . . .	50
3.3.2	90° Hop Funnel PixTech Cathode . . . . .	52
3.3.3	60° Hop Funnel with/without the Metal Hop Bottom Electrode . . . . .	56
3.3.4	Experimental Summary . . . . .	58
<b>4</b>	<b>Simulation . . . . .</b>	<b>60</b>
4.1	Overview . . . . .	60
4.2	Lorentz 2E Description . . . . .	60

4.3	Basic Simulation Setup . . . . .	63
4.3.1	Field Emitters . . . . .	64
4.3.2	Secondary Electron Boundaries . . . . .	67
4.3.3	Electrodes . . . . .	67
4.3.4	Simulation Stability . . . . .	68
4.3.5	Data Interpretation . . . . .	70
4.4	Metal Hop Bottom Electrode Simulation . . . . .	70
4.4.1	Results . . . . .	71
4.5	Ramping Simulation . . . . .	72
4.5.1	Voltage Step Stability . . . . .	74
4.5.2	Simulation Results for Case 1 . . . . .	76
4.5.3	Simulation Results for Case 2 . . . . .	90
4.5.4	Simulation Results for Case 3 . . . . .	95
4.5.5	Simulation Summary . . . . .	107
4.5.6	Simulation Comparison with Experiment . . . . .	107
<b>5</b>	<b>Conclusions . . . . .</b>	<b>109</b>
	<b>Bibliography . . . . .</b>	<b>113</b>

## LIST OF TABLES

2.1	The number of electrons per ray used in the Lorentz 2E simulation performed by Lester et al. [6]. . . . .	37
4.1	Summary of ramping simulations performed. . . . .	75

## LIST OF FIGURES

2.1	Potential barrier at the boundary between vacuum and metal. The work function is defined by $\phi$ , and the lowering of the work function from the applied electric field is $\Delta\phi$ [11]. . . . .	7
2.2	Ungated FEA examples. . . . .	7
2.3	Diagram of a cell in a gated FEA [11]. . . . .	8
2.4	Gated FEA examples. . . . .	8
2.5	Diagram of one cell of a gated field emitter array with a ballast resistor. . . . .	12
2.6	Classical view of electron interactions within an atom. Image provided by Radboud University Nijmegen, <a href="http://www.vcbio.science.ru.nl/en/feem/eds/">http://www.vcbio.science.ru.nl/en/feem/eds/</a> [17] . . . . .	12
2.7	Normalized secondary electron yield data for some polymers as found by Willis and Skinner [20, 22] compared to the model found by Lye and Dekker [19] and Baroody [18]. . . . .	18
2.8	Analytical secondary electron yield curves proposed by Vaughan and compared to Lye and Dekker's formula for $\delta_{max} = 2$ and $E_{pmax} = 500 eV$ . The point at which the unity gain reference line intersects with the curve corresponds to the energy where for every incoming electron there will be one secondary electron. The first crossover of Vaughan's formula in this example occurs at an energy $E_p = 70 eV$ . . . . .	18

2.9	Diagram of the cross-section of the hop funnel. The funnel is rotationally symmetric about the center axis. . . . .	23
2.10	Example I-V curve showing the three hop funnel operation regions. . . . .	23
2.11	Hopping trajectory model [8]. . . . .	28
2.12	Electron-transmission curve (I-V curve) through a cylinder from Monte Carlo simulations performed by Hendriks et al. [8]. . . . .	28
2.13	Simulated steady-state potential distribution along the surface of the cylinder for (a) $V_L = 600 V$ and (b) $V_L = 1000 V$ [8]. . . . .	30
2.14	Hop funnel model simulated in Lorentz2E by Lester et al. [6]. . . . .	30
2.15	Anode current vs. time from the Lorentz2E simulations of a hop funnel for various hop voltages performed by C. Lester et al. [6]. . . . .	32
2.16	Simulated and experimental hop funnel anode current characteristics performed by Lester et al. [6]. . . . .	32
2.17	Current stability study from Lester et al. [6]. . . . .	35
2.18	Double funnel design used to increase energy uniformity of the electron beam [24]. . . . .	37
3.1	The hop funnels used in the experiments. The blue part is the LTCC, the silver is the silver paste, and the yellow material is Kapton tape used to suspend the funnel above the cathode. . . . .	41
3.2	Hop funnel diagram. . . . .	41
3.3	SEM image of the PixTech cathode showing the layout. . . . .	45
3.4	Experimental setup. The potential of the metal hop bottom electrode is equal to $V_{gate}$ if it is used. . . . .	45

3.5	Experimental I-V curves obtained from the 90° hop funnel without a metal hop bottom, for runs taken using the same test setup, using the Motorola cathode. . . . .	51
3.6	Experimental I-V curves obtained from the 90° hop funnel without a metal hop bottom, for runs taken from different test setups, using the Motorola cathode. . . . .	51
3.7	Experimental I-V curves obtained from the 90° hop funnel without a metal hop bottom, for runs taken using the same test setup, using the PixTech cathode. . . . .	53
3.8	Experimental I-V curves obtained from the 90° hop funnel without a metal hop bottom, for runs taken from different test setups, using the PixTech cathode. . . . .	53
3.9	Experimental I-V curves obtained from the 90° hop funnel with a metal hop bottom, for runs taken using the same test setup, using the PixTech cathode. . . . .	55
3.10	Experimental I-V curves obtained from the 90° hop funnel with a metal hop bottom, for runs taken from different test setups, using the PixTech cathode. . . . .	55
3.11	Experimental I-V curves obtained from the 60° hop funnel without a metal hop bottom, for runs taken using the same test setup, using the PixTech cathode. . . . .	57
3.12	Experimental I-V curves obtained from the 60° hop funnel with a metal hop bottom, for runs taken using the same test setup, using the PixTech cathode. . . . .	57

4.1	Hop funnel geometry created in Lorentz 2E used for all simulations. . . .	65
4.2	A close up on the boundaries modeling the FEA for the Lorentz 2E simulations. . . . .	65
4.3	Simulated I-V curves with and without a metal hop bottom. . . . .	73
4.4	The steady-state trajectories using a metal and a non-metal hop bot- tom. Primary electron trajectories emitted from the FEA are shown in yellow, and secondary electron trajectories are shown in the other colors. (a) Non-metal hop bottom shows a bulge in the trajectories along the wall at the funnel entrance caused by charging of the hop bottom. (b) Metal hop bottom shows no bulge because charge on the hop bottom is “bleed” away. . . . .	73
4.5	Ramp-up I-V curves with varying voltage step sizes of a hop funnel with $\delta_{max} = 2$ and $E_{max} = 300 eV$ . . . . .	75
4.6	Ramp-down I-V curves with varying voltage step sizes of a hop funnel with $\delta_{max} = 2$ and $E_{max} = 300 eV$ . . . . .	75
4.7	Simulated I-V curves for Case 1 showing a full ramp-up, down, and then back up procedure for $\delta_{max} = 2$ and $E_{max} = 300 eV$ ( $40 eV$ first crossover). . . . .	80
4.8	Plots of the steady-state electron ray trajectories and the corresponding initial condition voltage contour plots for a range of hop voltages for Case 1 ( $40 eV$ first crossover) ramp-up-first. The primary rays emitted from the FEA are yellow and the secondary rays are shown in the other colors. . . . .	81

4.9	(a) Distance from the funnel exit of the point at which the 50 V voltage contour line intersects the funnel wall, and (b) the point at which electron transport begins to take place along the funnel wall for Case 1 (40 eV first crossover) ramp-up-first. . . . .	82
4.10	Surface charge density along the funnel wall vs. the hop voltage during the ramp-up-first for Case 1 (40 eV first crossover). . . . .	82
4.11	Simulations of the ray trajectories and the corresponding voltage contour plots for a range of hop voltages for Case 1 (40 eV first crossover) ramp-down. The primary rays are yellow and the secondary rays are shown in the other colors. . . . .	85
4.12	(a) The point at which the 50 V voltage contour line intersects the funnel wall, and (b) the point at which electron transport begins to take place along the funnel wall for Case 1 (40 eV first crossover) ramp-down	86
4.13	Surface charge density along the funnel wall vs. the hop voltage during the ramp-down for Case 1 (40 eV first crossover). . . . .	86
4.14	Simulations of the ray trajectories and the corresponding voltage contour plots for a range of hop voltages for Case 1 (40 eV first crossover) ramp-back-up. The primary rays are yellow and the secondary rays are shown in the other colors. . . . .	88
4.15	(a) The point at which the 50 V voltage contour line intersects the funnel wall, and (b) the point at which electron transport begins to take place along the funnel wall for Case 1 (40 eV first crossover) ramp-back-up. . . . .	89
4.16	Surface charge density along the funnel wall vs. the hop voltage during the ramp-back-up for Case 1 (40 eV first crossover). . . . .	89

4.17	I-V curves for Case 2 showing a ramp-down after starting at $V_{hop} = 650 V$ and then a ramp-back-up for $\delta_{max} = 2$ and $E_{max} = 300 eV$ (40 eV first crossover). . . . .	92
4.18	Simulations of the ray trajectories and the corresponding voltage contour plots for a range of hop voltages for Case 2 (40 eV first crossover) ramp-down-first. The primary rays are yellow and the secondary rays are shown in the other colors. . . . .	93
4.19	(a) The point at which the 50 V voltage contour line intersects the funnel wall, and (b) the point at which electron transport begins to take place along the funnel wall for Case 2 (40 eV first crossover) ramp-down-first. . . . .	94
4.20	I-V curves for Case 3 showing a full ramp-up, down and then back up procedure for $\delta_{max} = 2$ and $E_{max} = 500 eV$ (70 eV first crossover). . . . .	97
4.21	Simulations of the ray trajectories and the corresponding voltage contour plots for a range of hop voltages for Case 3 (70 eV first crossover) ramp-up-first. The primary rays are yellow and the secondary rays are shown in the other colors. . . . .	98
4.22	(a) The point at which the 80 V voltage contour line intersects the funnel wall, and (b) the point at which electron transport begins to take place along the funnel wall for Case 3 (70 eV first crossover) ramp-up-first. . . . .	99
4.23	Surface charge density along the funnel wall vs. the hop voltage during the ramp-up-first for Case 3 (70 eV first crossover). . . . .	99

4.24	Simulations of the ray trajectories and the corresponding voltage contour plots for a range of hop voltages for Case 3 ( $70\text{ eV}$ first crossover) ramp-down. The primary rays are yellow and the secondary rays are shown in the other colors. . . . .	102
4.25	(a) The point at which the $80\text{ V}$ voltage contour line intersects the funnel wall, and (b) the point at which electron transport begins to take place along the funnel wall for Case 3 ( $70\text{ eV}$ first crossover) ramp-down.	103
4.26	Surface charge density along the funnel wall vs. the hop voltage during the ramp-down for Case 3 ( $70\text{ eV}$ first crossover). . . . .	103
4.27	Simulations of the ray trajectories and the corresponding voltage contour plots for a range of hop voltages for Case 3 ( $70\text{ eV}$ first crossover) ramp-back-up. The primary rays are yellow and the secondary rays are shown in the other colors. . . . .	105
4.28	(a) The point at which the $80\text{ V}$ voltage contour line intersects the funnel wall, and (b) the point at which electron transport begins to take place along the funnel wall for Case 3 ( $70\text{ eV}$ first crossover) ramp-back-up. . . . .	106
4.29	Surface charge density along the funnel wall vs. the hop voltage during the ramp-back-up for Case 3 ( $70\text{ eV}$ first crossover). . . . .	106

## LIST OF ABBREVIATIONS

**MVED** – Microwave Vacuum Tube Electron Device

**FEA** – Field Emitter Array

**pFED** – Printable Field Emission Display

**SEM** – Scanning Electron Microscopy

**SEY** – Secondary Electron Yield

**UHV** – Ultra High Vacuum

**I-V curve** – Transmitted Current Vs. Hop Voltage

## CHAPTER 1

### INTRODUCTION

#### 1.1 Overview

The demand for reliable electron sources capable of generating high current density is great. Their use in Microwave Vacuum Electron Devices (MVEDs) [1] is essential. Traditionally, thermionic cathodes are used for the electron source. Thermionic cathodes allow for current densities up to  $100 A/cm^2$  [1], have a long operational life, and are resistant to the harsh environments created by MVEDs. There are also many limitations on the use of thermionic cathodes. The cathodes require a heating source that reduces efficiency and degrades the cathode. The cathodes also have very slow “turn-on/off” times ( $> 10^{-8} s$ ) [2], which prevent much modulation of the beam. These, along with other limitations, restrict the use of the cathodes. Field Emitter Arrays (FEAs) are an alternate electron source that do not have the negative properties of their thermionic counterpart.

Field emission is a property that has been known for over a century but has not been fully exploited as an MVED electron source because of the low current density. Recent semiconductor processing techniques have allowed the development of FEAs, which can contain thousands of tiny field emitters packed in a small area ( $< 1 mm^2$ ) [3]. These relatively new FEAs require a lower turn on voltage and can obtain current densities of  $< 10 A/cm^2$  [1] with the possibility of more [2]. FEAs are

more efficient, allow a modulation of the beam, provide easy spatial control, and have many advantages over their thermionic counterpart; however their use in MVEDs has not become mainstream because of two fundamental weaknesses: (i) the reliability and poor lifetime of the emitters and (ii) the relatively low current densities.

To protect the FEAs and to increase the uniformity and density of the beam [4], the use of electron hop funnels has been proposed. Hop funnels are holes or funnels fabricated into an insulating material. The narrow end (exit) is surrounded by an electrode, referred to here as the hop electrode, and the wide end (entrance) is where the electrons enter the funnel. Electrons are emitted up and into the funnel, pulled up by the electric field created by the hop electrode, and hop along the funnel wall via secondary electron transport. The electrons eventually exit the funnel as a denser and more uniform beam [4, 5]. These hop funnels can be sized anywhere from tens of  $\mu m$  to a few  $mm$ . The funnels described in this thesis are in the  $mm$  range.

A characteristic that is of interest in hop funnels is the relationship between the hop electrode voltage and the transmitted current, referred to here as the “I-V characteristic.” From the I-V characteristic the electric field necessary to sustain electron transport in the funnel and the secondary electron emission characteristics of the funnel dielectric can be studied. Experimental measurements of this relationship showed signs of hysteresis in the I-V characteristic [6]. The I-V curve shows that ramping the hop voltage from low to high yields different results than ramping from high to low. This characteristic has been largely ignored by much of the literature [6–8]. The purpose of this thesis is to characterize this hysteresis and to model it using a simulation software Lorentz 2E [9].

There are several possible causes of the I-V hysteresis. One mechanism was thought to be charging on the bottom of the funnel, at the funnel entrance. To

investigate this mechanism, a metal layer was added to the hop bottom to “bleed” the charge away and prevent charging. Experiments and simulations were performed to test this theory and showed no change in the hysteresis. The results of these experiments are presented.

It was then proposed that the hysteresis is a fundamental characteristic of the funnel operation. To test this theory, a new method to simulate the I-V curve using Lorentz 2E was used in order to recreate the hysteresis in the simulation. This simulation work represents the bulk of the thesis research. Lorentz 2E is a particle trajectory code that has been modified to model the electron transport mechanism. Original simulations to model the I-V curve used zero surface charge on the funnel wall for each voltage simulated along the I-V curve. This technique captured the general shape of the I-V curve but could not model the hysteresis since there is no “ramping” of the voltage from one state to the next. In the new work done in this thesis, at each discrete voltage step, the steady-state surface charge of the previous voltage step is used as the initial condition of the current voltage step. In this way, an effective “ramping” of the hop voltage can be recreated.

The simulations and experiments performed are presented and compared. The correlation between surface charge, electron transport, voltage contours, and the I-V characteristic are also shown. A general explanation of the cause of the hysteresis is proposed. No analytical study has been proposed and is beyond the scope of this work.

## CHAPTER 2

### BACKGROUND

#### 2.1 Field Emission

Field emission is a quantum mechanical phenomenon in which electrons tunnel through a potential barrier at the surface of a solid under the influence of an applied electric field [10]. Electric fields on the order of  $10^7 V/cm$  are required to get appreciable currents [11]. This emission is distinct from thermionic and photoemission where electrons are excited into vacuum from heat or from photon bombardment. At the boundary between the metal and the vacuum, there exists a potential barrier, often called the work function, which electrons must overcome to escape into vacuum, as shown by  $\phi$  in Fig. 2.1. When there exists an electric field, the potential barrier is lowered by  $\Delta\phi$  as shown in Fig. 2.1.

The lowering of the potential barrier is given by

$$\Delta\phi = \left( \frac{eE}{4\pi\epsilon_0} \right)^{1/2} \quad (2.1)$$

where  $E$  is the electric field ( $V/m$ ),  $e$  is the elementary charge ( $1.6 \times 10^{-19} C$ ), and  $\epsilon_0$  is the permittivity of vacuum ( $8.85 \times 10^{-12} F/m$ ). Using this shape of the energy barrier, Fowler and Nordheim derived expression an expression for the tunneling current density versus the external electric field [10]. A version of this expression is

shown in Equation (2.2) [11].

$$J = \frac{e^3 E^2}{8\pi h \phi t^2(y)} \exp \left[ \frac{-8\pi(2m)^{1/2} \phi^{3/2}}{3heE} v(y) \right] \quad (2.2)$$

$J$  is the current density ( $A/m^2$ ),  $y = \Delta\phi/\phi$ ,  $h$  is Planck's constant,  $m$  is the electron mass ( $kg$ ), and  $t(y)$  and  $v(y)$  are the Nordheim elliptic functions. To the first approximation  $t^2(y) = 1.1$  and  $v(y) = 0.95 - y^2$ . Combining Equations (2.1) and (2.2) along with the approximations, Equation (2.3) is derived.

$$J = 1.42 \times 10^{-6} \frac{E^2}{\phi} \exp \left( \frac{10.4}{\phi^{1/2}} \right) \exp \left( \frac{-6.44 \times 10^7 \phi^{3/2}}{E} \right) \quad (2.3)$$

Plotting  $\log(J/E^2)$  vs.  $1/E$  yields a straight line with a slope proportional to the work function of the material to the 3/2 power,  $\phi^{3/2}$ . This formula applies to materials at a temperature equal to  $0^\circ\text{K}$ ; however the error involved is negligible for moderate temperatures around  $300^\circ\text{K}$  [11].

## 2.2 Field Emitter Arrays

Field Emitter Arrays consist of an array of sharp tip or edges. The scale of the tips of the FEAs are  $\sim 1 \mu m$  with the radius of curvature typically  $< 10 nm$ . There exists many different types of field emitters varying in geometry, number of electrodes, materials, and size, but the concept is the same throughout: a sharp point in a region of high electric field that is used to pull the electrons out into vacuum via field emission.

### 2.2.1 Ungated FEAs

The simplest FEAs are arrays of emitter tips. An external electrode, usually placed above the FEA, is then required to create the electric field necessary to induce field emission. This type of structure is often referred to as a diode configuration. Applying a voltage across the electrodes will induce field emission from the tips. Examples of this are carbon nanotubes, tip-on-post, *ZnO* nanorods and many more, some of which are shown in Fig. 2.2.

### 2.2.2 Gated FEAs

A slightly more complicated FEA would be a gated FEA. Gated FEAs contain two electrodes: the emitter and the gate. The cathode would contain an array of sharp points, the emitters, and each point is surrounded by the gate electrode. A diagram of one element of a gated FEA is shown in Fig. 2.3.

Applying a potential between the gate and the emitter creates the necessary electric field to cause field emission. The electrons follow the electric field lines and leave the emitter-gate region. A third electrode is needed to control where the electrons go after they leave the emitter-gate region. Usually the third electrode is placed directly above the cathode, with a potential greater than the gate electrode. In many cases, without the third electrode, the electrons will collect at the gate. Examples of gated FEAs are Spindt-type [3, 11], lateral, silicon, carbon nanofiber, and many more, some of which are shown in Fig. 2.4. The field emitters used in the experiments described here are a Spindt-type emitter, an example of which is shown in Fig. 2.4b.

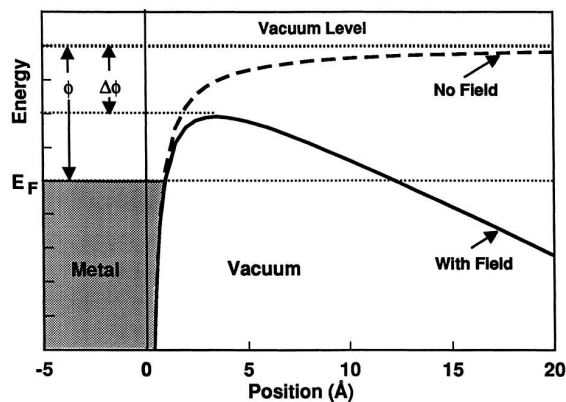
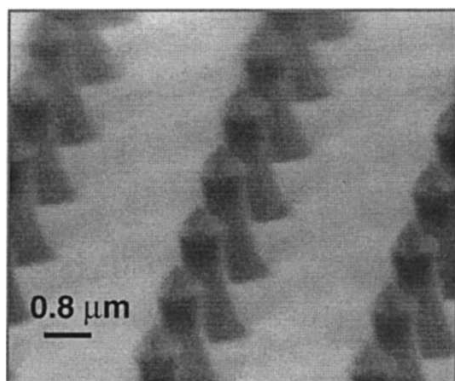
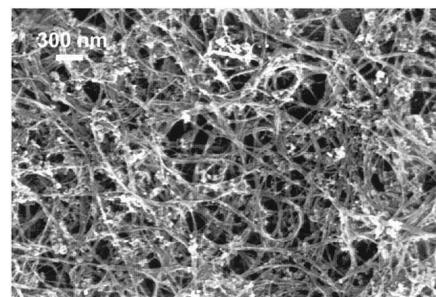


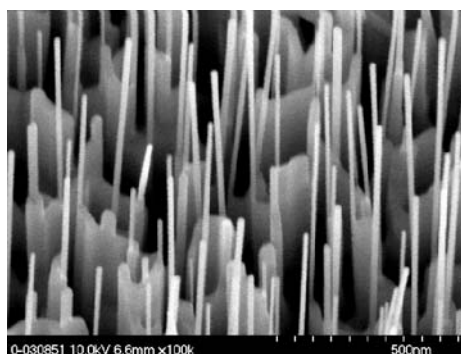
Figure 2.1: Potential barrier at the boundary between vacuum and metal. The work function is defined by  $\phi$ , and the lowering of the work function from the applied electric field is  $\Delta\phi$  [11].



(a) Ungated Si tip-on-post FEA [11].



(b) Carbon nanotubes [12].



(c) ZnO nanorods [13].

Figure 2.2: Ungated FEA examples.

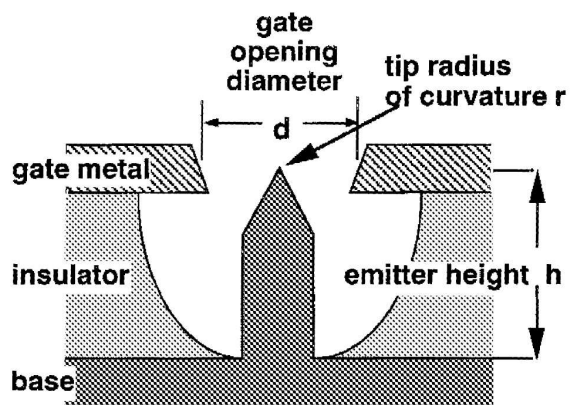
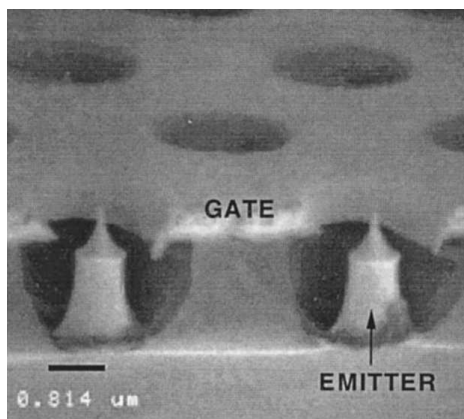
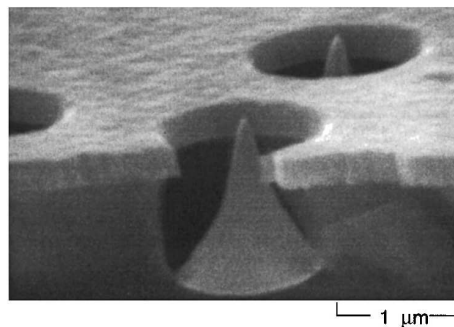


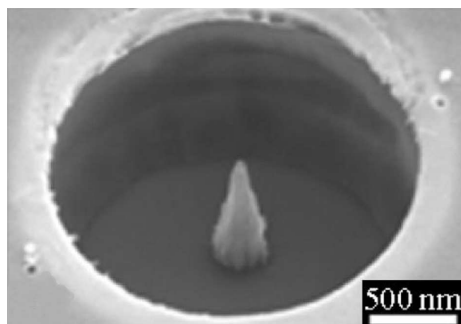
Figure 2.3: Diagram of a cell in a gated FEA [11].



(a) Gated Si tip-on-post FEA [11].



(b) Spindt-type FEA [11].



(c) Carbon nanofiber emitter [14].

Figure 2.4: Gated FEA examples.

### 2.2.3 Characteristics

Emission from the tips can be described by the Fowler-Nordheim Equation (2.2). The required potential applied to the gate necessary for emission depends on the work function of the material and field enhancement effects.

A sharp point in an electric field allows for an increased electric field in the region of the point, which is known as field enhancement. The radius of curvature of the tip and the gate opening diameter greatly affect the field enhancement factor. The tip height and tip position are much less critical [11].

The work function is determined by the material. The lower the work function, the lower the necessary electric field needed to cause emission. This effect would be consistent for the material; however minute surface impurities can drastically change the work function of the emitter tip. Oxidization and monolayers of adsorbed surface contaminants are two common examples of impurities.

### 2.2.4 Issues for FEAs

Because of the difference in geometries and work functions from tip-to-tip, each tip behaves drastically different. “Hero” emitters, ones with a lower work function and/or higher field enhancement factor, will emit much greater current than emitters with poor work functions and/or field enhancement factors. This deviation causes a non-uniformity in current along the array. This difference in current is unavoidable; however solutions exist to minimize this difference. By using a ballast resistor on the emitters, the current can be “self” regulating [15]. The ballast resistor is placed on the input of each emitter cell as shown in Fig. 2.5. The more current the emitter draws, the higher the voltage drop across the resistor and the lower the electric field between

the gate and the emitter. This ballast resistor improves the uniformity throughout the array [15].

One concern for the reliability of all FEAs is the susceptibility of the FEA to backward ion bombardment. At higher pressures, the residual gas can ionize from the emitted electrons, and the ions can be slammed back into the emitters by the electric field. This bombardment could damage the emitter tips causing a decrease in the field enhancement factor. This mechanism limits the use of FEAs to vacuum pressures less than  $10^{-6} \text{ Torr} - 10^{-8} \text{ Torr}$  [11], and in some cases lower current. High current density ( $> 0.1 \text{ A/cm}^2$ ) will increase ionization of the residual gas and increase bombardment of the cathode.

Oxidation is the biggest threat to the lifetime of the FEAs [16]. The residual oxygen in the vacuum or from the materials in the system can ionize near the emitter and oxidize the emitter material. Oxidation increases the work function of the emitter tip, making it less effective. This mechanism is differentiated from backward ion bombardment in that the oxygen ion is adsorbed onto the material, which raises the work function, versus damage to the emitter by impact (sputtering) with an ion, which reduces the field enhancement factor. The observed changes in emission current due to oxidation were found to be reversible [11]. By operating the cathode in vacuum pressures less than  $10^{-7} \text{ Torr}$ , the desorption of oxygen molecules can take place. This process is often called “burn in.” Another method to cause desorption of oxygen is to heat the cathode to high temperatures.

## 2.3 Electron Wall Interactions

Upon a bombardment of a material with a beam of electrons, many different interactions can occur. Much research on electron wall interactions have been done in the field of Scanning Electron Microscopy (SEM). Figure 2.6 shows different electron interactions that are of interest. Interactions A (secondary electron emission) and B (electron backscatter) are the most common types of interactions and are discussed in more detail.

### 2.3.1 Secondary Electron Emission

Secondary electron emission is a phenomenon where electrons are emitted from a surface upon a bombardment with particles [18, 19]. Secondary emission can be caused from any particle type, but the focus of this thesis is on secondary electron emission from electron bombardment. The interaction between the primary electrons and the internal secondary electron is fundamentally a quantum mechanical interaction, but a classical approach gives insight to the mechanism.

Interaction A in Fig. 2.6 shows secondary electron emission. A primary electron penetrates the material where it collides with another electron in the lattice of one of the atoms of the material. The primary electron scatters away, but it excites the secondary electron to a higher energy sufficient to allow it to escape the atom, and eventually the material into vacuum. This is an inelastic interaction, and the secondary electron has substantially less energy than the primary that created it.

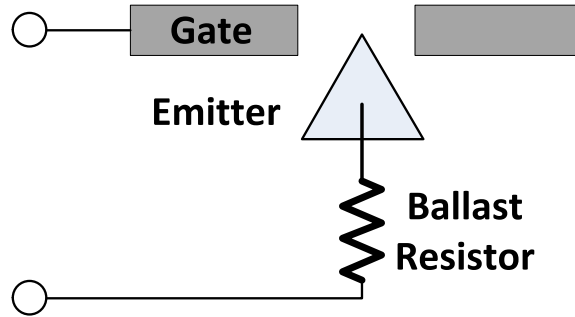


Figure 2.5: Diagram of one cell of a gated field emitter array with a ballast resistor.

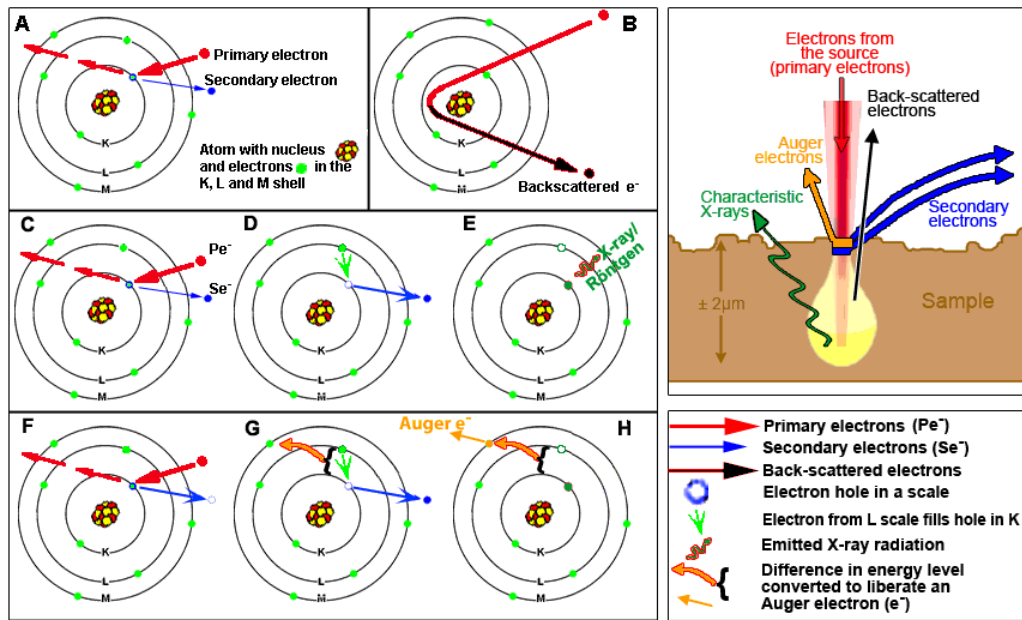


Figure 2.6: Classical view of electron interactions within an atom. Image provided by Radboud University Nijmegen, <http://www.vcbio.science.ru.nl/en/fesem/eds/> [17]

### 2.3.1.1 Secondary Electron Yield (SEY)

As the primary electron scatters away in interaction A in Fig. 2.6, it has a chance of producing another secondary electron. The number of secondary electrons produced from an electron wall interaction is closely related to the energy of the primary electron. Traditional methods to experimentally find this relationship are done by bombarding a voltage-biased material with electrons at different energies and measuring the number of electrons coming off the material through replacement current [20]. This test is complicated for insulators because no replacement current can be measured. And as the material charges up, the primary energy becomes difficult to be determined, and current cannot be measured. There are a few clever methods to measure the SEY of insulators. One way is to coat the insulator with a metal on one side and to bombard electrons onto the other side of the material. The metal electrode can be modeled as a capacitor, and as the insulator charges up, displacement current can be measured on the electrode, and the SEY can be deduced [20]. This and other methods [21] to measure SEY are difficult to implement, and a simpler and accurate method is desired. The use of hop funnels may be able to provide a new way to measure the SEY of materials and is one motivation for the work done in this thesis.

The purity of the sample is essential to the accuracy of the SEY measurements. Contaminants on the surface of the material drastically change the secondary electron yield. Nevertheless, methods to get around these problems have been implemented, and relatively accurate measurements have been produced. The measurements performed have produced a universal relationship between primary electron energy and secondary emission yield for all materials, and an example is shown in Fig. 2.7 [20, 22]. Here,  $\delta$  is the secondary electron emission yield,  $\delta_{max}$  is the maximum SEY for

the material,  $E_p$  is the energy of the primary electron, and  $E_{pmax}$  is the energy of the primary electrons at which the maximum SEY occurs. The normalized curves in Fig. 2.7 closely resemble each other; hence the reason it is called a universal curve. A few analytical curves, Lye and Dekker [19] and Baroody [18], are also plotted in Fig. 2.7, which are explained in Section 2.3.1.2.

Secondary yield depends on two factors: the production of secondaries and the probability of escape. Let  $n(x) dx$  represent the number of secondaries produced at a depth between  $x$  and  $dx$  below the surface. Let  $f(x)$  be the probability of escape for that secondary. The expression for secondary yield would be

$$\delta = \int n(x) f(x) dx$$

All that is left to do is to come up with expressions for  $n(x)$  and  $f(x)$ . The derivation of these terms is not done here, but a few final expressions are presented. These expressions work fairly well; however experimental results sometimes deviate, and a large amount of experimental information is needed to adjust the curve to fit the data.

### 2.3.1.2 Lye and Dekker Formula

The first formula for SEY was derived from a quantum perspective in 1950 by Baroody [18]. This formula deviated from experimental results, specifically in the high-energy region, but produced the general trend in the observed secondary electron yield.

Baroody's formula, not shown here, was modified by Lye and Dekker to improve the accuracy [19]. The modification is still a physical phenomenon based on the energy loss law; however the power  $n$ , in (2.5), is unknown and is empirically found in order

to fit experimental data. The formula is shown below

$$\frac{\delta}{\delta_{max}} = \frac{1}{g_n(z_m)} g_n \left( z_m \frac{E_p}{E_{pmax}} \right) \quad (2.4)$$

where

$$g_n(z) = \frac{1 - \exp(-z^{n+1})}{z^n} \quad (2.5)$$

$\delta$  is the secondary electron yield, and  $E_p$  is the primary electron energy. The parameters of the material that describe the secondary electron yield curve are  $\delta_{max}$ , maximum secondary electron yield, and  $E_{pmax}$ , the energy at which the maximum occurs.  $z_m$  is the value of  $z$  for which  $g_n(z)$  is maximum;  $n$  is an adjustable value. Lye and Dekker found that for the experimental results they were using,  $n = .35$  works well for lower electron energies and  $n > .35$  works better for higher energies. The value for  $n$ , however, can vary drastically from material to material and is usually found empirically to match experimental results. A plot of this formula is shown in Fig. 2.7, and compared to experimental results of various polymers [20, 22].  $n = 2.0$  is a good model for polymers as shown by the figure. The dashed line,  $n = 1.35$ , is for metals, semiconductors, and high-density insulators. Another plot of Lye and Dekker's formula is shown in Fig. 2.7, and compared with the other formulas described in this thesis.

### 2.3.1.3 Vaughan Formula

Vaughan created a strictly empirical formula, (2.6), to describe the secondary yield in the low-energy region,  $0 V$  to  $E_{pmax}$  [23]. This formula described experimental results much better in that region but deviated in the high-energy region. He later com-

bined his formula with Lye and Dekker's to form a combined formula that describes experimental data a little bit better across the range. Vaughan's combined formula is the one used in the simulation software, Lorentz 2E, which is used in this thesis. Vaughan's empirical formula is

$$\frac{\delta}{\delta_{max}} = (ve^{1-v})^k \quad (2.6)$$

where

$$v = \frac{E_p - E_0}{E_{max} - E_0}$$

The value for  $k$  can be found in many different ways, but the "generic" formula proposed by Vaughan is

$$k = \frac{k_1 + k_2}{2} + \frac{k_1 - k_2}{\pi} \arctan(\pi \ln v)$$

where  $k_1 = .62$  and  $k_2 = .25$ . These values for  $k_1$  and  $k_2$  were determined to fit experimental data the best according to Vaughan, and these are the values used by Lorentz 2E. There are, however, different ways to get a more accurate  $k$  value having prior information about the measured data. Also,  $E_0$  is another empirical value designed to fit the curve, and Lorentz 2E uses  $E_0 = 0$ . To combine formulas (2.4) and (2.6), Vaughan found where the expressions intersect with a good degree of accuracy

$$v_3 = \frac{1}{k_2} - .25$$

and if the secondary emission yields,  $\delta_1$  and  $\delta_2$ , were known by expressions (2.6) and

(2.4), respectively, then the combined formula would be

$$\delta = \frac{\delta_1 + \delta_2}{2} - \frac{\delta_1 - \delta_2}{\pi} \arctan(\pi \ln v/v_3) \quad (2.7)$$

According to Vaughan, this formula gives improved performance in all regions. A plot of the non-normalized formulas for  $\delta_{max} = 2$  and  $E_{pmax} = 500 \text{ eV}$  is shown in Fig. 2.8.

The difference between Lye and Dekker and Vaughan's formulae in the low-energy region is the desired characteristic that Vaughan was analyzing. The difference of the formulae in the high-energy region was an unwanted consequence that poorly resembled experimental data. The combined formula takes the best from both and gives an improved formula in all regions. The combined formulae can be tweaked by the many constants to match slight variations in the curve from material to material. Vaughan's formulae may not be physically meaningful, or its physical meaning is unknown because of its empirical nature, but its improved accuracy is the reason why it is used in Lorentz 2E. The unity gain reference line is plotted in Fig. 2.8 to show the energy at which when one electron hits the material one is born. There are two points at which this occurs, a low-energy crossover, referred to here as the first crossover, and the high-energy crossover. The first crossover is an important aspect of electron transport and will be discussed in Section 2.4.

#### 2.3.1.4 Angle Dependence

The secondary electron yield also depends on the impact angle. If a primary beam strikes at an oblique angle, the secondary electron yield will be larger due to the shallower escape paths of the secondary electrons [20]. This dependence begins to fade

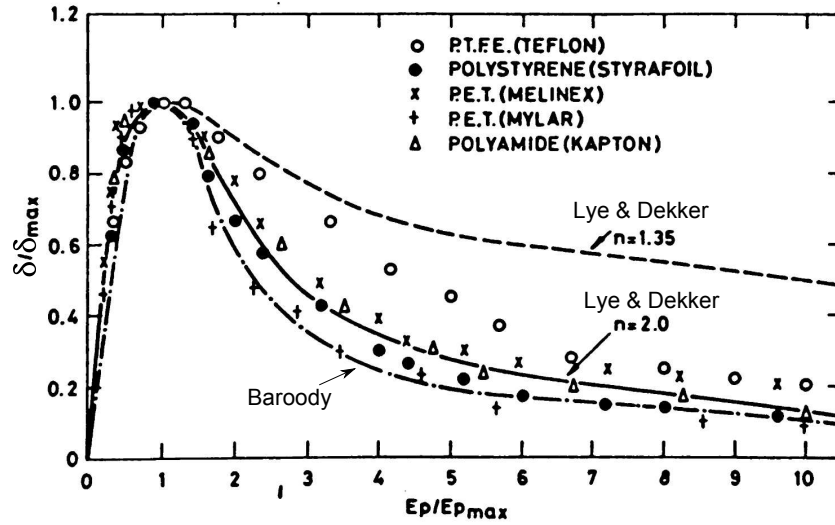


Figure 2.7: Normalized secondary electron yield data for some polymers as found by Willis and Skinner [20, 22] compared to the model found by Lye and Dekker [19] and Baroody [18].

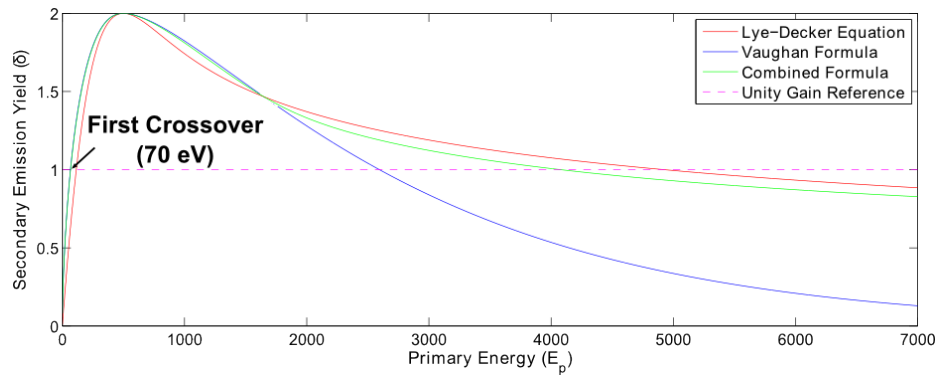


Figure 2.8: Analytical secondary electron yield curves proposed by Vaughan and compared to Lye and Dekker's formula for  $\delta_{max} = 2$  and  $E_{pmax} = 500$  eV. The point at which the unity gain reference line intersects with the curve corresponds to the energy where for every incoming electron there will be one secondary electron. The first crossover of Vaughan's formula in this example occurs at an energy  $E_p = 70$  eV.

at incident energies below  $100\text{ eV}$  [8], which is generally the case in the application of this thesis and is, therefore, ignored for simplicity.

### 2.3.2 Backscattering

Interaction B in Fig. 2.6 shows a backscattered electron. The primary electron enters the material, interacts with the nucleus of the atom, and changes its direction where it is allowed to escape the material. This scatter is usually a highly elastic collision, and the primary electron loses little energy. Differentiating between a secondary electron and a backscattered electron is done by taking into account the energy of the electron that comes off the material. Secondary electrons have energies with a distribution  $< 10\text{ eV}$  while scattered electrons have energies related to the energy of the primary electron, and usually of similar magnitude [8].

### 2.3.3 Other Interactions

The other interactions in Fig. 2.6 show different interactions that are beyond the scope of this thesis, but they show the endless possibilities of the events that may take place. Many types of collisions can take place between particles, and many combinations of collisions can take place. In the hop funnel experiments, the most likely collisions are interactions A and B, and for the energies and materials used in this thesis, interaction A is the dominating interaction. For simplicity, interaction A is the only interaction modeled upon electron bombardment of a material.

The probability of other interactions taking place in the hop funnel experiments is high enough that they will occur in the experiment; however the effects are small when compared to secondary emission because the occurrence of these interactions are significantly lower. The general behavior of the hop funnel is dominated by

the secondary emission properties, and would be slightly modified by the electron backscatter and less-so by the other interactions. In future and more sensitive work involving the determination of the secondary electron yield of the material, backscattering should be modeled. In the work done in this thesis, only the general shape of the I-V curve is needed.

## 2.4 Electron Transport

For this work, electron transport describes the mechanism by which electron current is sustained across an insulator via secondary electron emission. When an electron hits an insulating structure, it may be backscattered or a secondary electron may be generated. If a lateral electric field is present along the surface of the insulator, secondary electrons will travel along the surface, through the vacuum, gain energy, and then may collide with the insulator once again. The electron may again be backscattered or generate a secondary electron. These secondary electrons will also travel along the surface, and the cycle continues until the electrons have been collected at the exit or no new offspring is formed. Because of the way the electrons appear to “hop” down the wall, through the vacuum, this mechanism is often referred to as electron hopping transport, not to be confused with the quantum hopping transport mechanism.

For electron transport to take place, a simultaneous perpendicular and parallel electric field to the wall is needed in order to force the electrons back to the wall. To sustain electron transport, the average secondary electron yield through the geometry must be equal to unity. If the yield is not unity, the wall will become charged, thus affecting the electric field and the electron trajectories. The wall will charge up to a

point where the conditions are either favorable for electron transport or they are not. This is a self-regulating process that will charge the wall so that the average number of secondaries emitted per incoming electron equals unity, corresponding to the first crossover [8], shown in Fig. 2.8. If unity cannot be achieved, the surface charge on the wall will repel incoming electrons, preventing electron transport. An extensive study on this mechanism was performed by Hendriks et al. [8], which is summarized in Section 2.6.1.

## 2.5 Hop Funnel

The design of a hop funnel is essentially, as the name suggests, a funnel, which is made of an insulating material. The narrow end is surrounded by an electrode that is called the hop electrode. Figure 2.9 shows a diagram of a hop funnel.

The wide end of the funnel faces the electron source, which in this case is a FEA. Electrons emitted from the FEA are pulled up by the electric field created by the hop electrode. Some of the primary electrons have a chance of flying straight through the funnel exit, but the majority of the primary electrons will hit the funnel wall. The primary electrons that hit the walls have a chance of producing secondary electrons. If the electric field created by the hop electrode is favorable, electron transport will occur and transmit current through the funnel. If the electric field is not favorable, the funnel wall will charge negatively and repel incoming electrons.

The relationship between the hop electrode voltage and transmitted current (I-V characteristic) allows a study of the electric field required to cause electron transport in the funnel and of the secondary electron emission characteristics of the funnel material. An example I-V curve found experimentally is shown in Fig. 2.10. This

figure was obtained experimentally from the 60° funnel made from low temperature co-fired ceramic (LTCC) described in Section 3.2.1.

Generally, as will be discussed in throughout this thesis, the shape of the I-V curves vary, but the curve shown in Fig. 2.10 is a good example for explaining the general trend. There are three regions of operation of the funnel: the zero-gain region, the transition region, and the unity-gain region. In the zero-gain region, the electric field created by the hop electrode is not strong enough to allow for hopping transport to take place, and nearly all the electron trajectories are reversed back to the cathode. In the transition region, there are a different combination of events that happen in order to allow some of the electrons through and not others. The unity-gain region occurs when the potential on the hop electrode is high enough to pull the electrons towards the exit and to allow for unity-gain electron transport. The mechanisms behind the curve are explained in Section 4.5.

## 2.6 Prior Work

There are a few key papers that discuss hop funnels. Hendriks et al. [7, 8] did an extensive study on electron hopping transport across insulators. An analytical formula and explanation was proposed to describe this phenomenon. The work by Hendriks et al. is summarized in Section 2.6.1. Lester et al. [6] compared experimental I-V curves with simulations of the hop funnel design. They showed that modeling of the mechanism can accurately recreate the I-V curves and is explained in more detail in Section 2.6.2. Liu Min et al. [5], Lei Wei et al. [24], and Xiaobing Zhang et al. [25] did a study on the transverse energy component of electrons leaving the funnels and proposed ways to improve the energy uniformity. Tuck et al. [4] used

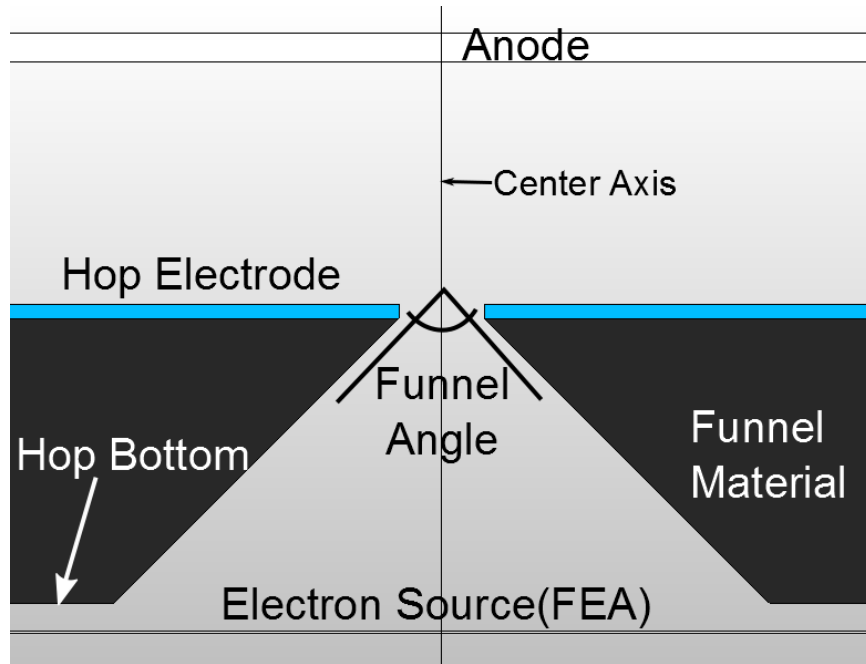


Figure 2.9: Diagram of the cross-section of the hop funnel. The funnel is rotationally symmetric about the center axis.

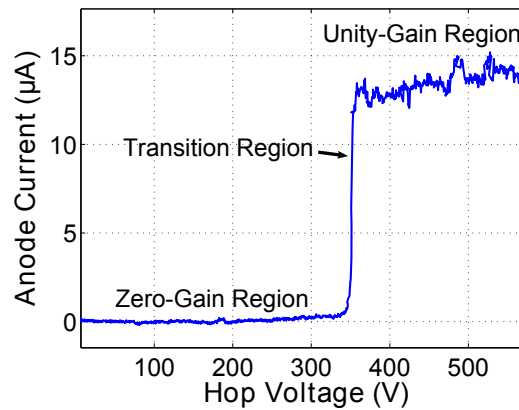


Figure 2.10: Example I-V curve showing the three hop funnel operation regions.

tiny hop funnels ( $\approx 300 \mu m$ ) for their printable field emission displays (pFED). They showed a dramatic increase in uniformity of the electron beam.

### 2.6.1 Hopping Transport Study

The paper by Hendriks et al. [8] focuses on the “hopping” nature of the electrons along an insulated surface with a parallel electric field applied. An analytical formula is proposed and is compared with simulated and experimental results. To obtain the analytical solution, three assumptions were made: (i) the electric field is homogenous, (ii) the surface is a plane, and (iii) the electron current remains constant along the plane. An expression was found that defines the condition where electron transport takes place.

$$\int_0^\infty \int_0^{\frac{1}{2}\pi} \int_0^{2\pi} \Phi(E_l, \theta_l, \varphi_l, r) [\delta(E_l, \theta_l) - 1] d\varphi_l d\theta_l dE_l = 0 \quad (2.8)$$

$\Phi(E, \theta_l, \varphi_l, r)$  represents the probability distribution for electrons landing at wall position  $r$ , with energy  $E_l$ , at an angle of incidence  $\theta_l$ , and an azimuthal angle  $\varphi_l$ .  $\delta(E_l, \theta_l)$  represents the secondary electron yield of the material when it is hit by an electron at an energy of  $E_l$  and at an angle of incidence  $\theta_l$ . Expression (2.8) basically states that electron transport takes place when the average secondary electron yield throughout the geometry is equal to unity.

#### 2.6.1.1 Low-Hopping Approximation

To come up with an analytical expression for the resulting electric fields of electron transport, the hopping trajectories were studied [8]. Figure 2.11 shows the hopping trajectory and the associated vectors.

Using the equations of motion, they found that the distance traveled in the  $\xi$  direction is given by

$$\Delta\xi = \frac{4E_s F_{\parallel}}{eF_{\perp}^2} \cos^2\theta_s + \frac{4E_s}{eF_{\perp}} \cos\theta_s \sin\theta_s \cos\varphi_s$$

where  $\theta_s$  is the take off angle, and  $\varphi_s$  is the take off angle difference from the  $\xi$  direction,  $E_s$  is the energy of the secondary electron, and  $F_{\parallel}$  and  $F_{\perp}$  are the electric fields in the parallel and perpendicular direction, respectively. The maximum trajectory height is

$$\Delta\zeta = \frac{E_s}{eF_{\perp}} \cos^2\theta$$

The landing energy is given by

$$E_l = E_s \left( 1 + \frac{4F_{\parallel}^2}{3F_{\perp}^2} \cos^2\theta_s + \frac{4F_{\parallel}}{F_{\perp}} \cos\theta_s \sin\theta_s \cos\varphi_s \right)$$

and the time of flight is

$$t = \frac{(8mE_s)^{1/2}}{eF_{\perp}} \cos\theta_s$$

The secondary electron energy is described by  $E_s = \frac{1}{2}m(\nu_{\xi}^2 + \nu_{\eta}^2 + \nu_{\zeta}^2)$ , where  $\nu_{\xi}$ ,  $\nu_{\eta}$  and  $\nu_{\zeta}$  are the velocity components in each Cartesian direction. The important thing to note in these equations is that the landing energy depends on the  $F_{\parallel}/F_{\perp}$  ratio and not on the total electric field. Therefore, the number of secondary electrons formed also depends on the  $F_{\parallel}/F_{\perp}$  ratio. To ensure stability of the current, the average number of secondary electrons per incoming electron is equal to unity. For this to occur, Hendriks et al. found that the ratio must be constant throughout the

wall and must satisfy

$$\frac{F_{\parallel}}{F_{\perp}} = \left( \frac{E_I - 2E_0}{4E_0} \right)^{\frac{1}{2}}$$

where  $E_I$  is the lowest energy at which the secondary electron yield becomes unity (the first crossover), and  $2E_0$  is the averaged launching kinetic energy. To find the potential distribution in the space surrounded by the walls where hopping transport takes place, while ensuring the above constraints are satisfied, Laplace's equation is solved with the following boundary condition:

$$\frac{\delta V}{\delta l} = \mu \frac{\delta V}{\delta n}$$

where the constant  $\mu$  is the  $F_{\parallel}/F_{\perp}$  ratio,  $\delta V/\delta l$  is the derivative parallel to the surface, and  $\delta V/\delta n$  is the derivative normal to the surface. This boundary condition ensures that the  $F_{\parallel}/F_{\perp}$  ratio is preserved. The method of finding the electric field using the above boundary conditions is called the low-hopping approximation.

### 2.6.1.2 Electron Transport Through a Cylindrical Tube

Hendriks et al. tested the electron transport mechanism using a few different geometries with a Monte Carlo simulation to compare with the low-hopping approximation and experimental results. One of the analyzed geometries was an insulating cylinder with electrodes on both ends. The cylinder had a radius  $R = 1 \text{ mm}$  and a length  $L = 50 \text{ mm}$ . In the simulation, the electrons were injected on one end with an energy of  $50 \text{ eV}$  and with velocity directions isotropically distributed, and a study of the electron transmission through the cylinder vs. the voltage applied across the

electrodes was performed. The transmission vs. voltage characteristic is shown in Fig. 2.12.

The study shows that there is a critical voltage at which the transmission current goes from zero to full transmission. This curve resembles the transmission characteristics of hop funnels shown in Fig. 2.10. This similarity is to be expected, as the cylinder is essentially a funnel with a  $0^\circ$  angle. To see why the cylindrical insulator behaves this way, the potential distributions along the surface from the Monte Carlo simulations are shown in Figure 2.13.

At  $V_L = 600 V$ , shown in Fig. 2.13a, the entrance part of the tube charges negatively, which repels the incoming electrons, and current is not allowed to pass through. This negative charging is due to the fact that secondary electrons formed in this region do not hop very far due to the weak electric field. The primary and secondary electrons deposit their charge near the entrance, thus charging that region of the wall negatively. At  $V_L = 1000 V$ , shown in Fig. 2.13b, the walls become positively charged. This is due to the fact that initially more than one secondary electron is formed per primary in this region, and they are pulled down the cylinder by the strong electric field. This causes the wall to charge positively, which in turn attracts the newly formed secondary electrons so that they do not travel as far down the cylinder. The wall charges so that eventually the average SEY in the region and throughout the cylinder will be unity (the first crossover). The electric field decreases exponentially in the first part of the tube, which corresponds to a rotationally symmetric distribution similar to what is seen with the low-hopping approximation, also shown in the figure. The potential distribution starts to deviate from the low-hopping approximation as soon as the hopping heights exceed that of the diameter of the tube, and electrons start hitting the other side of the tube. The

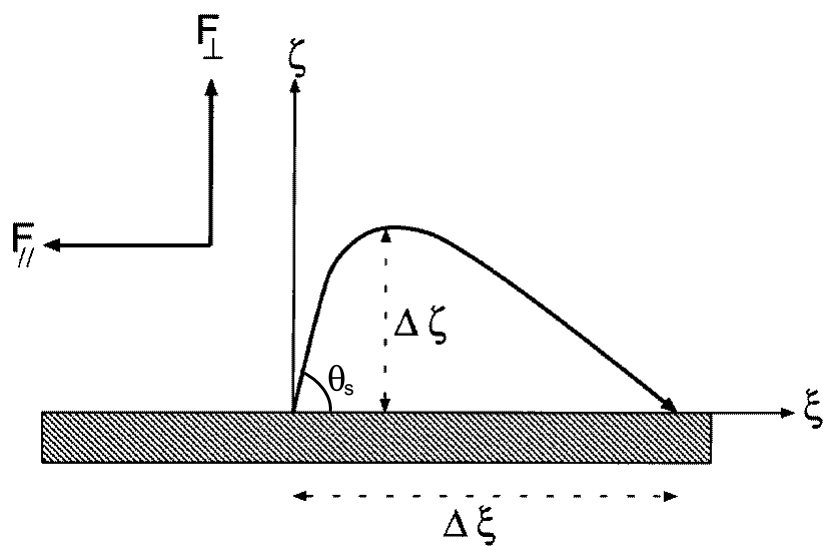


Figure 2.11: Hopping trajectory model [8].

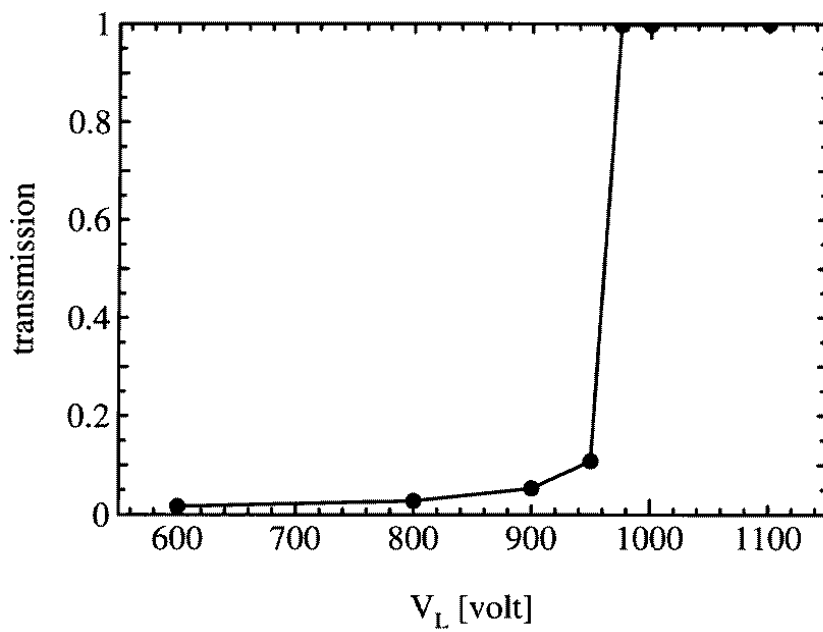


Figure 2.12: Electron-transmission curve (I-V curve) through a cylinder from Monte Carlo simulations performed by Hendriks et al. [8].

parallel electric field becomes more uniform thereafter in order to pull the electrons down the tube. After this happens, the rotational symmetry breaks down. The spatial distribution was found to vary in time and is easily disturbed by external influences.

### 2.6.2 Hop Funnel from Low Temperature Co-Fired Ceramic

A study was done by Lester et al. [6] that compared the results of experimental hop funnel I-V data to that of a simulation using Lorentz 2E. This study focused on the validity of the Lorentz 2E simulation to match the results found in the experiments. The stability, exiting electron energy, and exit current were studied. The setup is virtually identical to the experiments and simulations described in this work and is explained briefly here but in greater detail in Sections 3.2 and 4.3. The simulations were performed using Lorentz 2E. The basic hop funnel geometry is shown in Fig. 2.14.

The thickness of the hop funnel is  $1\text{ mm}$ ; the radius of the exit hole is  $0.2\text{ mm}$ ; the radius of the funnel entrance is  $1.2\text{ mm}$ ; and the distance from the cathode to the anode is  $2\text{ mm}$ . The primary electrons shown in Fig. 2.14, also referred to here as primary rays, are emitted from the FEA in a way that represents the typical behavior of a FEA. Each ray represents a number of electrons and the charge associated with that electron group. The material of the hop funnel shown in Fig. 2.14 is labeled as LTCC (Low Temperature Co-Fired Ceramic) whose secondary electron characteristics are unknown, but the values simulated are in the range of  $\delta_{max} = 1.75 - 3.0$  to and  $E_{pmax} = 420 - 500\text{ eV}$ . Not knowing the secondary electron characteristics of the material is undesirable, but one of the goals of the research by Lester et al. was to determine the secondary electron characteristics of the material by comparing the I-V characteristics of the simulation to the experimental results. In Fig. 2.14, the

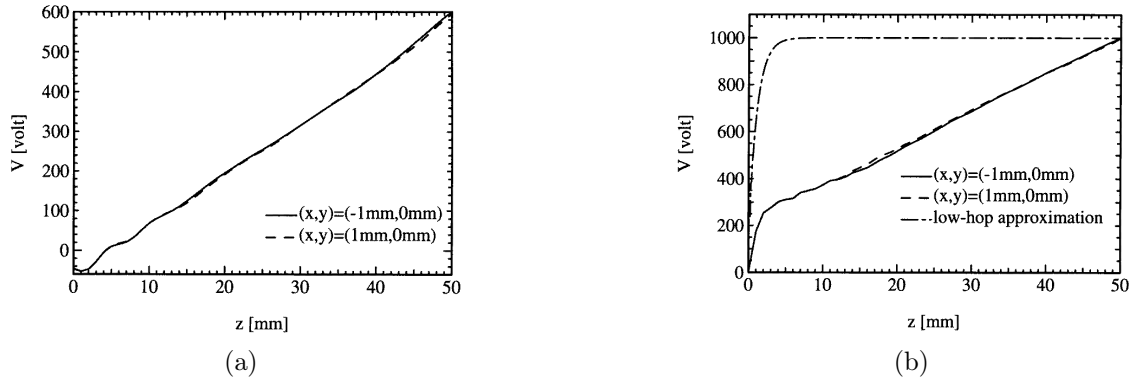


Figure 2.13: Simulated steady-state potential distribution along the surface of the cylinder for (a)  $V_L = 600$  V and (b)  $V_L = 1000$  V [8].

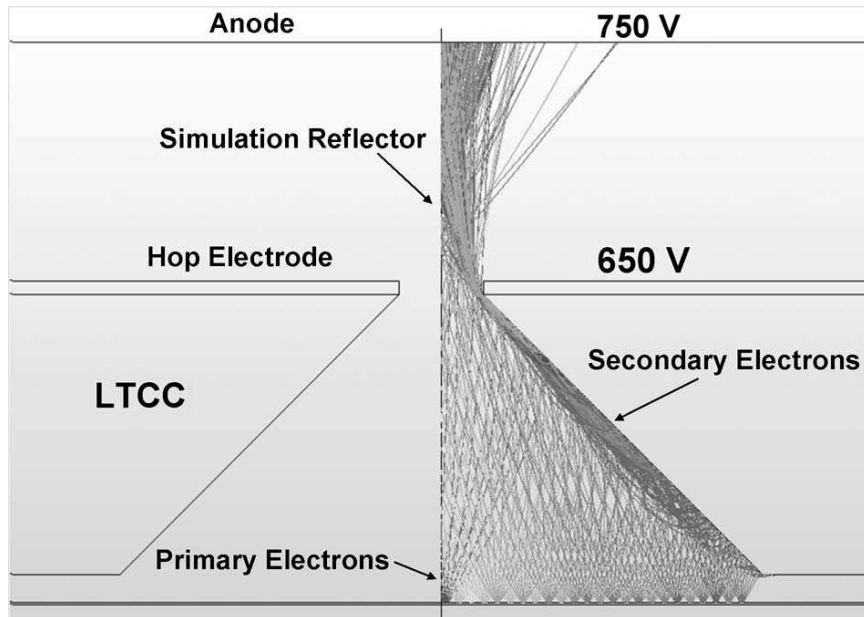


Figure 2.14: Hop funnel model simulated in Lorentz2E by Lester et al. [6].

potential of the hop electrode is sufficient for the rays to hop up the wall, through vacuum, via electron transport, and exit the funnel, ending at the anode. By varying the hop electrode voltage and running the simulation many times to steady-state, the general behavior of the funnels was studied. The anode current evolution through time for each simulation is shown in Fig. 2.15, and the transmission vs. hop voltage graph is shown in Fig. 2.16.

Figure 2.15 shows the simulated anode current through all the iterations at various hop voltages. As the simulation starts, the walls start to charge up negatively, which can be seen by the less than unity current on the anode at the beginning of each run. There are two mechanisms as to why the wall charges negatively. If the energy of the primary electron is below the first crossover, then less than one electron will be produced causing the wall to charge negatively. If the energy of the primary electron is above the first crossover, more than one electron will be produced, which will start to charge the wall positively; however the newly formed secondary electrons have energies far below the first crossover, and if the electric field present in the funnel pulls the secondary electrons up into the wall without gaining sufficient energy above the first crossover, they will be collected causing a net negative charge to be deposited on the wall. If the electric field is too weak, the walls will keep charging more negatively until the incoming primary electrons are repelled. If the electric field is favorable, the wall still charges negatively, but even with the negatively charged walls, the electric field remains strong enough to pull the secondary electrons up the wall with energies above or equal to the first crossover, allowing electron transport to take place.

The negative charging of the funnel wall during full transmission is different than the positive charging of the cylinder as found by Hendriks et al. [8], explained in

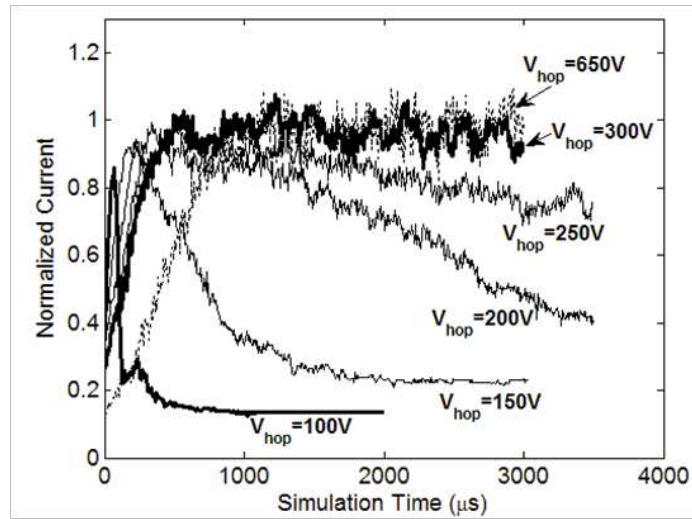


Figure 2.15: Anode current vs. time from the Lorentz2E simulations of a hop funnel for various hop voltages performed by C. Lester et al. [6].

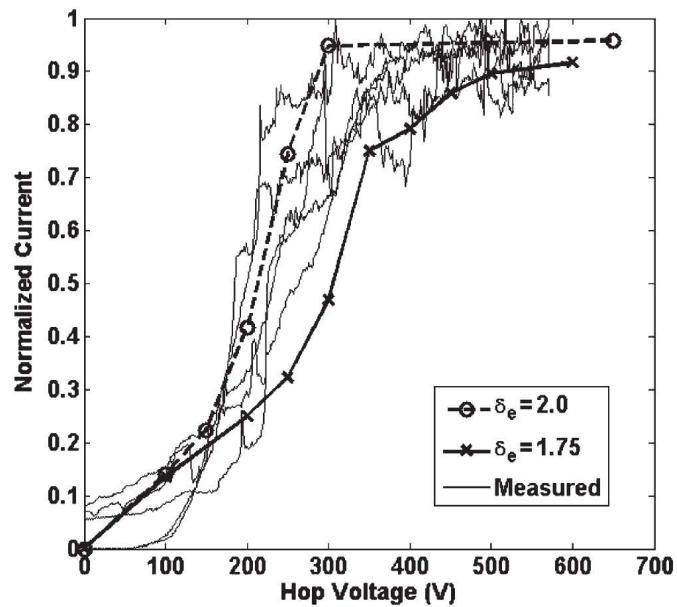


Figure 2.16: Simulated and experimental hop funnel anode current characteristics performed by Lester et al. [6].

Section 2.6.1.2. The difference is attributed to the angle of the funnel wall. With a  $0^\circ$  funnel angle, like the cylinder, the initial lateral electric field pulls secondary electrons farther down the wall, causing more electrons to leave the area, thus charging positively. With a  $90^\circ$  funnel angle, the electric field pulls the secondary electrons along the wall, but they collide with the wall before they gain a sufficient amount of kinetic energy to collide at energies above the first crossover because of the funnel angle. More electrons are deposited on the wall in this region, thus charging negatively. Once at steady-state, the negativity charged walls still allow primary electrons to collide with energies around the first crossover and also allow the secondary electrons to travel farther up the wall, thus gaining enough energy to form new secondaries.

The secondary electron characteristics of LTCC are not known; however the group managed to find parameters that matched the I-V curve fairly well as shown in Fig. 2.16. Figure 2.16 also shows a wide range of I-V curves observed experimentally. The context of the curves are not published in the paper; however in analyzing the data, the I-V curve depends on whether the voltage is being ramped up or down. This hysteresis will be described in Section 3.3.1. The “ramp-up” I-V curves are relatively similar from experiment to experiment, and the “ramp-down” curves are relatively similar from experiment to experiment. The simulated curve represents the basic trend in the transmission characteristics of the hop funnel; however the hysteresis was not modeled.

There were three basic discretizations studied in order to make the simulation times reasonable but still allow a limited amount of error and stability issues.

1. The coulombs per electron ray
2. The number of rays

### 3. The number of surface charge elements on the wall

Lester et al. focused on one and two. For the third discretization, they used 100 surface charge elements along the wall. More information on the effect of the number of surface charge elements is discussed in Section 4.3.2. The charge per ray can be found by  $\Delta Q = I \cdot \Delta t / N$ , where  $N$  is the total number of rays,  $\Delta t$  is the time step, and  $I$  is the total injected current. To study the effects of the charge per ray size and the number of rays on the stability of the current, nine test cases were studied, which are shown in Table 2.1. Each column represents a constant charge per ray size but varying number of rays. By maintaining a constant time step and the number of rays ratio,  $\Delta t / N$ , a constant charge per ray can be maintained, and the effect of the number of rays on simulation stability can be studied. Each row represents the effect of keeping the number of rays constant but varying the charge per ray.

The simulation was run with the total emitted current  $I = 1 \mu A$ , the hop electrode voltage  $V_{hop} = 600 V$ , and the anode voltage  $V_{anode} = 800 V$ . The secondary electron parameters chosen for the funnel were  $\delta_e = \delta_{max} = 3.0$ ,  $W_m = E_{pmax} = 420 eV$ , and  $W_{avg} = 5 eV$ .  $W_{avg}$  is the average energy of the emitted secondary electrons. The simulation was run from start up until steady-state where the stability of the current was studied. Figure 2.17 shows the anode currents of each case in Table 2.1 after the simulation has reached steady-state.

The general trend in the data is that with more rays and less charge per ray the anode current is more stable. This is to be expected because as  $N \rightarrow \infty$  and  $\Delta t \rightarrow 0$ , the simulation should stabilize. The 50 ray case shown in Figure 2.17c is surprisingly stable for all cases. The reason is unknown for the stability of 50 rays. The chosen simulation parameters that yield fairly stable results and with reasonable

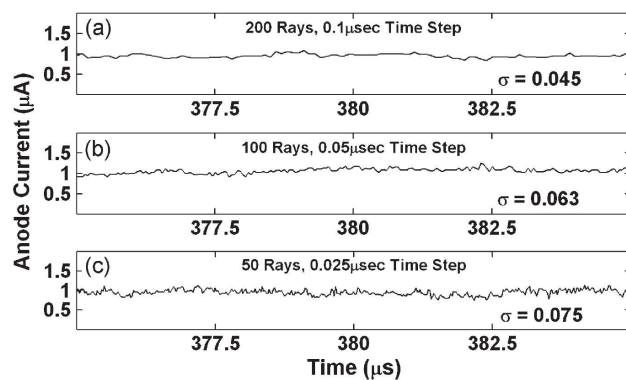
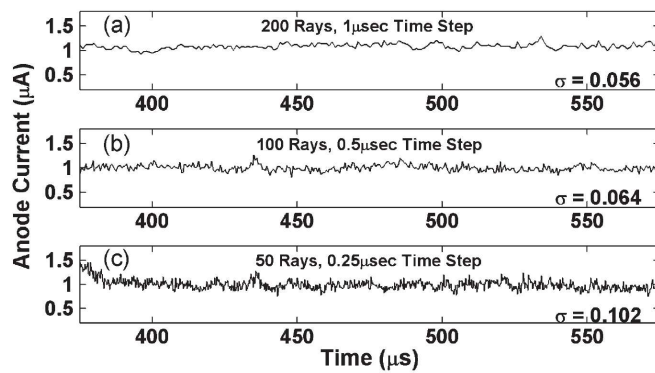
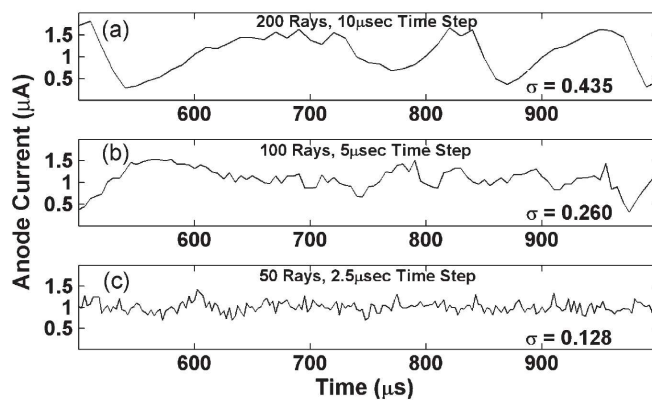
(a) 3.1 *ke/ray*(b) 31 *ke/ray*(c) 310 *ke/ray*

Figure 2.17: Current stability study from Lester et al. [6].

simulation times was  $\Delta t = 5 \mu s$  with 200 rays. The work in this thesis will build on this preliminary modeling.

### 2.6.3 Transverse Energy Study

Liu Min et al. [5], Lei Wei et al. [24], and Xiaobing Zhang et al. [25] analyzed the transverse energy component of the electrons leaving the funnel. By moving the emission source relative to the funnel entrance, they could control the number of primary electrons exiting the funnel. They found that the transverse energy component of secondary electrons leaving the funnel is smaller than that of the primary electrons. By allowing only secondary electrons through, the energy of the electrons leaving the funnel can be controlled. To prevent primary electrons from leaving the funnel, they moved the electron source away from the funnel entrance, and as a result some current was lost underneath the hop bottom.

To prevent the primary electrons from leaving the funnel and to prevent a loss of current, in a prior article, Lei Wei et al. proposed a double funnel design [24]. The double funnel design is shown in Fig. 2.18. This design gives no direct path for the primary electrons to escape the funnel, and mainly secondary electrons are allowed to leave. This provides a much greater energy uniformity of the beam.

### 2.6.4 Printable Field Emitter Display (pFED)

Tuck et al. [4] used hop funnels for a field emission display. The FEA used in the work emitted a non-uniform beam across the array. Tiny ( $\approx 300 \mu m$ ) funnels were used on each pixel of the 5.2 *inch* diagonal display to improve spatial uniformity of the electron beam. Not only did the funnels improve the performance of the display,

Table 2.1: The number of electrons per ray used in the Lorentz 2E simulation performed by Lester et al. [6].

	<b>3.1 (ke/ray)</b>	<b>31 (ke/ray)</b>	<b>310 (ke/ray)</b>
$\Delta t_1 (\mu\text{s}) / N_1$	0.1 / 200	1 / 200	10 / 200
$\Delta t_2 (\mu\text{s}) / N_2$	0.05 / 100	0.5 / 100	5 / 100
$\Delta t_3 (\mu\text{s}) / N_3$	0.025 / 50	0.25 / 50	2.5 / 50

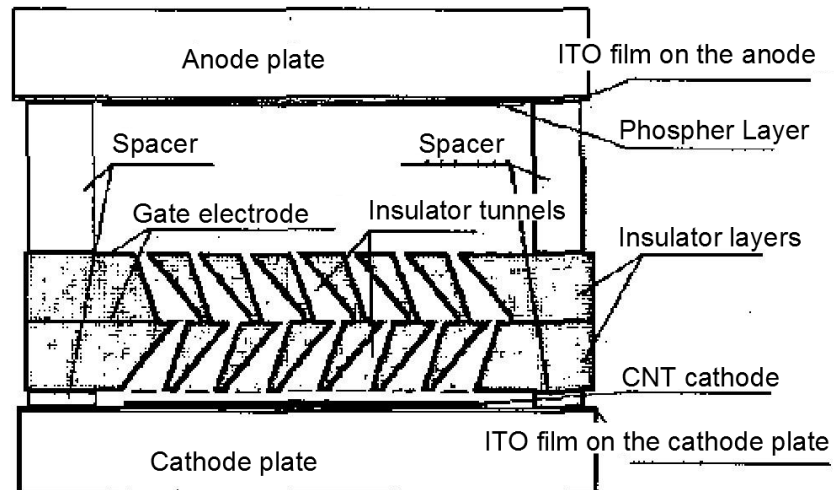


Figure 2.18: Double funnel design used to increase energy uniformity of the electron beam [24].

they also provided structural protection of the carbon-based field emitters used in the work.

## CHAPTER 3

### EXPERIMENT

#### 3.1 Overview

The experiment described here includes the work done in this thesis and the work described in Section 2.6.2. The experiment was designed to recreate the same conditions that caused the hysteresis observed by Lester et al. [6] and to try to find the cause. Initially, it was theorized that charging on the hop bottom could be the cause of the hysteresis. To test this theory, a variation of the original experiment was implemented to rule out charging on the hop bottom. A silver layer was deposited on the hop bottom in order to prevent charging. This layer is referred to here as the metal hop bottom. Also, two different hop funnel angles,  $60^\circ$  and  $90^\circ$ , were tested to determine the effect on the current versus the funnel angle.

#### 3.2 Experimental Setup

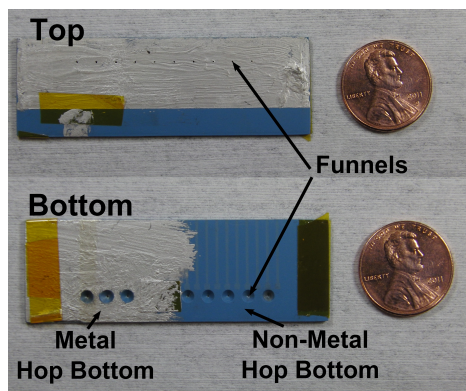
##### 3.2.1 Hop Funnel

The material used to fabricate the hop funnel in the following experiments is DuPont 951 Green Tape low temperature co-fired Ceramic (LTCC) [26]. LTCC is a good material for vacuum and outgasses very little upon electron bombardment. LTCC is an easily machinable material in its green state, and the access to the tools and

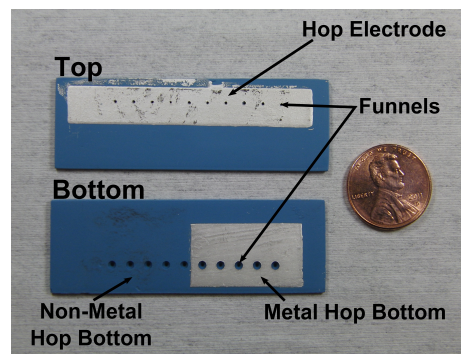
material at the university made it a good choice for this work. The secondary electron characteristics of the material is unknown, which is undesirable; however it is not completely necessary to know these values to observe the hysteresis and study electron hopping transport. The metal used for the hop electrode and the metal hop bottom for all the funnels is silver paste.

LTCC is sold in thin flexible sheets. The sheets are cut to the appropriate dimensions and are then heat pressed (laminated) together at  $75^{\circ}\text{C}$  to form a block of the desired thickness. The material is still somewhat malleable and can be easily worked with. In some funnels, the silver paste was screen printed onto the block where the funnels would be. One metal layer is the hop electrode, and one layer would be the hop bottom electrode, if it is needed. In other funnels the silver paste would be applied later. To create the funnel, the block is milled with an angled bit corresponding to the desired angle of the funnel. Finally, the structure is fired at  $860^{\circ}\text{C}$  to harden it. The LTCC structure shrinks almost uniformly by about 12% in each direction and comes out of the oven as an extremely hard and fairly brittle structure. At this point the LTCC cannot be milled or manipulated and cracks easily. If the hop electrode or the metal hop bottom electrode was not applied pre-firing, the layers would be hand painted using silver paint. The  $60^{\circ}$  funnels used the screen-printing method and the  $90^{\circ}$  ones did not. Pictures of the funnels are shown in Fig. 3.1 and a diagram of the funnel is shown in Fig. 3.2.

The hand-painted funnels were less effective than the screen-printed funnels. Because of unwanted silver paste in the funnel exit, leakage current to the hop electrode was common and on the order of the anode current. The screen-printed electrodes showed substantially less current on the hop electrode. The difference in the quality of the funnels most likely introduces unwanted I-V curve effects between the funnels.



(a) 90° funnel with hand painted silver electrodes



(b) 60° funnel with screen printed silver electrodes

Figure 3.1: The hop funnels used in the experiments. The blue part is the LTCC, the silver is the silver paste, and the yellow material is Kapton tape used to suspend the funnel above the cathode.

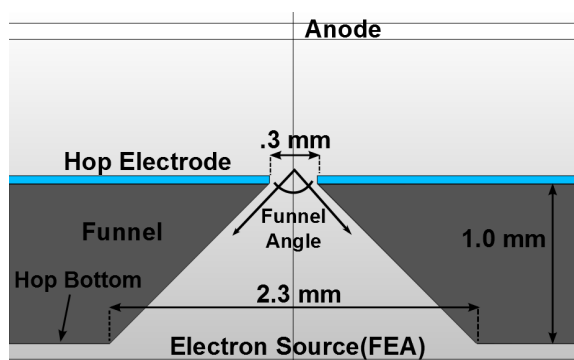


Figure 3.2: Hop funnel diagram.

It is impossible at this point to determine what these unwanted effects are; however similar behavior of the hysteresis was observed in both funnels, enough to be able to study the hysteresis mechanism.

### **3.2.2 Field Emitter Arrays**

Two types of FEAs were used in these experiments. A cathode developed by PixTech was used for the experiments done by the author, and cathodes developed by Motorola [15] were used by the previous researchers [6] whose results are presented here as well. Both of the cathodes are Spindt-type emitters. An example of a Spindt-type is shown in Fig. 2.4b.

#### **3.2.2.1 PixTech Cathodes**

The FEAs used in the experiment were fabricated by PixTech for use in their Field Emission Displays around the year 2001. The cathodes originally were inside the PixTech displays. To remove the cathode, the display had to be disassembled by breaking the glass frit seal. This is a delicate procedure, and many cathodes and phosphor screens were damaged in the removal process. Many of the experiments were performed with a cracked cathode. The main side effect of using a cracked cathode is an increase in short circuits between gates to the emitters. This causes an increase in “leakage” current, which is discussed in more detail later.

The cathodes were fabricated on a Borosilicate glass substrate. The emitters are a Molybdenum Spindt-type [3] with ballast resistors. An example of a Spindt-type is shown in Fig. 2.4b. The gates are made of Niobium laid out across the substrate and around the holes. An image of the emitter array is shown in Fig. 3.3.

The emitter electrodes are on the bottom of the structure, and the gate electrodes are on the top. Each pixel consists of thousands of emitters. To turn on a desired section, the gate is given a positive potential ( $\sim 80 V$ ) relative to the emitter. The arrays are laid out in an X-Y addressable format. The location at which the address lines crossover is the section that will turn on (display pixel). To keep the other sections from turning on, the electrodes must be reversed biased.

The PixTech cathodes used in these experiments were not designed for this application, and unwanted characteristics were unavoidable. After the cathodes were removed from the display, physically connecting to the gate and emitter lines was tedious, and it was difficult to pinpoint the exact location of emission. To connect to the traces, a layer of silver paste was placed over the desired traces. To connect to a lead wire, the end of the wire was “sandwiched” between two layers of silver tape, which was then adhered to the silver paste layer. To align the funnel onto the point of emission, one must follow the traces the crossover point. Placement of the funnel was done visually and set in place by Kapton tape. An exact centering of the beam under the hop funnel is unlikely, and it is very likely that some of the current was emitted under the hop bottom.

Leakage current in the cathode caused by short circuits between the gates and the emitters within the cathode is another problem. To reverse bias the other sections to prevent them from turning on, the leakage current would be on the  $50-100 mA$  range, which can heat up and damage the cathode. For this reason, all the other sections were left floating and were commonly seen to emit current. This stray current is an unwanted source of charge that can deposit itself somewhere and affect the results.

The leakage current was also observed to increase linearly through use. This “run-away” leakage prevented the use of a current controlled emitter source. Using a

current controlled source would be ideal because it allows a known and clean source of current. Without it, a constant voltage on the gate is used, and the resulting emission current is very noisy. Such noise was not seen before the cathodes were de-sealed.

The cathode was designed to be used with a  $300\text{ V}$  anode at a  $200\ \mu\text{m}$  gap, and neither ion nor electron back bombardment was a concern. As a result, the dielectric surface around the gates was not a concern, so the cathode has no way to bleed charge. Any reverse trajectories or ions in the hop funnel configuration that find their way to the substrate will deposit their charge. Charging of the dielectric will deform the beam optics and most likely affect the outcome of the experiments as will be seen in Section 3.3. The PixTech cathodes used in the experiment start to emit current at around  $40\text{ V}$ , and at voltages greater than  $80\text{ V}$  the leakage and susceptibility of arcs makes use in this region difficult.

### 3.2.2.2 Motorola Cathodes

The Motorola cathodes are also a Spindt-type emitter and have a very similar layout to the PixTech cathodes. An example of a Spindt-type is shown in Fig. 2.4b. These cathodes were designed to be experimental cathodes, and contain regions with different layouts. The exact makeup of the cathode is unknown and contain differences between them.

### 3.2.3 Mechanical Setup

To measure the hop funnel exit current, an anode is placed over the funnel as shown in Fig. 3.4. The anode is held at ground potential, through a current measurement resistor ( $V_{measure} < 2\text{ V}$ ), while the cathode is biased to a negative potential.

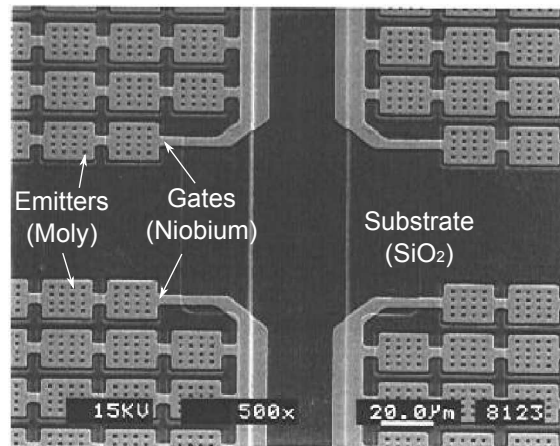


Figure 3.3: SEM image of the PixTech cathode showing the layout.

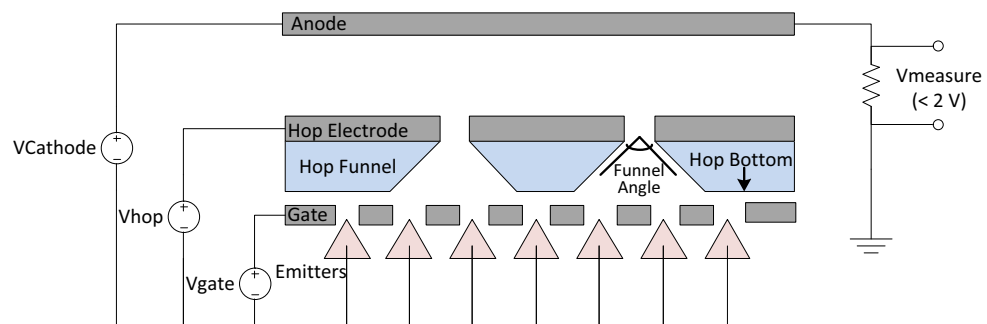


Figure 3.4: Experimental setup. The potential of the metal hop bottom electrode is equal to  $V_{gate}$  if it is used.

The hop funnel is suspended above the cathode as close as possible, typically  $< 1\text{ mm}$ . The anode is placed above the hop electrode by about  $1\text{ cm}$ . The distance between the hop electrode and anode is found to have little or no effect on the measured current. The potential difference between the hop electrode and the anode also is found to have little effect on the current so long as the electric field is sufficient to attract and collect the electron current.

The cathode is biased negatively relative to the anode by  $V_{cathode}$ .  $V_{cathode}$  ranges anywhere from  $700\text{ V}$  to  $3000\text{ V}$ . The gate electrode and the hop electrode are biased positively with respect to the emitters by  $V_{gate}$  and  $V_{hop}$ , respectively.  $V_{gate}$  ranges from  $40\text{ V}$  to  $80\text{ V}$ , and  $V_{hop}$  ranges from  $0\text{ V}$  to  $550\text{ V}$ . If the metal hop bottom electrode is used, the potential was fixed to the gate potential  $V_{gate}$ . Having the gate and hop bottom electrode potentials be equal, the electric field disturbance created by the hop bottom electrode is minimized.

### 3.2.4 Measurement and Control Setup

The entire cathode/hop structure is biased negatively. Much of the control circuitry and the power supplies for the hop electrode and the cathode are floated as well. A LabVIEW Virtual Interface (VI) was created to control the power supplies. To communicate with the floating potential, a D/A converter and analog opto-isolators were used. The emitter, gate, and hop currents also must be measured from the floating potential, and circuitry to accurately measure and record them is not currently implemented. On the Earth ground side, the anode current is measured across a resistor to ground and read into the LabVIEW VI through an A/D converter.

### 3.2.5 Procedure

To gather the I-V curves, the following procedures are used for the experiments.

#### Calibration

1. Slowly ramp the cathode voltage to the desired potential,  $V_{cathode} \approx 1000 V$ . For the safety of the equipment, the supply is “potted,” meaning the voltage is increased slowly to values above the desired potential in order to ensure no arcs occur.
2. Initialize the hop voltage to the maximum,  $V_{hop} = 550 V$ , in order to ensure full transmission.
3. “Burn-in” the cathode to desorb oxygen on the emitters.
4. Slowly ramp up the gate voltage while observing the transmitted current on the anode until the desired current is reached. This anode current is considered the total emitted current.

#### Measure I-V Curves

1. While keeping the gate voltage constant so that the cathode is constantly emitting current, lower the hop voltage to zero. This information is not recorded.
2. Ramp up the hop voltage from  $V_{hop} = V_{hop-min} \rightarrow V_{hop-max}$ , over a desired time,  $t_{ramp} \approx 10 s$  while recording the anode current.
3. When the hop voltage reaches the maximum,  $V_{hop} = V_{hop-max}$ , hold the voltage constant for a desired time,  $t_{pause} \approx 10 s$ .

4. Ramp down the hop voltage from  $V_{hop} = V_{hop-max} \rightarrow V_{hop-min}$ , over a desired time,  $t_{ramp} \approx 10$  s while recording the anode current.
5. This constitutes a full ramp-up-down procedure. Repeat Steps 2 - 4 to gather many ramping curves.

### 3.3 Experimental Results

Three different types of hop funnels were tested, and two different cathodes were used. The I-V curves were obtained for hop funnels with and without a metal layer on the hop bottom and with different hop funnel angles. Once the setup was placed into the vacuum chamber, the general behavior of the I-V curves obtained was fairly consistent between ramp-up-down procedures. However, if the setup was changed in any manner (i.e., allowing the chamber to go up to atmosphere and then back to vacuum, without touching anything) the I-V curves would change. This sort of behavior reiterates the notion that the electron transport mechanism in the hop funnel is very susceptible to external forces as found by Hendriks et al. [8]. Also, current spikes and degradation of current over time, within the same setup, was common. This changing current is most likely caused from the inconsistencies in the cathode operation as explained in Section 3.2.2.1 and later in this section.

The inconsistency in the curves from setup to setup suggests external forces at work. A change in the initial conditions of the setup can cause drastic changes in the I-V characteristics. The purity of the sample has been found to affect the SEY characteristics drastically in many secondary emission experiments [20] and may affect the I-V curves of hop funnels in a similar manner. Slight changes in the work function of the cathode can cause major shifts in current, which can also affect the I-V curves.

Charging of a dielectric is the most likely source of the inconsistency within the same setup. At times, when ramping the current up and down repeatedly, the current would degrade each cycle, until very little to no current was observed. To regain the current, usually one of two things occurred. If an arc or surface flashover occurred on or near the cathode, the current would occasionally “reset”. Also, by shutting down the experiment for a prolonged period of time and by restarting the experiment at a later time, the current would also reset. Both of these things lead to the conclusion of unwanted electrical charging on or near the cathode, most likely the charging of the cathode (FEA) dielectric.

By running the hop funnel in the zero-current or transition region, where there are many reverse trajectories, the substrate is likely to charge up. The charging of the cathode itself is a likely source of “erratic” behavior. The same experiments performed in this thesis should be run with a cathode that has a charge bleed layer to try to get more consistent results, and either confirm or disprove the cathode charging theory. However, such cathodes are not available to our group.

For each test case, there are two series of plots. One series will show the consistency from one setup. The consistent series is presented in the order in which the I-V curves were gathered. The second series will show the range of different results observed for all the setups. The order of the second series is not necessarily in the order in which they were performed. The timing of the ramps was found to have little effect on the I-V curves, so the ramping times are not presented here. Many of the mechanisms behind the results are left unexplained as it is difficult to draw conclusions from the varying results. Much of the explanations on the behavior of the funnels is explained from simulations in Chapter 4.

### 3.3.1 90° Hop Funnel Using Motorola Cathode

These experiments were run by Lester et al. [6]. The original publication did not include the context of the curve, whether it was during a ramp-up or ramp-down. The following plots are a reevaluation of the raw data, including the context of the curves. Figure 3.5 shows I-V curves of the same setup, showing the consistent hysteresis of the I-V curves in the same setup. Figure 3.6 shows the range in results that can be observed from setup to setup.

Figure 3.5 plainly shows the hysteresis. The ramp-down transition region occurs at a lower voltage than the ramp-up. There are a few reasons why this might happen, but as will be seen later, sometimes the opposite is true.

During the ramp-downs, Fig. 3.5 shows a traditional I-V curve as would be expected from previous research [8]. The ramp-up shows two levels of transmission with two steep transition regions. This variation is commonly observed in many of the I-V curves and has no definite explanation. One possible explanation may be that there are small imperfections on the funnel wall that cause discrete levels of transmission. Cross-sectional images of the funnel are needed to help confirm this, which are unavailable and left for future work. There seems to be an evolution of the ramp-up curve in Fig. 3.5. The 2nd transition occurs at higher voltages on each run through until it occurs at the highest voltage, shown in Fig. 3.6b and 3.6c. After the ramp-up, the hop voltage is kept at maximum for a period of time on the order of the ramp time, and it is during this time that the second transition in Fig. 3.6b and 3.6c occurs. This evolution of the curve indicates a progressive charging occurring somewhere. Most likely the charging occurs on the cathode, during the zero-gain or transition region from the reverse trajectories.

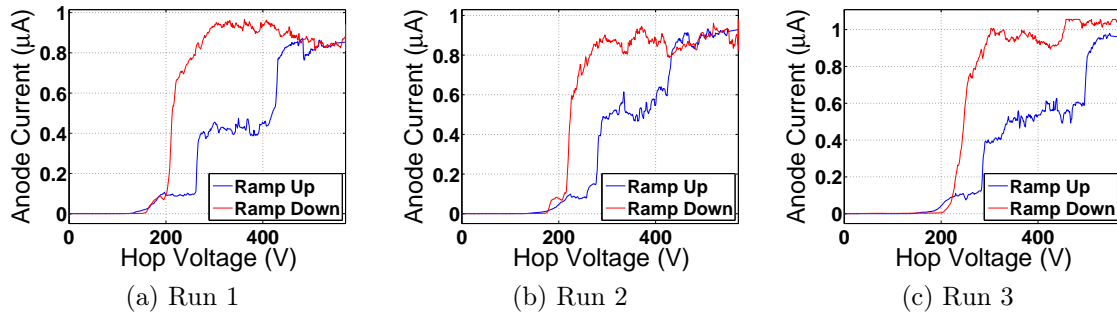


Figure 3.5: Experimental I-V curves obtained from the  $90^\circ$  hop funnel without a metal hop bottom, for runs taken using the same test setup, using the Motorola cathode.

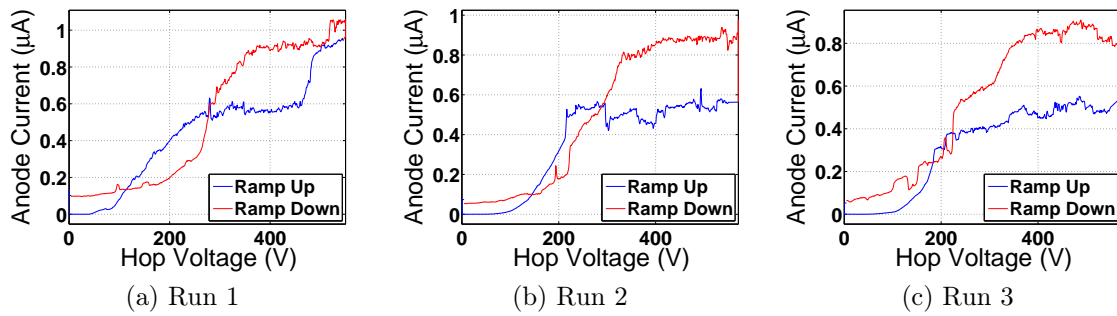


Figure 3.6: Experimental I-V curves obtained from the  $90^\circ$  hop funnel without a metal hop bottom, for runs taken from different test setups, using the Motorola cathode.

### 3.3.2 90° Hop Funnel PixTech Cathode

Two different types of 90° hop funnels were used with the PixTech cathodes: one with a metal hop bottom and one without. The funnels used in this experiment are the same as used in Section 3.3.1, but with a silver paste metal layer brushed on the hop bottom of half of the funnels. A picture of the funnel is shown in Fig. 3.1a and a diagram of the funnel geometry is shown in Fig. 3.2.

#### 3.3.2.1 No Metal Charge Hop Bottom Electrode

The I-V curves for the 90° funnel without the metal hop bottom are shown in Fig. 3.7 and 3.8. Figure 3.7 shows the ramp-down transition occurring at lower voltages than the ramp-up, which is opposite of what was observed in Fig. 3.5. The consistency of the hysteresis within one setup is also confirmed by Fig. 3.7. Figure 3.8 shows a pretty wide range in the shape of the I-V curves. Figure 3.8b shows almost no hysteresis. The slight differences between the ramp-up and ramp-down, however, are consistent within each curve gathered that day. Figure 3.8c shows a familiar step that was observed in Fig. 3.5 and was repeatable; however this time it occurs during the ramp-down. Figure 3.8a also shows some similarities with Fig. 3.6b and 3.6c, but it should be mentioned that this result was not repeatable.

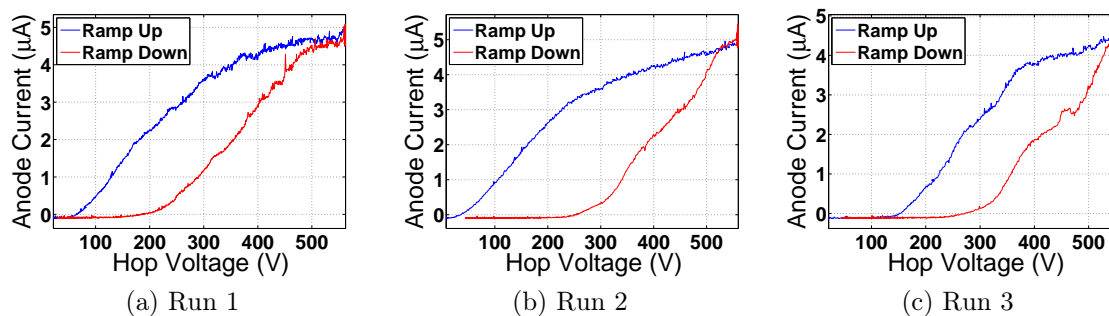


Figure 3.7: Experimental I-V curves obtained from the  $90^\circ$  hop funnel without a metal hop bottom, for runs taken using the same test setup, using the PixTech cathode.

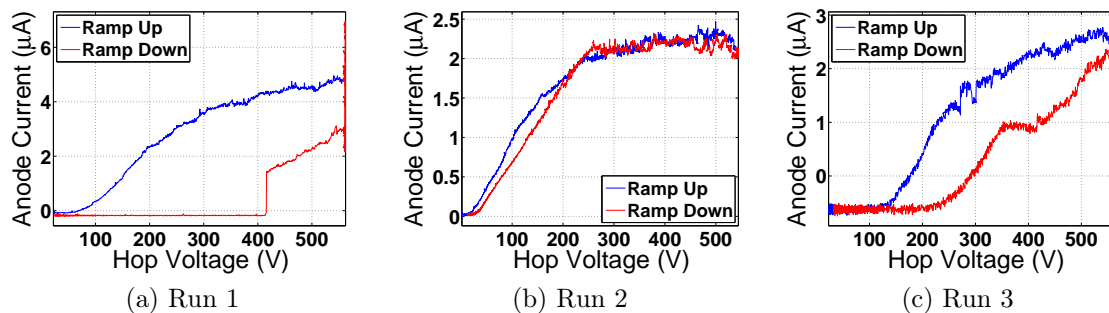


Figure 3.8: Experimental I-V curves obtained from the  $90^\circ$  hop funnel without a metal hop bottom, for runs taken from different test setups, using the PixTech cathode.

### 3.3.2.2 With Metal Hop Bottom Electrode

Figures 3.9 and 3.10 show the I-V curves obtained for the 90° funnel with the metal hop bottom. From Fig. 3.9 and 3.10, it is immediately apparent that the hysteresis is still present. This result indicates that charging on the bottom alone is not the source of hysteresis. There may be some correlation with hysteresis and charging on the bottom, but from the experimental data presented here, no conclusions can be drawn. Some theories derived from the simulations describing how charging on the bottom may affect the I-V curves are presented in Section 4.4.1.

A whole range of I-V curve shapes can be observed from Fig. 3.9 and 3.10, similar to the setup without the metal hop bottom. It can be safe to say that the metal bottom has little effect on the shape of the I-V curve and that the overall shape of the curve is defined by some other mechanism.

Figure 3.9 is a great example of the evolution of the curve on each ramp. The ramp-down I-V curve starts out smooth and slowly evolves a knee. This is typical sort of behavior, and is evidence of unwanted charging of a dielectric.

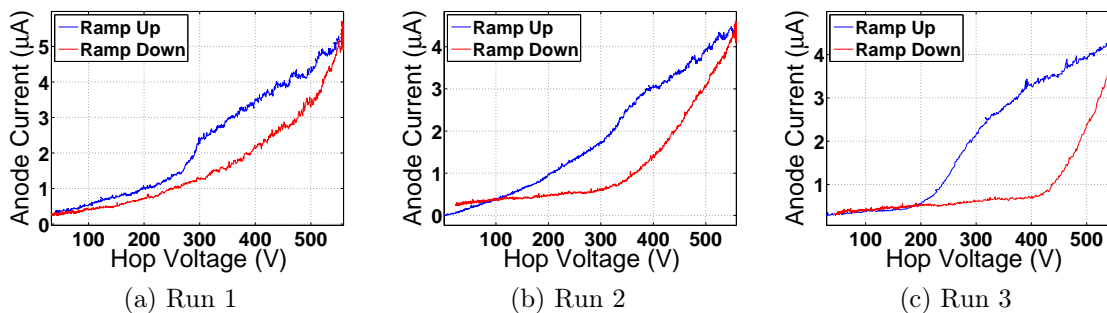


Figure 3.9: Experimental I-V curves obtained from the  $90^\circ$  hop funnel with a metal hop bottom, for runs taken using the same test setup, using the PixTech cathode.

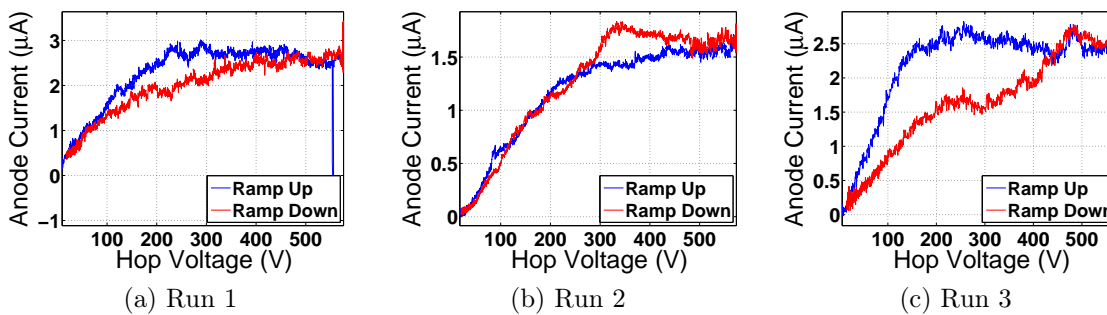


Figure 3.10: Experimental I-V curves obtained from the  $90^\circ$  hop funnel with a metal hop bottom, for runs taken from different test setups, using the PixTech cathode.

### 3.3.3 60° Hop Funnel with/without the Metal Hop Bottom Electrode

The following experiments were performed in one day. For this reason, the plots are all very similar and show no range in results as the previous cases do. These hop funnels were also brand new, and the silver paste was screen printed. The leakage to the hop electrode was virtually non-existent.

#### 3.3.3.1 No Metal Hop Bottom Electrode

The I-V curves for the 60° hop funnel without the metal hop bottom are shown in Fig. 3.11. The I-V curves show a sharp knee on both the ramp-up and ramp-down. A slight evolution of the knee is also present on the ramp-up. The knee gets less and less sharp on each ramp. The ramp-down curve remains fairly consistent.

#### 3.3.3.2 With Metal Hop Bottom Electrode

The I-V curves for the 60° hop funnel with the metal hop bottom are shown in Fig. 3.12. Once again, the metal has little effect on the hysteresis and the curve shape. The I-V curves in Fig. 3.12 show a slight difference from Fig. 3.11 in the unity-gain region but not beyond the experimental error. The evolution of the knee on the ramp-up is present and almost identical to the evolution seen in non-metal hop bottom shown in Fig. 3.11.

The sharp knee in both figures is also significant. This is attributed to the steeper slope of the hop funnel. With a steep slope, the transmission curve should look more like that of a cylinder as found by Hendriks et al. [8], shown in Fig. 2.12.

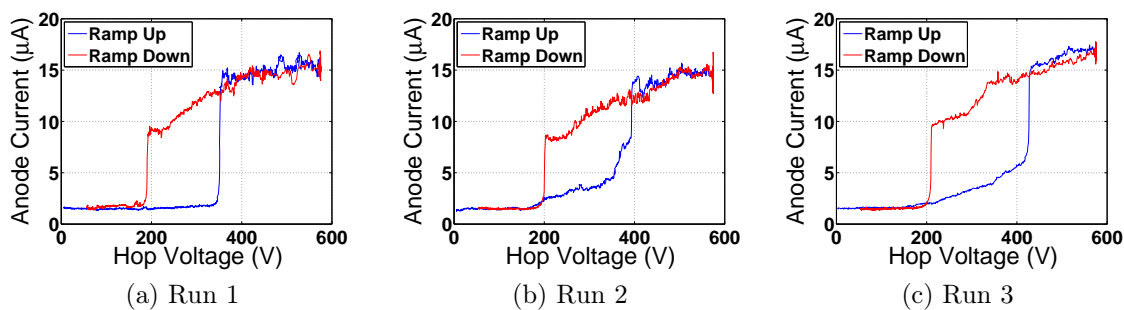


Figure 3.11: Experimental I-V curves obtained from the  $60^\circ$  hop funnel without a metal hop bottom, for runs taken using the same test setup, using the PixTech cathode.

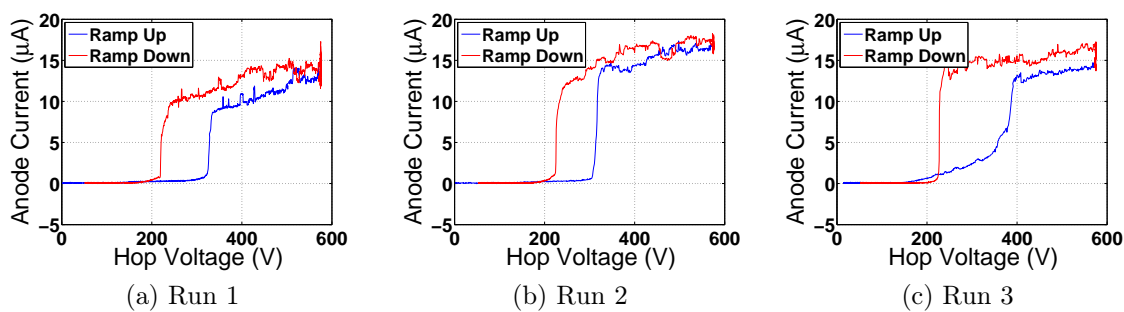


Figure 3.12: Experimental I-V curves obtained from the  $60^\circ$  hop funnel with a metal hop bottom, for runs taken using the same test setup, using the PixTech cathode.

### 3.3.4 Experimental Summary

The experimental results may be summarized as follows:

- The metal hop bottom has little effect on the hysteresis.
- Hysteresis is always observed, even in the cases where it is small.
- Within the same setup, the I-V curve shape is fairly consistent.
- The evolution of the I-V curve may not be a characteristic of the funnel, but is most likely due to unwanted charging of the dielectric on the cathode. More experiments with a cathode with a charge bleed layer need to be performed to confirm this.
- Changing the setup in any way significantly alters the I-V curve.
- The slope of the transition region gets steeper with a steeper funnel angle. More tests are needed to confirm this.

Regardless of the erratic behavior, important observations can be made. One of the main consistencies in the experiment is, ironically, the inconsistency. This is typical with secondary electron emission with too many unknowns. Subtle changes in the initial state of samples can change the results drastically. The purity of the sample and the initial charge on the surface will affect the behavior, not to mention stray current and charging around the active region. Whenever dealing with secondary electron emission, great care in the preservation of the samples, and in the experiment need to be taken in order to get consistent results.

Also, hysteresis in the current was almost always observed. Even in the cases where the hysteresis was minute, “blips” in the current consistently revealed themselves when ramping one way and not the other within the same experiment.

It should also be noted that the hop funnels are expected to be used only in the unity-gain regime. The pFED work [4] demonstrated that when the funnels are only operated in this regime, the results are very consistent.

## CHAPTER 4

### SIMULATION

#### 4.1 Overview

In this section, the I-V characteristics of hop funnels are modeled in Lorentz 2E. Simulations were performed to see the effect of charging on the hop bottom and to see the effect of using a metal hop bottom. To simulate the hysteresis mechanism, a method to simulate a “ramping” of the voltage of the hop electrode was developed and simulated. The electron trajectories, the surface charge of the funnel wall, and the voltage contours were all analyzed to find the cause of hysteresis.

#### 4.2 Lorentz 2E Description

Lorentz 2E version 8 is a two-dimensional serial (it uses one processor core) particle trajectory code developed by Integrated Software [9]. The software allows the user to build the geometry and to simulate and analyze the electric fields and particle trajectories. The geometry is defined by different types of boundaries.

**Emitters:** These are the source of the electron rays. There are many different emission regimes to choose from, but in the assigned current regime the direction, energy, number of rays, and the current can be specified.

**Collectors:** These are boundaries that collect particles upon collision (conductors).

**Reflectors:** These are a simulation boundaries where particles are reflected and electric fields are symmetric. These reflectors are used to simulate symmetric geometries (e.g., rotationally symmetric cylindrical coordinates).

**Secondary Emitters:** These boundaries generate secondary electrons upon collision by a primary electron. The secondary emission characteristics of the boundary are based on the empirical Vaughan Formula [23], shown in Equation 2.7. The user specifies the maximum secondary emission yield,  $\delta_{max}$ , the energy at the maximum yield,  $E_{max}$ , and the average energy of the secondary electron,  $W_{avg}$ . The dependence of the secondary emission yield on the angle of the primary electron is not modeled. The angle of the emitted secondary electrons are not random, but there is an angle dependence. The first secondary electron is emitted normal to the surface; the next two are emitted at an angle of  $\pm 45^\circ$  from the normal.

**Potential Boundary:** These are the boundaries that represent an equipotential surface such as the cathode and hop funnel electrodes

To calculate the electric field, the simulation uses either the boundary element method (BEM), finite element method (FEM), or a hybrid. Fast and accurate field predictions were achieved with the BEM, which is used in this work. As opposed to choosing a two-dimensional grid as in FEM or finite difference methods, the BEM uses elements along the boundaries. Elements along the boundaries of the simulation are chosen to get a desired degree of accuracy in the field predictions. In order to get accurate field predictions, regions that contain corners or turns should contain many elements while regions with slowly varying boundaries can use fewer elements. It should be noted that the surface charge is also modeled on these elements.

The software uses a Runge-Kutta method to calculate the particle trajectories. The options include a constant step 4th order Runge-Kutta (RK4), an adaptive step 5th order Runge-Kutta (RK5), and an adaptive step Bulirsch-Stoer. The RK5 method was used in these simulations. In the RK5 method, each particle trajectory has its own time stepping scheme independent of the other trajectories. Typically, the time steps were in the range of  $1 \times 10^{-11} s - 5 \times 10^{-11} s$ . Depending on where the particle is, a particular time step is automatically altered. Each trajectory is referred to as a ray, and each time step of the ray is referred to as a point.

The emitted rays are created from the emitter boundary. The user specifies the amount of current, the number of rays, and the time step. The surface charge time step is independent of the trajectory time step and is used solely for the calculation of the charge per ray for the surface charge iteration. Each surface charge time step is referred to as an iteration. The charge in each ray is defined by

$$\Delta Q = I \frac{\Delta t}{N} \quad (4.1)$$

where  $\Delta Q$  is the charge per ray,  $I$  is the assigned current per emitter boundary,  $N$  is the number of divisions, and  $\Delta t$  is the iteration time step.

Surface charging is modeled along secondary emitter boundaries. Surface charge is calculated using the same boundary elements used for the electric field calculations. The charge is deposited on each wall element and then interpolated with the neighboring element using a polynomial interpolation. The user specifies the maximum number of iterations, the time step of the iterations, and the convergence criteria. The convergence criteria is related to the relative change in surface charge of the elements. If no convergence is obtained, the simulation iterates only to the maximum

number of iterations. The step size is specified in seconds and determines the charge in each ray.

The surface charge iterative method works as follows:

1. Calculate the electric fields based on the geometry and potential boundaries, including wall surface charge
2. Emit primary electron rays and track the trajectories.
3. Emit and track all secondary ray trajectories, and then all secondary electrons they produce.
  - (a) The energy of the secondary electrons is constant and equal to the estimated average energy ( $W_{avg} = 5 eV$ ).
  - (b) The direction of the emitted secondaries is chosen between  $45^\circ$ ,  $90^\circ$  or  $135^\circ$  from the wall surface.
4. Update the surface charge on the surface charge on the wall elements.
5. Check for convergence.
  - (a) If the surface charge converges or the maximum number of iterations is met, end the simulation
  - (b) If no convergence is met, go to Step 1.

### 4.3 Basic Simulation Setup

The geometry of the hop funnel simulation was generated in Lorentz 2E and is shown in Fig. 4.1. The geometry consists of the FEA, the sloped funnel wall, the hop

electrode, and the collecting anode. The model is cylindrically symmetric, so electrons are reflected at the simulation reflector. The dimensions of the funnel geometry in the simulation are the same as the experiment shown in Fig. 3.2. The thickness of the hop funnel is  $1\text{ mm}$ ; the exit holes radius is  $0.2\text{ mm}$ ; the radius of the funnel entrance is  $1.2\text{ mm}$ ; and the distance from the cathode to the anode is  $2\text{ mm}$ .

### 4.3.1 Field Emitters

The model for the emitters is designed to represent both the emitting nature of the emitting points and the voltage potential created by the gate electrode. Figure 4.2 shows a diagram of the emitter geometry.

The emitters are modeled by small arc bumps on the boundary. Each of the bumps are emitting boundaries and emit particles normal to the arc. The gate is modeled by the boundary below the emitters. This boundary is defined as both a collector and a potential boundary. The potential of the gate boundary would match the voltage needed to be applied to cause emission on the array. For the PixTech cathodes, a voltage of  $65\text{ V}$  is close to what was used in the experiment and is applied to the gate boundary. The energy of the emitted rays is  $55\text{ eV}$ .

Field emission, using the Fowler Nordheim equation, is a phenomenon that could be modeled in the simulation, but is unnecessary. The computations needed to perform this would further increase the simulation time with minimal, if any, gains. Also, given the nature of any FEA and its variation of field tips, the Fowler Nordheim scheme poorly models the FEA anyway. From experimental data gathered about the emitted electrons of FEAs, a better model uses a distribution of emitted angles. To simplify this even further, the energy of all electron rays are emitted near the gate voltage

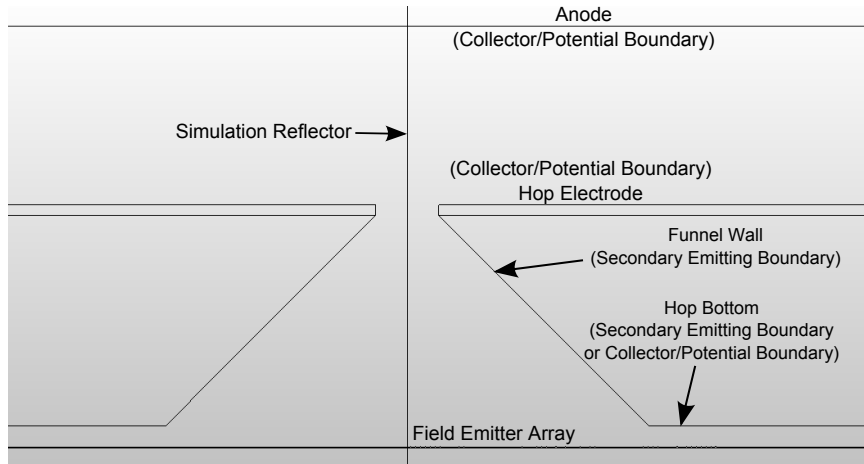


Figure 4.1: Hop funnel geometry created in Lorentz 2E used for all simulations.

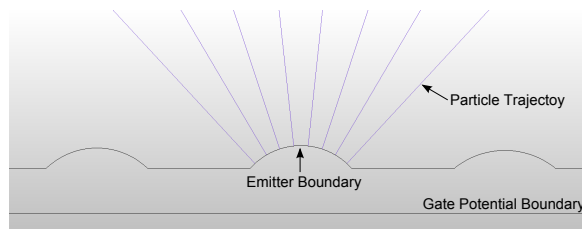


Figure 4.2: A close up on the boundaries modeling the FEA for the Lorentz 2E simulations.

To get a stable and accurate simulation, the correct number of rays and charge per ray needs to be chosen for the emitter boundary. Much analysis on simulation parameters were performed by Lester et al. [6] to find a balance between simulation time and accuracy as explained in Section 2.6.2. The parameters chosen for this work are the same as chosen in that reference.

**Time Step:**  $5 \mu s$

**Total Number of Rays:** 192

**Total Current:**  $1 \mu A$

Using Equation (4.1), the charge per ray would be  $2.6 \times 10^{-14} C$ . 192 rays also gives a sufficient spread of electrons across the funnel. It should be noted that Lester et al., along with the findings in this simulation, found that with these parameters, the surface charge along the funnel wall yields widely varying values from segment to segment. This variation is undesirable, but in order to decrease this effect, the number of rays must be increased dramatically, at least 10 times, and the simulation time increases by the same order. Even with this widely varying surface charge, however, the simulations in their experiment and the ones in this thesis, matched experimental results. This suggests that the surface charge “oscillations” are centered about the correct value.

It should also be noted that the emitted beam is not uniform. The emission rays are uniformly distributed when viewing the model in two-dimensions, but when accounting for the rotational symmetry, the beam current is denser in the center. This is not desirable, but this implementation will keep the model simpler.

### 4.3.2 Secondary Electron Boundaries

The secondary electron boundaries include all of the insulating boundaries of the funnel. The secondary electron characteristics of the material are unknown; hence the secondary parameters,  $\delta_{max}$  and  $E_{max}$ , are somewhat arbitrary. Lester et al. found that the behavior of the hop funnel simulation was closely related to the 1st crossover point of the secondary electron curve. In fact, there is a continuum of  $\delta_{max}$  and  $E_{max}$  values that give the same first crossover point and also yield the same I-V curve. Two different sets of parameters are used in this thesis:  $\delta_{max} = 2$ ,  $E_{max} = 500 \text{ eV}$  and  $\delta_{max} = 2$ ,  $E_{max} = 300 \text{ eV}$ . These parameters correspond to first crossovers of  $70 \text{ eV}$  and  $40 \text{ eV}$ , respectively.

The number of elements on the secondary electron boundaries has to be sufficient to allow secondary electrons to “hop” to an adjacent segment. If secondary electrons are not allowed to hop to another segment, “overcharging” of the segments can occur. Since the charge in each ray is fairly high, one “stationary” secondary electron can have drastic effects on the charging of the funnel wall. In the funnel region, 300 segments yields a segment length slightly smaller than the minimum hopping length; therefore 300 segments were chosen for the simulations.

### 4.3.3 Electrodes

The electrodes in the simulation are both collector and potential boundaries, and these electrodes create the electric fields and collect the current. No secondary electrons are generated at the electrodes.

**Anode:** The anode’s voltage was chosen to allow a sufficient electric field in the interaction region. The voltage was chosen to be at least  $100 \text{ V}$  higher than the

hop electrode at all voltages tested, which is 850  $V$  for most simulations. Some hop voltages exceeded 850  $V$  and the anode potential was modified in those cases to keep the 100  $V$  difference from the hop electrode.

**Hop Electrode:** The goal of the simulation is to find the relationship between the voltage on the hop electrode and the exit current. The voltage on the hop electrode varies from 0  $V$  to 1000  $V$ .

**Gate:** To simulate the potential applied to the gate electrode on the FEA, 55  $V$  is applied to the gate boundary.

**Hop Bottom:** In some simulations, a metal hop bottom electrode was used. The potential on the electrode is set to the gate potential, 55  $V$ , in order to minimize the field effects created by the electrode and to match the experiment.

#### 4.3.4 Simulation Stability

##### 4.3.4.1 Surface Charge Stability

The surface charge convergence criteria depends on the relative surface charge change. This value is set to  $1 \times 10^{-7}$ , which is a very strict criteria. Values lower than this give many false convergences. With the strict convergence criteria, the surface charge of the secondary emitting funnel wall rarely converges in the simulation setup. To get a balance between speed and accuracy, the charge per ray is large. If charge from one ray is deposited or removed from the section, the convergence criteria will not be met because of the large charge per ray. The only time the surface charge iteration converges is when no charge is deposited on the wall. Even without meeting the surface charge convergence criteria, steady-state can still be achieved. During

steady-state, the surface charge may be rapidly changing, but the average surface charge on the wall will remain constant. This is what is defined as steady-state.

#### 4.3.4.2 Steady-State Current

The variation of the current on the anode is what is mainly used to determine when the simulation has reached steady-state. The current of each iteration is determined by the number of rays hitting the anode. With the total current,  $I = 1 \mu A$ , and the total number of rays,  $N = 192$ , the current per ray is  $I_{ray} = I/N = 5.2 nA$ . The current cannot be monitored while the simulation is running, so to reach steady-state the user must estimate and implement the maximum number of iterations needed. The initial behavior of a simulation run is a changing trend in the current due to the initial charging of the wall. The end behavior is an oscillation about an average current. Figure 2.15 shows general current vs. time curves of the hop funnel simulation.

The number of iterations needed to get to steady-state depend on the initial conditions of the simulation. It depends on how much charging of the walls is needed to reach steady-state. With no initial surface charge on the walls, as done by Lester et al., the number of iterations needed are quite high ( $> 300$  iterations with  $\Delta t = 5 \mu s$ ). With an initial surface charge on the walls close to the one needed for steady-state, fewer iterations are needed to reach steady-state. This is because the initial charge on the walls is relatively close to the steady-state charge, thus less charging time is needed. This approach is used in the “ramping” simulations done here.

#### 4.3.4.3 Convergence Criteria

Typically, the convergence is defined by the user via the maximum number of iterations. The surface charge along the surface of the funnel may be rapidly changing,

but the average charge throughout the funnel will be stable and as result the current will be stable on the anode. The stability of the current on the anode is what is used as the reference of steady-state.

#### **4.3.5 Data Interpretation**

To create the I-V curves, the anode current must be read in from multiple simulations. First, the anode current from one simulation is read in for each iteration. Since the current is somewhat noisy, the anode current is averaged over the last 25% of the emissions. A stable anode current for all the simulations is observed no later than the last 25% of the iterations. The anode current is read in from all simulations in this way and plotted against the hop voltage.

### **4.4 Metal Hop Bottom Electrode Simulation**

Initially, it was thought that charging on the hop bottom could be the source of hysteresis in the I-V curves. As shown in Section 3.3, experiments were performed to test this theory. While these experiments were being performed, simulations were implemented to see the effect on adding a metal electrode on the hop bottom. These simulations wouldn't explain the source of the hysteresis but would give insight into the trajectories.

Experimentally, the precision on the point of emission is limited, and most likely emitters under the hop bottom are being turned on. The emitter "bumps" were extended underneath the hop bottom to recreate this situation, and two different simulations were run: one with a metal hop bottom and one without. The goal of

these simulations is to find out how charging on the hop bottom modifies the I-V curve. The procedure to gather the I-V curves was as follows:

1. Set the voltage on the hop electrode.
2. Launch the trajectories with an uncharged hop funnel surface until steady-state.
3. Output the anode current.
4. Repeat Steps 1 - 3 to get the desired data points on the I-V curve.

With the initial condition of the uncharged surface, the charging times are relatively long. The number of iterations to reach steady-state was from 300 to 600 iterations, depending on the particular voltage step. Each hop voltage simulation took about 20 hours to reach steady-state on a Intel Xeon w3530 4-core 2.9 GHz machine. The software is a serial code and only utilizes one core.

#### 4.4.1 Results

Figure 4.3 shows the Lorentz simulated I-V curves with and without metal on the hop bottom. The metal hop bottom slightly shifts the I-V curve to the left. Another way to think of it is that by introducing emitters under the non-metal hop bottom, the I-V curve is shifted left. By emitting electrons into the hop bottom, the corner near the entrance of the funnel charges negatively, thereby disrupting any hopping trajectories that would be there otherwise. Figure 4.4 shows the steady-state trajectories of both cases with  $V_{hop} = 650 V$ . The plotted trajectories are from the last iteration of the simulation and are representative of the steady-state. The bulge in Fig. 4.4a is caused by the charge deposited there and on the hop bottom from the previous iterations.

Figure 4.4b shows no bulge because the metal hop bottom allows the charge deposited on the hop bottom to bleed away.

As found from the experiments, charging on the bottom is not the source of hysteresis. The simulations performed here show that charging on the bottom will shift the I-V curve to the right, the general shape being maintained. To find the source of the hysteresis, a virtual “ramping” of the voltage must be modeled.

## 4.5 Ramping Simulation

The software was designed to find steady-state responses to static inputs. The software iterates through many surface charge time steps in order to get the steady-state surface charge, but simulating a changing voltage is not an inherent function. To simulate a “ramp-up” of the voltage, discrete simulations were performed with the initial condition being the steady-state conditions of the previous simulation. One assumption was made: the changing voltage in the experiment is much slower (600 V in 20 s) than the time for the current to reach steady-state for each voltage ( $< 5$  ms). The procedure to ramp the voltage is shown below.

1. Initial uncharged wall simulation at either  $V_{hop} = 0$  V or  $V_{hop} = 650$  V.
2. After the anode current reaches a relative steady-state, save the wall surface charge and dump the trajectory data to a file.
3. Increment the hop voltage to the new value.
4. Import the surface charge from the previous voltage simulation.
5. Run the simulation with the new voltage and the surface charge from the previous step.

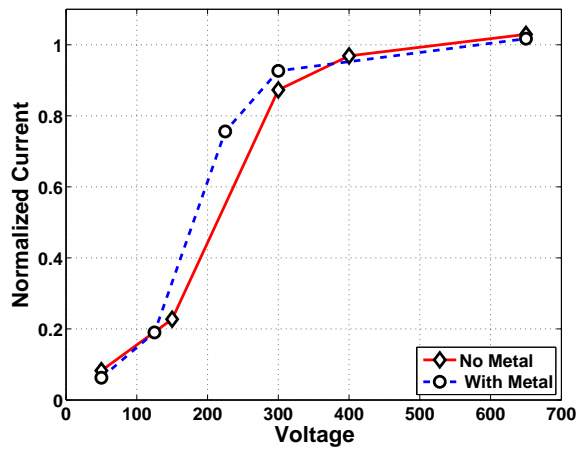


Figure 4.3: Simulated I-V curves with and without a metal hop bottom.

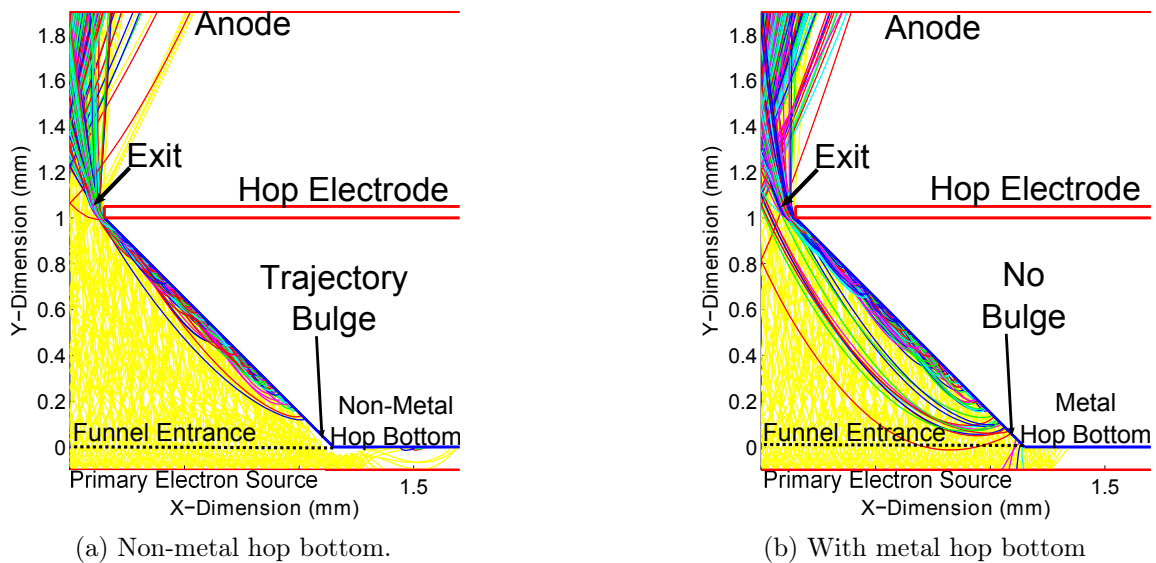


Figure 4.4: The steady-state trajectories using a metal and a non-metal hop bottom. Primary electron trajectories emitted from the FEA are shown in yellow, and secondary electron trajectories are shown in the other colors. (a) Non-metal hop bottom shows a bulge in the trajectories along the wall at the funnel entrance caused by charging of the hop bottom. (b) Metal hop bottom shows no bulge because charge on the hop bottom is “bleed” away.

6. Repeat Steps 2–5 for the desired voltage ramp.

Three test cases were simulated. All the simulations used a  $90^\circ$  hop funnel. A ramp-up-down-up procedure was performed for funnels with  $\delta_{max} = 2$  and  $E_{max} = 300\text{ eV}$ , and  $\delta_{max} = 2$  and  $E_{max} = 500\text{ eV}$ . These SEY characteristics correspond to a  $40\text{ eV}$  and  $70\text{ eV}$  first crossover points, respectively. Also, a ramp-down-up procedure was performed on the  $40\text{ eV}$  first crossover funnel. All the “ramping” simulations used a non-metal hop bottom. Table 4.1 shows a summary of all the ramping simulations

To obtain realistic results in a reasonable time, the voltage step size must be chosen. For the fastest results, the maximum step size that produced accurate results was chosen. This choice was difficult to make, and a study was done as described in Section 4.5.1 to determine the best step size.

#### 4.5.1 Voltage Step Stability

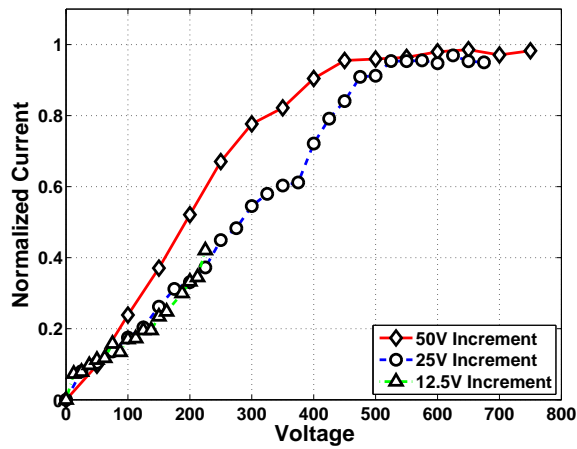
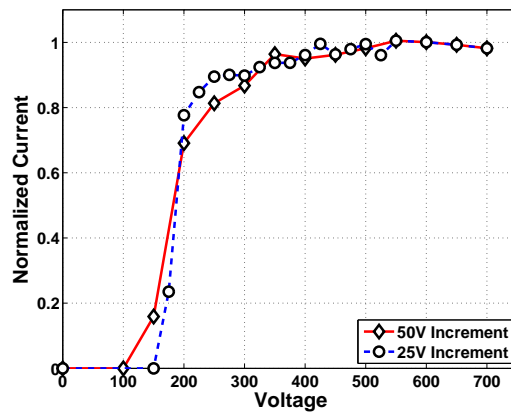
By using discrete voltage step sizes, a certain degree of error is introduced in the simulation. To minimize the error, the smallest step size possible should be used. To minimize simulation time, the largest step size should be used. In order to determine the step size, many different ramps were performed with varying step sizes. The simulated I-V curves with varying step sizes for both the ramp-up and ramp-down are shown in Fig. 4.5 and 4.6. The secondary characteristics of the material are  $\delta_{max} = 2$  and  $E_{max} = 300\text{ eV}$  corresponding to the  $40\text{ eV}$  crossover.

For the ramp-up case in Fig. 4.5, distinct differences can be seen in the  $50\text{ V}$  and  $25\text{ V}$  I-V curves but not between the  $25\text{ V}$  and  $12.5\text{ V}$  cases. The  $25\text{ V}$  step size seems like a good choice for minimizing the error while maximizing performance time.

For the ramp-down case shown in Fig. 4.6, the  $50\text{ V}$  and  $25\text{ V}$  increments seem to match fairly well. Of course, the transition region occurs over a  $100\text{ V}$  range, and

Table 4.1: Summary of ramping simulations performed.

Name	First Crossover	$\delta_{max}$	$E_{pmax}$	Ramp 1	Ramp 2	Ramp 3
Case 1	40 eV	2	300 eV	Up First	Down	Back Up
Case 2	40 eV	2	300 eV	Down First	Up	N/A
Case 3	70 eV	2	500 eV	Up First	Down	Back Up

Figure 4.5: Ramp-up I-V curves with varying voltage step sizes of a hop funnel with  $\delta_{max} = 2$  and  $E_{max} = 300 eV$ .Figure 4.6: Ramp-down I-V curves with varying voltage step sizes of a hop funnel with  $\delta_{max} = 2$  and  $E_{max} = 300 eV$ .

50 V does not resolve this region very well, so a 25 V step size should be used in this region. From these results, a 25 V step size is the best choice for the cases tested here. One should note that for materials with different secondary electron characteristics, a different maximum step size could be used. Because of time, many I-V curves presented here still used 50 V step sizes. This undoubtedly introduces some error to the curve; however the general shape of the curve is maintained, and the hysteresis is still visible. The I-V curves may be skewed by this step size, but the mechanisms behind the hysteresis are maintained.

#### 4.5.2 Simulation Results for Case 1

The secondary emission characteristics of the first funnel simulated were  $\delta_{max} = 2$  and  $E_{max} = 300 \text{ eV}$ , which corresponds to a 40 eV first crossover. Starting at  $V_{hop} = 0 \text{ V}$ , the voltage was ramped up to unity-gain, then ramped down to zero-transmission, and then back up again. The results are shown in Fig 4.7. The hysteresis is apparent.

##### 4.5.2.1 Case 1 Ramp-up Explanation

On the first ramp-up, the I-V curve looks fairly linear until full transmission (unity-gain) is reached. To visualize this effect, the electron trajectories and voltage contours are shown in Fig. 4.8. There are two mechanisms that define this behavior. One mechanism is the wall surface charging negatively on each increment of the hop voltage. On each step, the energies of the primary electrons hitting the wall are below the first crossover; therefore the wall charges negatively to the point where no electrons hit the walls. By incrementing the voltage for the next step, the initial surface charge restricts the energies of the primary electrons to below the first crossover, so the wall charges even more negatively. This mechanism, by itself, would continually charge

the wall more and more negatively, preventing unity electron transport from taking place. This mechanism is counteracted by the electric field penetration through the funnel exit.

As the hop voltage is increased from  $0\text{ V}$  to  $50\text{ V}$ , the electric field penetrates the funnel opening enough to allow some of the primary electrons through. This result can be seen in Fig. 4.8a where the trajectories of the simulated rays for the first step are plotted. The wall still charges negatively, and electron transport occurs nowhere along the walls. The next step, the electric field penetrates enough to cause electron transport to take place along the funnel wall immediately near the exit, and a linear variation is observed in the anode current. For each subsequent increment in hop voltage, the electric field penetrates the funnel exit farther, causing electron transport to take place farther and farther down the funnel incrementally.

The voltage contour plots in Fig. 4.8 show how the field penetrates through the exit of the funnel and the corresponding electron trajectories. These voltage contours were gathered before the first iteration at each voltage step ( i.e., the surface charge of the previous voltage step and the hop voltage of the current step). The contours represent the initial voltage distribution of the voltage step. The trajectories are at steady-state of the corresponding voltage step. Figure 4.8e shows a good example of the effect of the negatively charged wall. This region of negatively charged space is referred to here as the “charge sink” region. This region forms an electric field that prevents electrons from hitting the wall at an energy above the first crossover. The effect of the charge sink barrier can be seen by the corresponding trajectories shown in Fig. 4.8b. At the highest voltage of the ramp-up, the charge sink region is virtually non-existent in Fig. 4.8f, and secondary electron transport takes place on almost all of the wall except for near the funnel entrance.

The point at which electron hopping transport takes place is determined by the  $50\text{ V}$  contour line. To show this correlation, Fig. 4.9a shows the point along the funnel wall that intersects with the  $50\text{ V}$  contour line as a function of hop voltage, and Fig. 4.9b shows the point along the wall at which secondary electron transport takes place as a function of hop voltage.

As the hop voltage is increased, the  $50\text{ V}$  contour line moves linearly down the funnel wall. As the  $50\text{ V}$  contour moves, the secondary electron transport point follows. The initial electron energy of the primary electron is  $55\text{ eV}$ , which is emitted from a  $65\text{ V}$  potential. As the electron moves from  $65\text{ V}$  to the  $50\text{ V}$  contour,  $15\text{ eV}$  of energy is lost. The resulting energy is  $40\text{ eV}$ , which corresponds the first crossover of the secondary electron yield curve. For secondary electron transport to take place, the initial energies of the incoming electrons need to be above the first crossover; otherwise the wall will charge negatively, repelling any other incoming electrons. As this critical voltage contour moves down the wall, electrons with energies above the first crossover collide with that region of the wall, and secondary electron transport begins to take place in that region.

As secondary electron transport commences, that particular region of the wall starts to charge less negatively. Figure 4.10 shows the surface charge density along the funnel wall at different simulated hop voltage steps. Since there is a lot of noise in the surface charge density data, the plot shows a moving average of the simulated points along the wall to smooth the noise. Also, as the funnel wall joins the hop electrode, the charge on the funnel wall starts to deviate in order to match the boundary condition at this point. This portion of the funnel wall immediately near the exit swamps the rest of that data and is, therefore, cut out to reveal the important features.

The flat, slowly negative sloping region labeled “No Transport Region” shows the

portion of the wall in which secondary electron transport is not taking place. The “jagged” portion labeled “Transport Region” shows regions where secondary electron transport is taking place. Anywhere there is no electron transport, the wall continues to charge negatively as the hop voltage is raised, which counteracts the gain in hop voltage. As the electric field penetrates the funnel, the surface charge shows a ridge labeled “Transport Boundary,” where it sharply charges less negatively. The ridge slowly moves down the funnel wall due to the  $50V$  contour line moving down the funnel as the hop voltage is increased. The transport boundary almost makes it all the way down the wall except for the region near the entrance. The electron transport region of the surface charge plot also shows a slow negatively sloping curve along the hop voltage axis. This negative slope is the self-regulating mechanism to keep the SEY characteristics of that portion of the wall at unity. This sudden surface charge change at the transport boundary puts that region of the wall into a new “state.” With electron transport occurring along the wall, it becomes more difficult to stop the mechanism, as is observed during the following ramp-down, shown in Section 4.5.2.2.

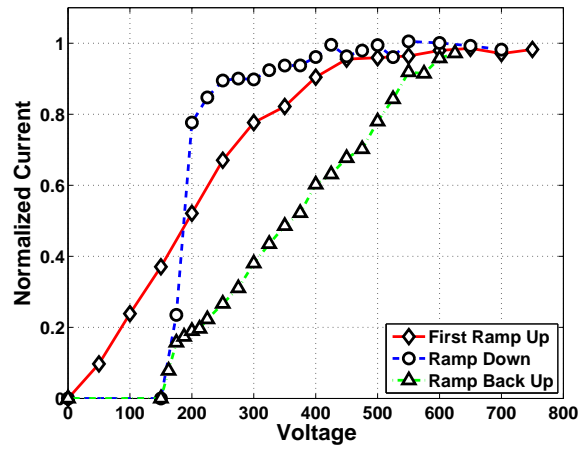


Figure 4.7: Simulated I-V curves for Case 1 showing a full ramp-up, down, and then back up procedure for  $\delta_{max} = 2$  and  $E_{max} = 300 eV$  ( $40 eV$  first crossover).

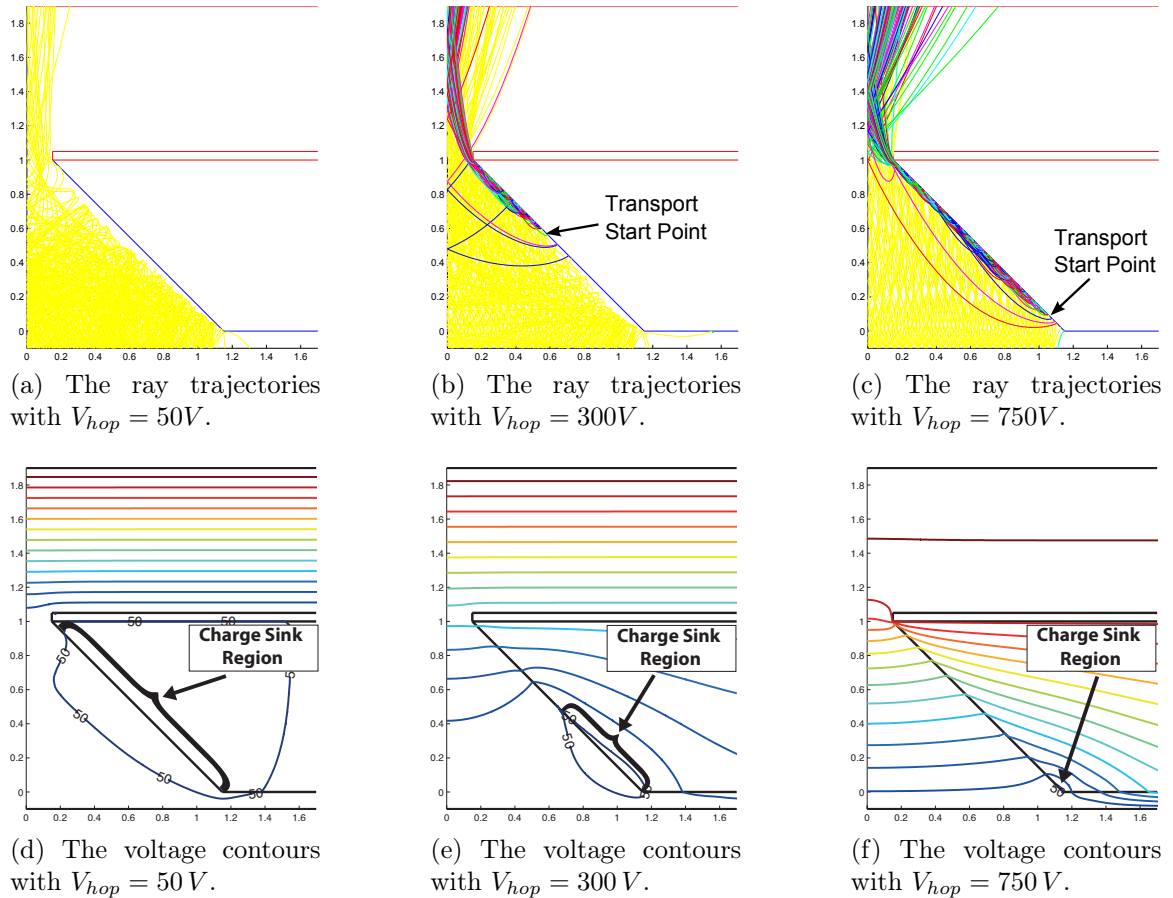


Figure 4.8: Plots of the steady-state electron ray trajectories and the corresponding initial condition voltage contour plots for a range of hop voltages for Case 1 ( $40 eV$  first crossover) ramp-up-first. The primary rays emitted from the FEA are yellow and the secondary rays are shown in the other colors.

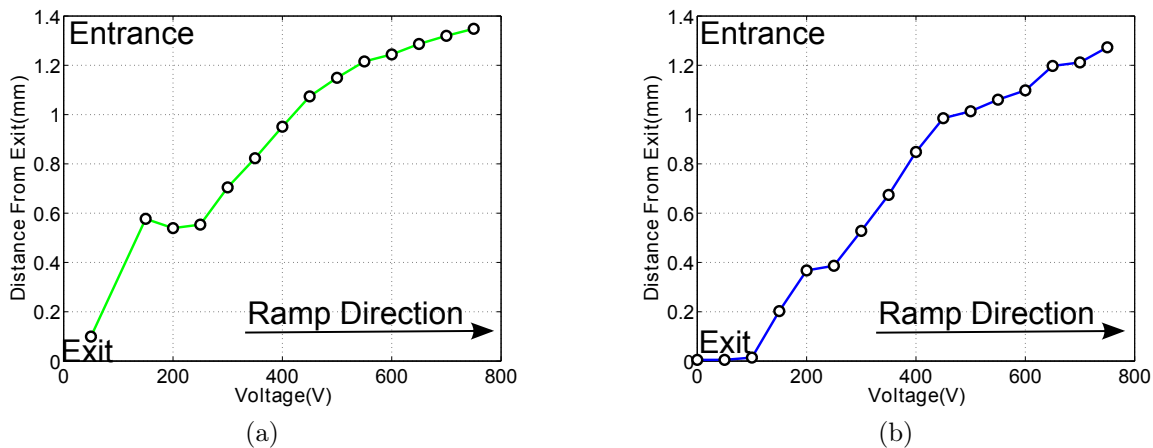


Figure 4.9: (a) Distance from the funnel exit of the point at which the 50 V voltage contour line intersects the funnel wall, and (b) the point at which electron transport begins to take place along the funnel wall for Case 1 (40 eV first crossover) ramp-up-first.

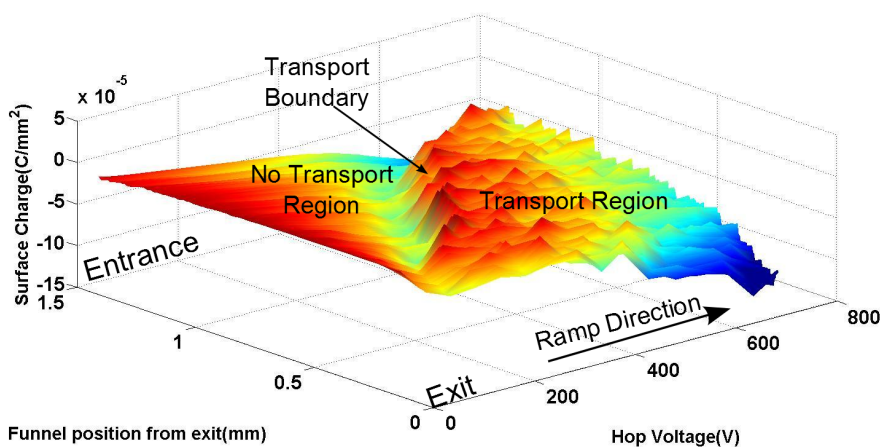


Figure 4.10: Surface charge density along the funnel wall vs. the hop voltage during the ramp-up-first for Case 1 (40 eV first crossover).

#### 4.5.2.2 Case 1 Ramp-Down Explanation

The ramp-down in Fig. 4.7 shows a “knee” occurring at around  $200\text{ V}$ . This knee is commonly observed in the experimental results as shown in Figs. 3.5, 3.11, and 3.12. To explain this behavior, the trajectories along with the corresponding voltage contours are shown in Fig. 4.11.

As the hop voltage is decreased, secondary electron transport continues to take place along the majority of the wall except for a region near the funnel entrance. This local charge sink region was left behind during the last voltage step of the ramp-up. By lowering the voltage, there is no way to remove this charge, and it will remain there for the entire ramp-down. As the hop voltage is lowered, the effect of the charge sink region slowly becomes more apparent, but has little effect on the movement of the  $50\text{ V}$  contour until a threshold.

The movement along the wall of the  $50\text{ V}$  contour and where secondary transport occurs is shown in Fig. 4.12. The  $50\text{ V}$  contour point slowly moves up the funnel wall as the hop voltage is decreased until around  $200\text{ V}$ , where it moves up the funnel rapidly. The correlation between the where secondary electron transport takes place and the  $50\text{ V}$  contour line is almost identical. The secondary electron transport moves about same magnitude as the  $50\text{ V}$  contour moves for all the curve except at  $175\text{ V}$ . At this point, the transport point moves up the funnel, past the  $50\text{ V}$  contour point of the initial condition.

The slow movement of the transport point is due to the movement of the  $50\text{ V}$  contour line, as seen in the ramp-up, but the sudden movement at  $175\text{ V}$  is from a different mechanism. At each decrement in hop voltage from  $525\text{ V}$  to  $200\text{ V}$ , the  $50\text{ V}$  contour line moves up the funnel slightly. The voltage gradient in the center

of the funnel and above the  $50 V$  contour is decreased, but it maintains a gradient sufficient to pull the secondary electrons up the funnel to gain at least  $40 eV$  of energy. The critical voltage step from  $200 V$  to  $175 V$  is when the gradient becomes insufficient. This is the point at which the majority of the negative charging along the wall occurs. Secondary electrons travel laterally across the funnel, are then reflected by the simulation reflector, and land very close to where they were created. Little energy is gained during this trajectory and the electrons deposit their charge. This large negative charging causes the movement of the hopping transport point up the funnel wall and is much greater than the initial movement of the  $50 V$  contour.

The surface charge density plot shown in Fig. 4.13 shows this sudden transition to the negative charging of the wall. The surface charge plot also shows how regions sustaining secondary hopping transport allow for a positive charging of that region during the ramp-down. This charging counteracts the lowering of the hop voltage. To maintain unity in these transport regions, the self-regulating nature of hopping transport charges the wall less negatively, and prevents current transmission loss. The transport boundary moves slowly up the funnel wall with the  $50 V$  contour until the knee. This negative charging caused by the weak electric field puts the funnel in a new “state.” Hopping transport is no longer taking place, and it becomes difficult to restart hopping transport because of the “new” negative charge deposited. This can be seen by the following ramp-up.

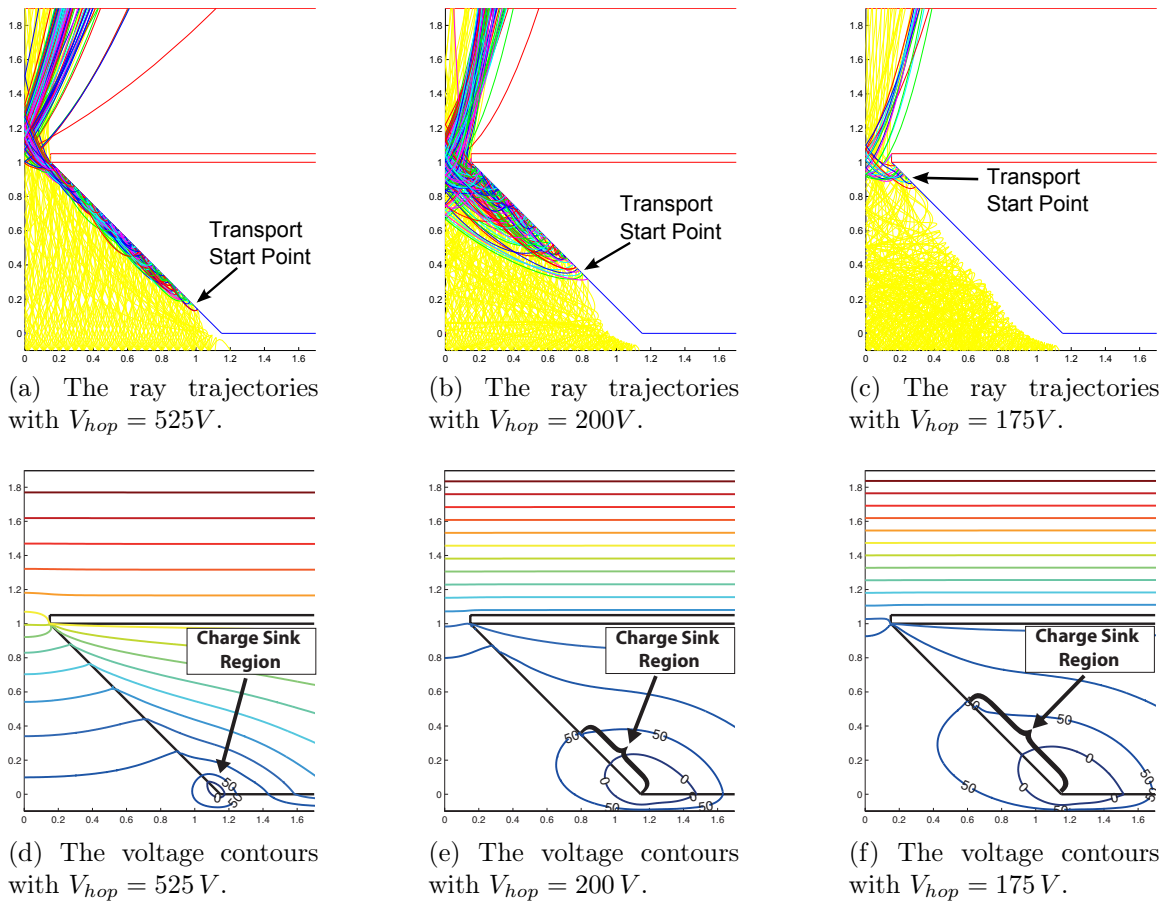


Figure 4.11: Simulations of the ray trajectories and the corresponding voltage contour plots for a range of hop voltages for Case 1 (40 eV first crossover) ramp-down. The primary rays are yellow and the secondary rays are shown in the other colors.

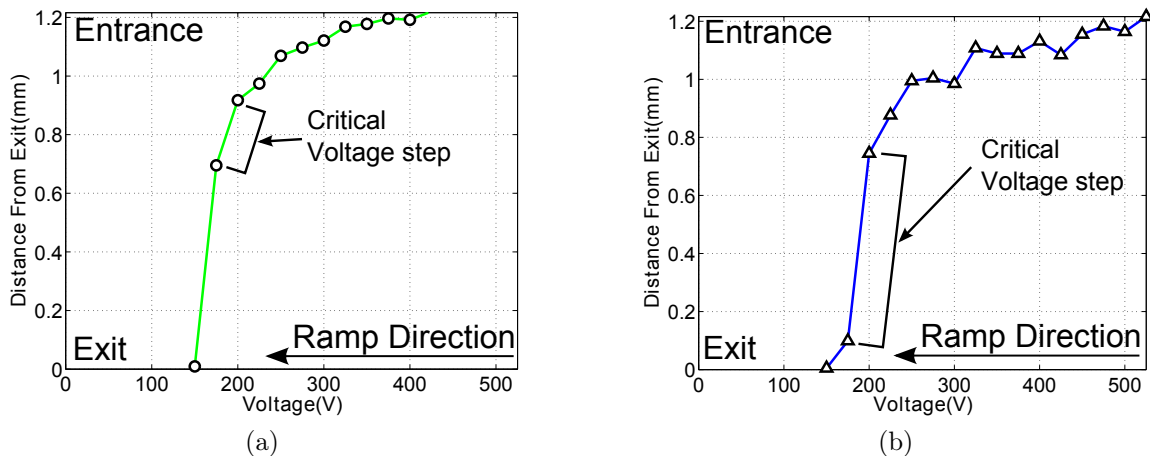


Figure 4.12: (a) The point at which the 50 V voltage contour line intersects the funnel wall, and (b) the point at which electron transport begins to take place along the funnel wall for Case 1 (40 eV first crossover) ramp-down

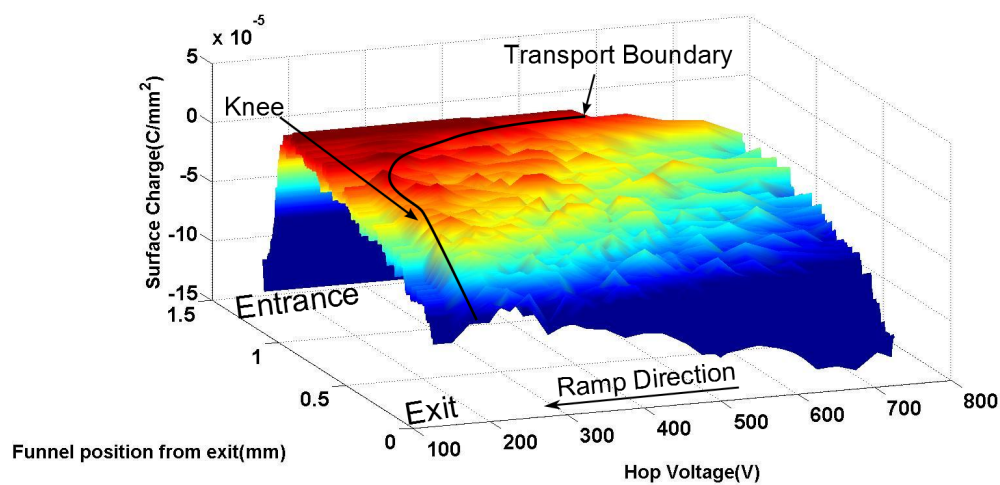


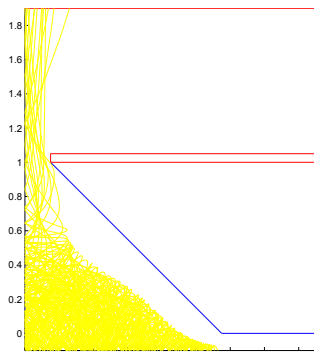
Figure 4.13: Surface charge density along the funnel wall vs. the hop voltage during the ramp-down for Case 1 (40 eV first crossover).

### 4.5.2.3 Case 1 Ramp-Back-Up Explanation

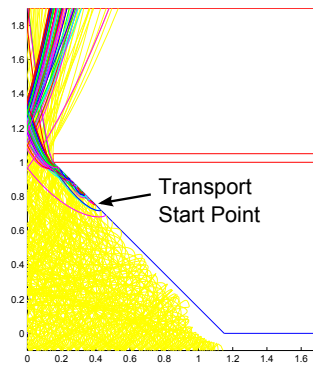
Similar to the first ramp-up, the I-V curve on this ramp is linear for the most part, but the curve is shifted to a higher voltage and has a sharp initial increase in current at the beginning of the ramp. The sharp increase is caused by some of the primary electrons starting to exit all at once. The slope thereafter is defined by the electric field penetrating the funnel. The difference from the first ramp-up is that now the funnel wall is already charged. The ray trajectories and voltage contours are shown in Fig. 4.14.

The movement of the 50 V contour line and the hopping transport point are shown in Fig. 4.15. The behavior of the hopping transport point is completely defined by the movement of 50 V voltage contour.

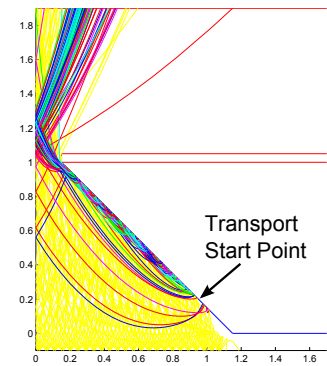
The surface charge density plot shown in Fig. 4.16 shows the similar “ridge” observed during the first ramp-up in Fig. 4.16, but the ridge in this case seems like more of a valley. The 40 V contour line precedes the 50 V contour line when going down the funnel. The 40 V contour allows electrons to hit the wall, but at an energy lower than the first crossover, thus, charging that region negatively. The next voltage step, the 50 V contour moves to that region, and allows electrons with energies greater than the first crossover. This initiates secondary electron transport in that region, and the region charges less negatively.



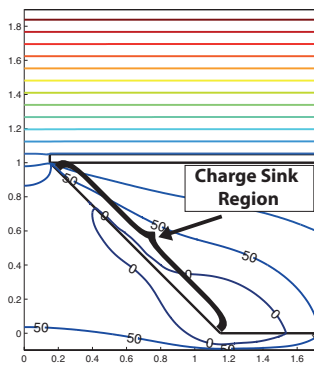
(a) The ray trajectories with  $V_{hop} = 162V$ .



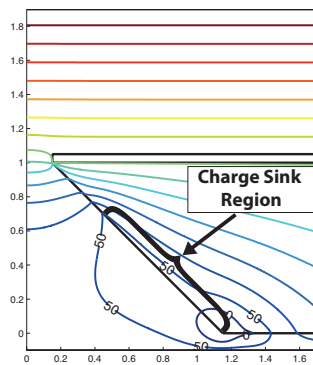
(b) The ray trajectories with  $V_{hop} = 400V$ .



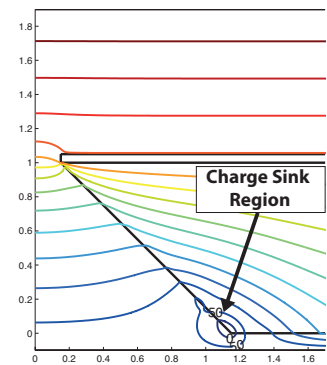
(c) The ray trajectories with  $V_{hop} = 625V$ .



(d) The voltage contours with  $V_{hop} = 162V$ .



(e) The voltage contours with  $V_{hop} = 400V$ .



(f) The voltage contours with  $V_{hop} = 625V$ .

Figure 4.14: Simulations of the ray trajectories and the corresponding voltage contour plots for a range of hop voltages for Case 1 ( $40 eV$  first crossover) ramp-back-up. The primary rays are yellow and the secondary rays are shown in the other colors.

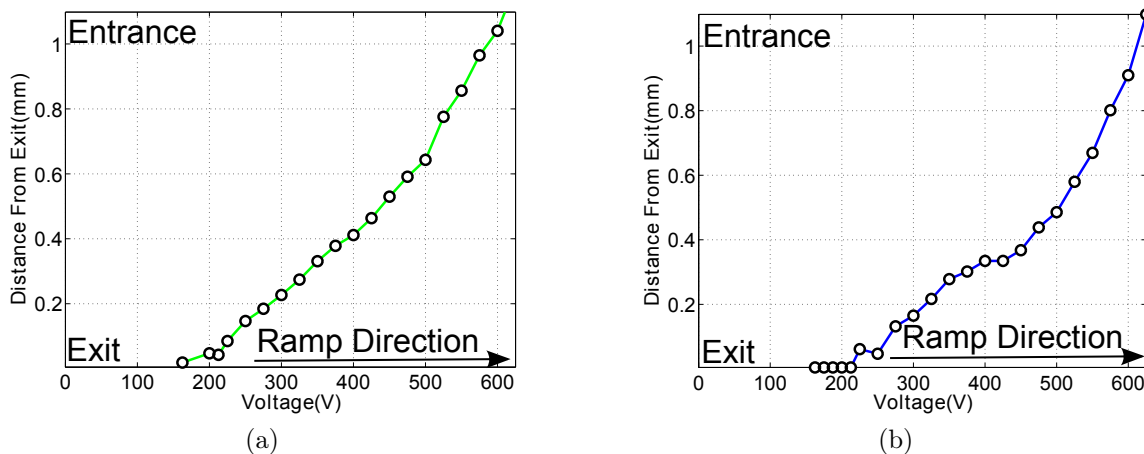


Figure 4.15: (a) The point at which the 50 V voltage contour line intersects the funnel wall, and (b) the point at which electron transport begins to take place along the funnel wall for Case 1 (40 eV first crossover) ramp-back-up..

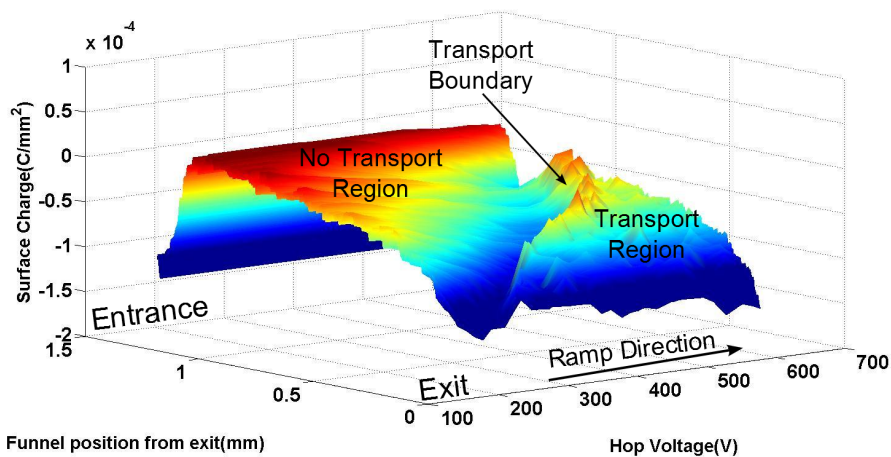


Figure 4.16: Surface charge density along the funnel wall vs. the hop voltage during the ramp-back-up for Case 1 (40 eV first crossover).

### 4.5.3 Simulation Results for Case 2

To initiate the experiments, the current is emitted through the funnel with the hop voltage at the maximum as described by the procedure in Section 3.2.5. To model this in the simulation, the hop voltage is initiated to  $650\text{ V}$  and ramped down first. The I-V curves are shown in Fig. 4.17. The behavior resembles the ramp-down and ramp-back-up behavior of Fig. 4.7 except the transition region during the ramp-down is much sharper and occurs at a lower voltage.

#### 4.5.3.1 Case 2 Ramp-Down Explanation

Figure 4.18 shows the electron ray trajectories along with the corresponding voltage contours. Electron transport takes place on almost all of the wall until a hop voltage of  $125\text{ V}$ . The critical voltage is at  $V_{hop} = 100\text{ V}$ , where almost all of the current is lost. The voltage contour plots from  $V_{hop} = 125\text{ V}$  to  $V_{hop} = 100\text{ V}$  shown in Fig. 4.18e and 4.18f look very similar. The change in the shape of the contours is minimal; however this step is when the critical voltage occurs.

The voltage contour gradient shown in Fig. 4.18e is very weak and produces the steady-state trajectories shown in Fig. 4.18b. The weak gradient produces very long hopping trajectories, but is still able to sustain electron transport. By lowering the voltage one more step, the gradient decreases even more as shown in Fig 4.18f, and the trajectories are no longer pulled up the funnel very far. The secondary electrons travel across the funnel, are then reflected by the simulation reflector, deposit themselves on the funnel wall, and charge the wall negatively. After the negative charging, the steady-state trajectories shown in Fig. 4.18c are observed.

The movement of the  $50\text{ V}$  contour line and the corresponding hopping transport

point is shown in Fig. 4.19. From  $600\text{ V}$  to  $125\text{ V}$ , the hopping transport point follows the  $50\text{ V}$  contour line. The movement of the  $50\text{ V}$  contour is much smaller than in Case 1. This smaller movement is attributed to the significantly smaller charge sink region. From  $125\text{ V}$  to  $100\text{ V}$ , the hopping transport point travels much farther than the small initial movement of the  $50\text{ V}$  contour. This is the critical voltage where the gradient of the voltage contours (electric field) is too weak to pull the secondary electrons up the funnel to gain energy above the SEY first crossover. The negative charging caused by the weak electric field is the cause of the movement of the transport point.

For brevity, the surface charge density is not shown. The surface charge density evolution looks very similar to Fig. 4.13. The total behavior of the hop funnel when ramping down first is very similar to ramping down after a ramp-up. The slight difference in the I-V curve is caused from the smaller charge sink region in the ramp-down-first case.

#### 4.5.3.2 Case 2 Ramp-Up Explanation

The ramp-up resembles the behavior of Case 1 during the ramp-back-up explained in Section 4.5.2.3. The behavior and the mechanism is the same, and for brevity, the trajectories, the transport start point, the  $50\text{ V}$  contour point, and the surface charge density are not shown.

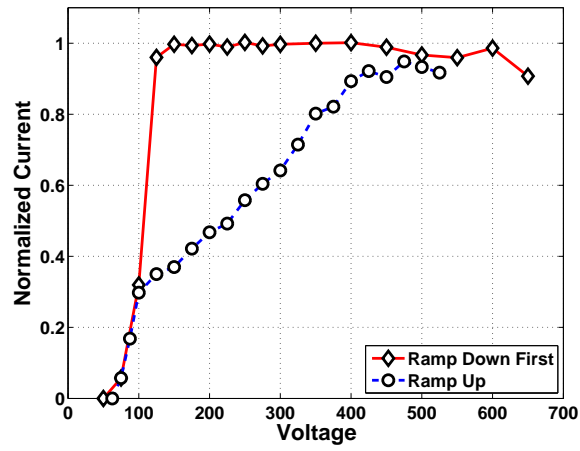


Figure 4.17: I-V curves for Case 2 showing a ramp-down after starting at  $V_{hop} = 650 V$  and then a ramp-back-up for  $\delta_{max} = 2$  and  $E_{max} = 300 eV$  ( $40 eV$  first crossover).

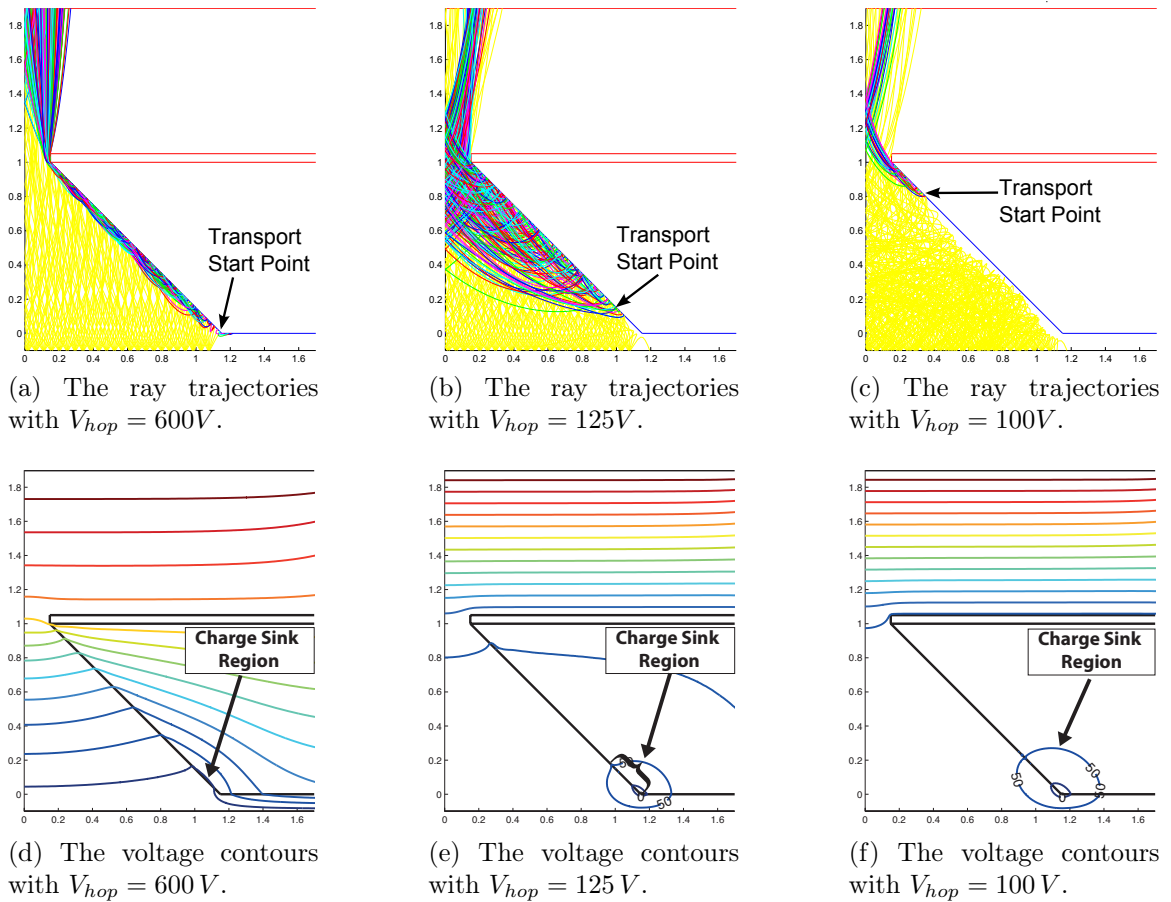


Figure 4.18: Simulations of the ray trajectories and the corresponding voltage contour plots for a range of hop voltages for Case 2 ( $40 eV$  first crossover) ramp-down-first. The primary rays are yellow and the secondary rays are shown in the other colors.

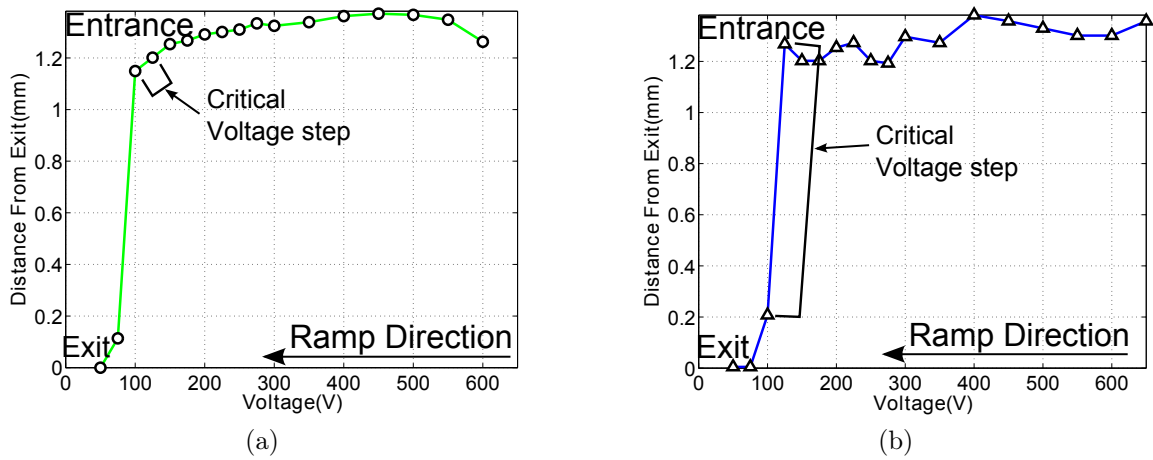


Figure 4.19: (a) The point at which the 50 V voltage contour line intersects the funnel wall, and (b) the point at which electron transport begins to take place along the funnel wall for Case 2 (40 eV first crossover) ramp-down-first.

#### 4.5.4 Simulation Results for Case 3

The next case tested was with a funnel material with  $\delta_{max} = 2$  and  $E_{max} = 500 eV$ , which corresponds to a  $70 eV$  first crossover. Starting at  $V_{hop} = 0 V$ , the voltage was ramped up to near unity-gain, then ramped down to zero-transmission, and then back up again. The results are shown in Fig 4.20. Immediately it is apparent that there are distinct differences on the ramp-down and ramp-back-up when compared to the  $40 eV$  Case shown in Fig. 4.7. These differences are due to the fact that during the ramp-up, the current never reached unity-gain.

##### 4.5.4.1 Case 3 Ramp-Up Explanation

Similar to the  $40 eV$  first crossover case, the slope of the I-V curve during the ramp-up is linear. This time, however, the slope is more shallow. The trajectories and the voltage contours are shown in Fig. 4.21. As the hop voltage is raised incrementally, both the contours and the secondary hopping transport point travel down the funnel wall incrementally. Figures 4.21c and 4.21f represent the highest voltage increment during the ramp-up before the ramp-down. In these figures, secondary hopping transport has not yet taken place on the entrance portion of the funnel wall. The charge sink region is much larger than that of the previous  $40 eV$  first crossover case. This larger charge sink region is there because of not ramping the hop voltage high enough to allow for unity transmission. The effects of the large charge sink region will be seen during the ramp-down.

Because the first crossover energy is higher than the previous case, the walls can charge more negatively. This negative charge counteracts the electric field more strongly and causes weaker field penetration through the funnel exit, which is the

reason for the relatively shallow slope. Also, the point at which electron transport takes place is correlated by the  $80\text{ V}$  voltage contour intersection with the funnel wall. The initial electron energy of the primary electron is  $55\text{ eV}$ , which is emitted from a  $65\text{ V}$  potential. As the electron moves from  $65\text{ V}$  to the  $80\text{ V}$  contour,  $15\text{ eV}$  of energy is gained, resulting in a collision energy of  $70\text{ eV}$ , which corresponds to the first crossover. The point at which the  $80\text{ V}$  voltage contour line intersects with the wall and the electron transport point is shown in Fig. 4.22. The figure shows the  $80\text{ V}$  voltage contour line traveling down the wall more slowly than that of the  $40\text{ eV}$  first crossover case. The surface charge density is shown in Fig. 4.23. This plot shows identical behavior to that in the  $40\text{ eV}$  first crossover case except that the magnitude of the negative surface charge density is greater.

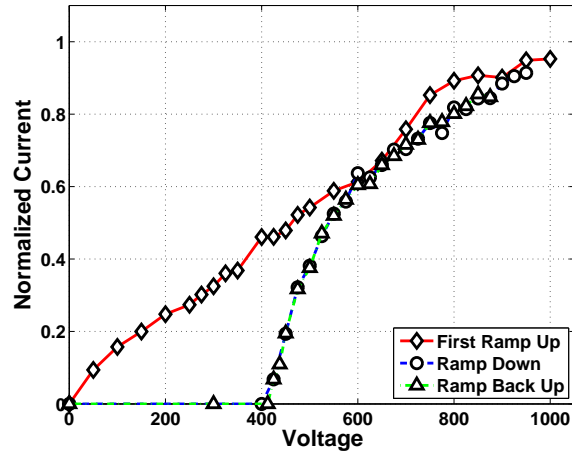
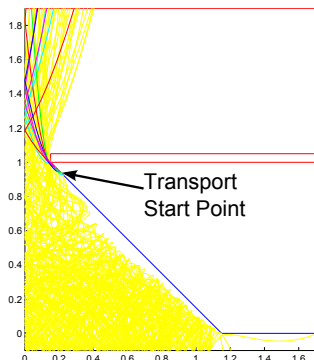
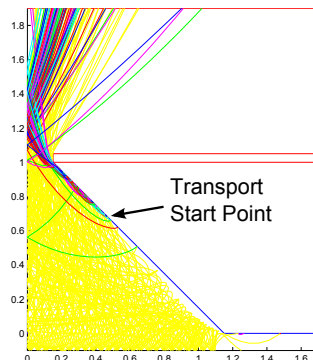


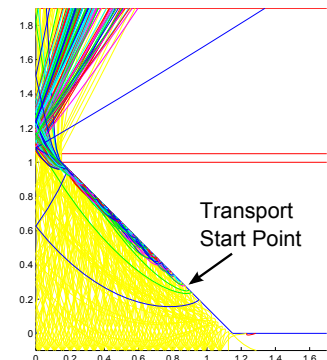
Figure 4.20: I-V curves for Case 3 showing a full ramp-up, down and then back up procedure for  $\delta_{max} = 2$  and  $E_{max} = 500 eV$  ( $70 eV$  first crossover).



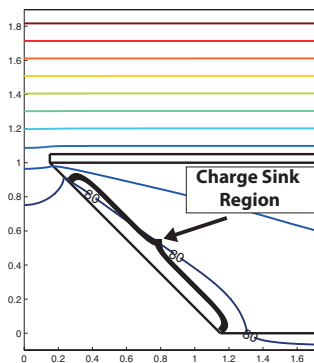
(a) The ray trajectories with  $V_{hop} = 200V$ .



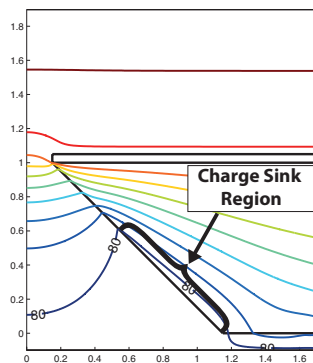
(b) The ray trajectories with  $V_{hop} = 700V$ .



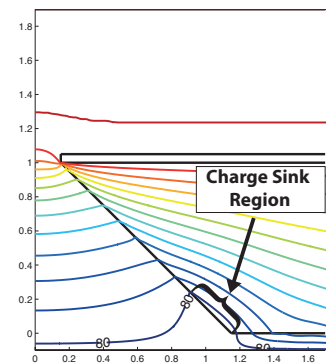
(c) The ray trajectories with  $V_{hop} = 1000V$ .



(d) The voltage contours with  $V_{hop} = 200V$ .



(e) The voltage contours with  $V_{hop} = 700V$ .



(f) The voltage contours with  $V_{hop} = 1000V$ .

Figure 4.21: Simulations of the ray trajectories and the corresponding voltage contour plots for a range of hop voltages for Case 3 ( $70 eV$  first crossover) ramp-up-first. The primary rays are yellow and the secondary rays are shown in the other colors.

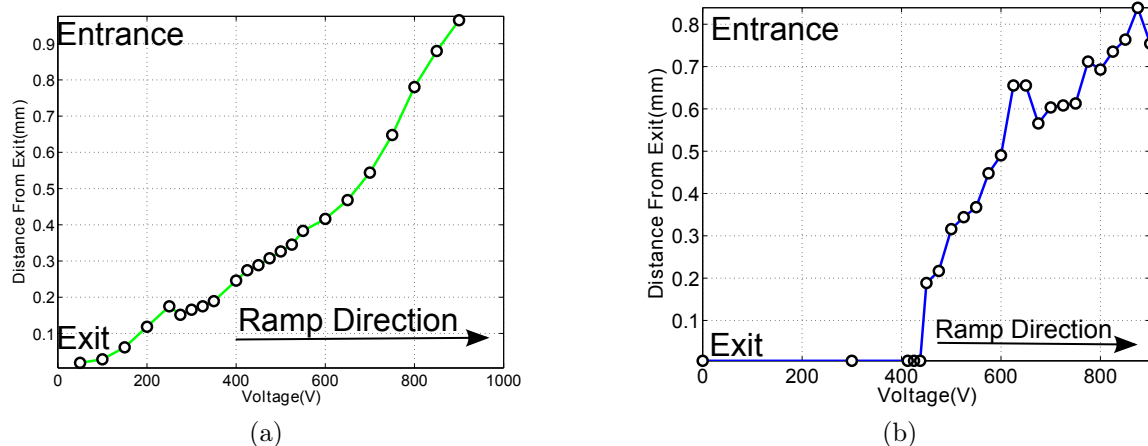


Figure 4.22: (a) The point at which the 80 V voltage contour line intersects the funnel wall, and (b) the point at which electron transport begins to take place along the funnel wall for Case 3 (70 eV first crossover) ramp-up-first.

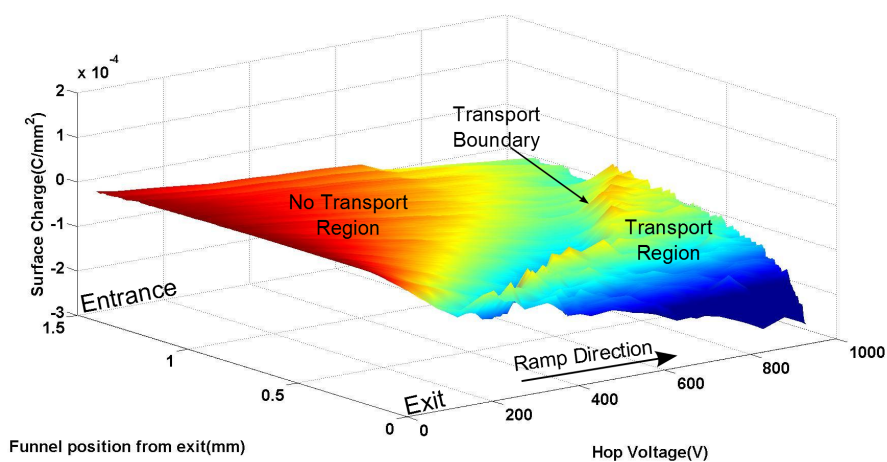


Figure 4.23: Surface charge density along the funnel wall vs. the hop voltage during the ramp-up-first for Case 3 (70 eV first crossover).

#### 4.5.4.2 Case 3 Ramp-Down Explanation

The  $70\text{ eV}$  first crossover ramp-down portion of the curve shown in Fig. 4.20 does not resemble that of the  $40\text{ eV}$  first crossover ramp-down shown in Fig. 4.7. The decay in anode current has a slight knee, and no sharp drop in current. Figure 4.24 shows the electron ray trajectories and the voltage contours. The trajectories on the first voltage step shown in Fig. 4.24a show a lack of hopping transport along the wall near the entrance. The corresponding voltage contour plot in Fig. 4.24d shows a huge charge sink region whose effect can be seen all the way to the cathode. The negative charge in the charge sink region was left behind during the ramp-up procedure. The ramp-up procedure did not go to a high enough hop voltage to induce transport in this region of the funnel. As result, this region never underwent the relative positive charging incurred by the transport region. A large charge sink region is left behind. The next voltage steps show how the charge “mountain” increases in size and affects larger portions of the cathode. Primary electrons emitted in this affected region cannot travel around this “mountain” of charge and are turned around.

Figure 4.24 shows the  $80\text{ V}$  contour intersection with the wall along with the corresponding hopping transport point. The transport point follows the  $80\text{ V}$  contour line closely. No critical voltage is observed, and the hopping transport start point is dominated by the  $80\text{ V}$  contour movement. The strong  $80\text{ V}$  contour movement stops electron transport long before the electric field mechanism can affect the electron trajectories.

As the charge mountain grows out, the  $80\text{ V}$  contour line moves with it and causes the secondary electron transport point to move with it. By bypassing the electric field mechanism, no intense charging of the surface occurs before hopping transport

is lost. The surface charge density is shown in Fig. 4.26. At the transport boundary, the wall charges slightly more negatively, but is barely visible and negligible. This explains the behavior on the ramp-back-up.

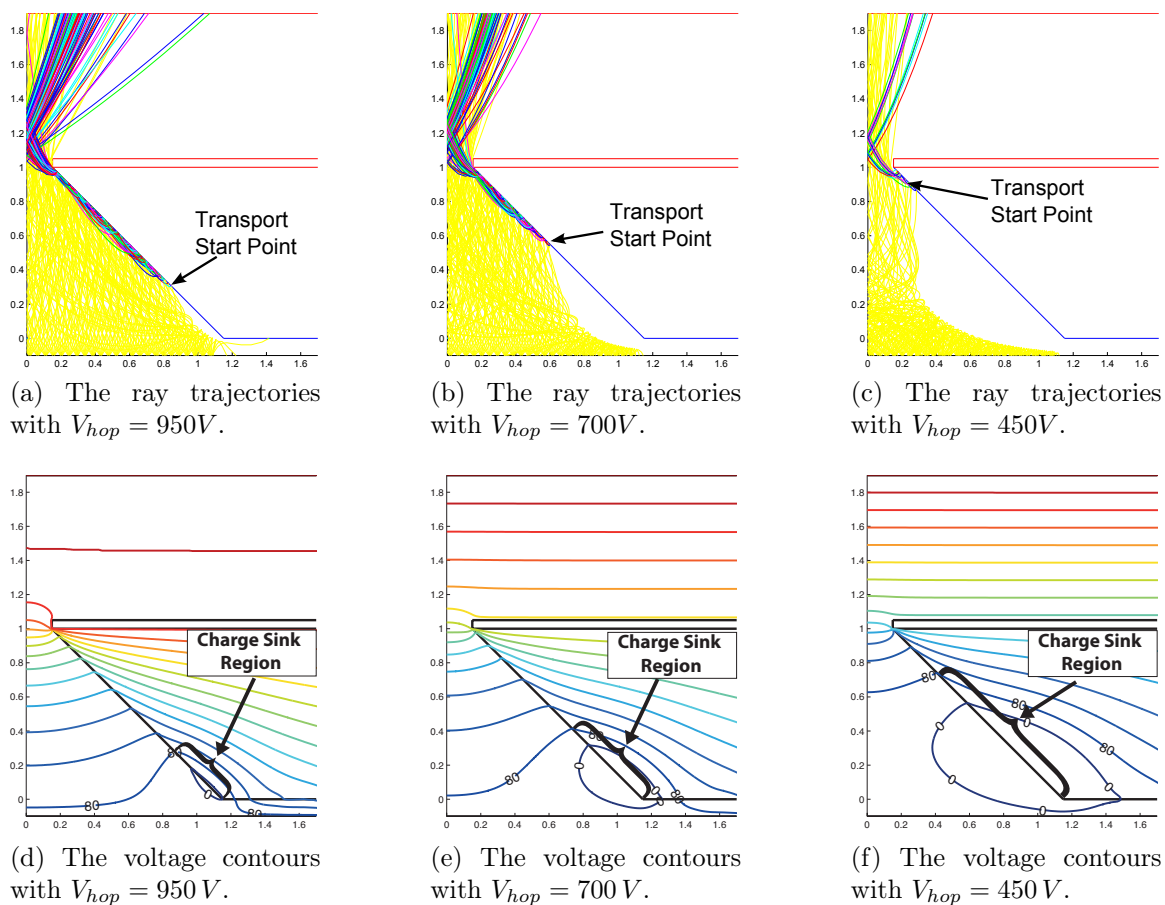


Figure 4.24: Simulations of the ray trajectories and the corresponding voltage contour plots for a range of hop voltages for Case 3 ( $70 eV$  first crossover) ramp-down. The primary rays are yellow and the secondary rays are shown in the other colors.

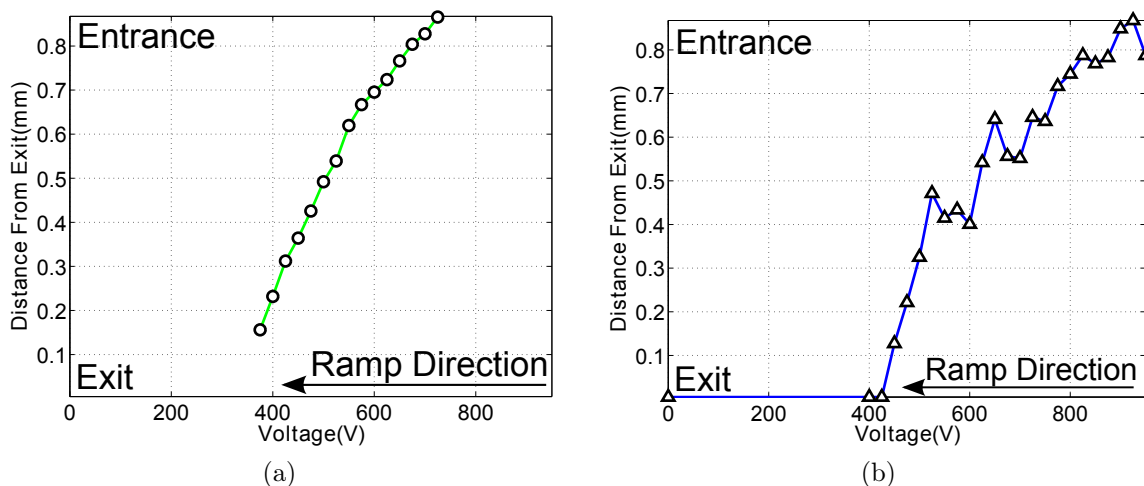


Figure 4.25: (a) The point at which the 80 V voltage contour line intersects the funnel wall, and (b) the point at which electron transport begins to take place along the funnel wall for Case 3 (70 eV first crossover) ramp-down.

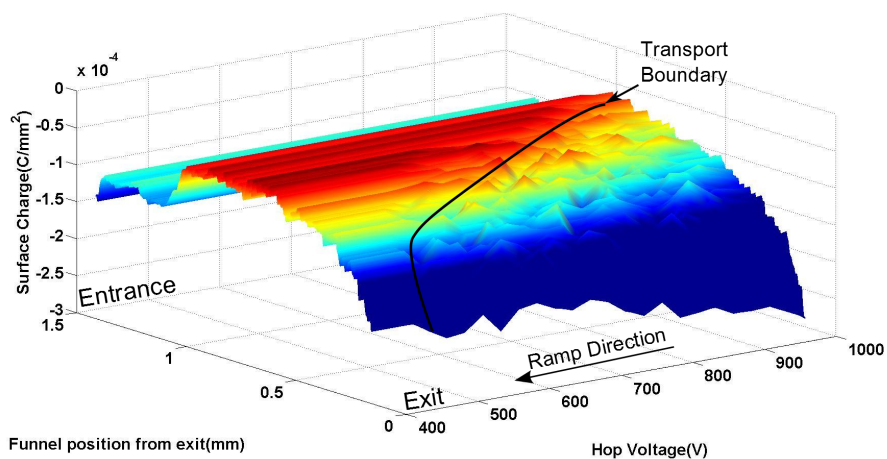


Figure 4.26: Surface charge density along the funnel wall vs. the hop voltage during the ramp-down for Case 3 (70 eV first crossover).

#### 4.5.4.3 Case 3 Ramp-Back-Up Explanation

The ramp-back-up almost exactly follows the ramp-down preceding it. The ray trajectories and voltage contours are shown in Fig. 4.27. The trajectory and voltage contour evolution are very similar to the ramp-down.

The movements of the  $80 V$  voltage contour and the hopping transport start point are also very similar to the ramp-down, and are shown in Fig. 4.28.

The surface charge density looks almost identical to the ramp-down and is shown in Fig. 4.29. The whole behavior of the ramp-back-up compared to the ramp-down is virtually identical. This similar result is caused by how the surface charge on the ramp-down was left unchanged by the transition from hopping transport to no hopping transport. The  $40 eV$  first crossover case showed a sharp negative charging on the transport boundary, which sets up the following ramp-up for different behavior. The  $70 eV$  first crossover ramp-down case shows no charge transition on the transport boundary. The funnel remains in the same “state”, which sets up the following ramp-up for the same path.

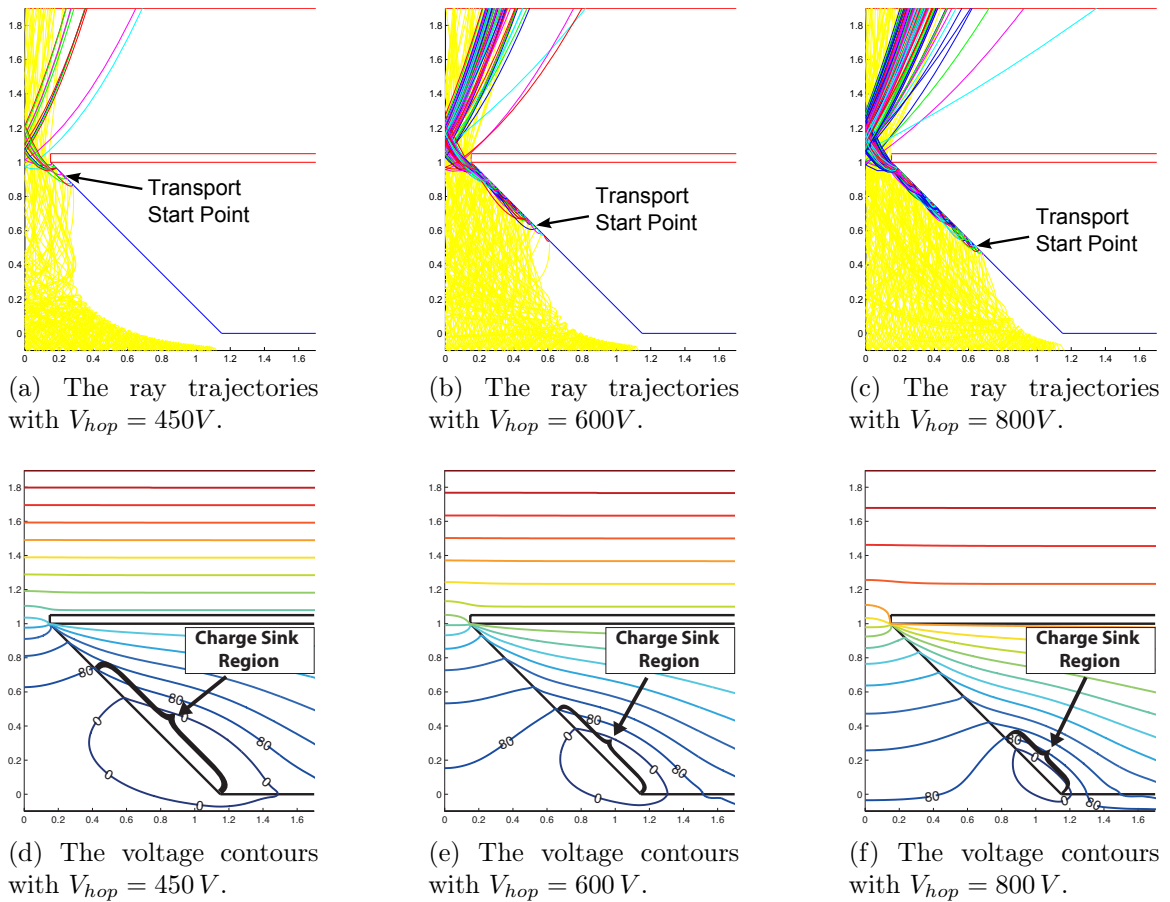


Figure 4.27: Simulations of the ray trajectories and the corresponding voltage contour plots for a range of hop voltages for Case 3 ( $70 eV$  first crossover) ramp-back-up. The primary rays are yellow and the secondary rays are shown in the other colors.

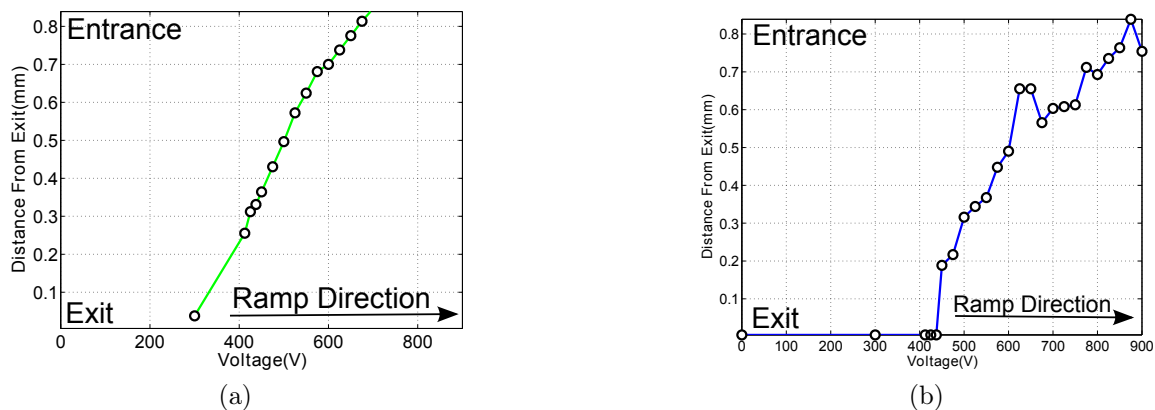


Figure 4.28: (a) The point at which the 80 V voltage contour line intersects the funnel wall, and (b) the point at which electron transport begins to take place along the funnel wall for Case 3 (70 eV first crossover) ramp-back-up.

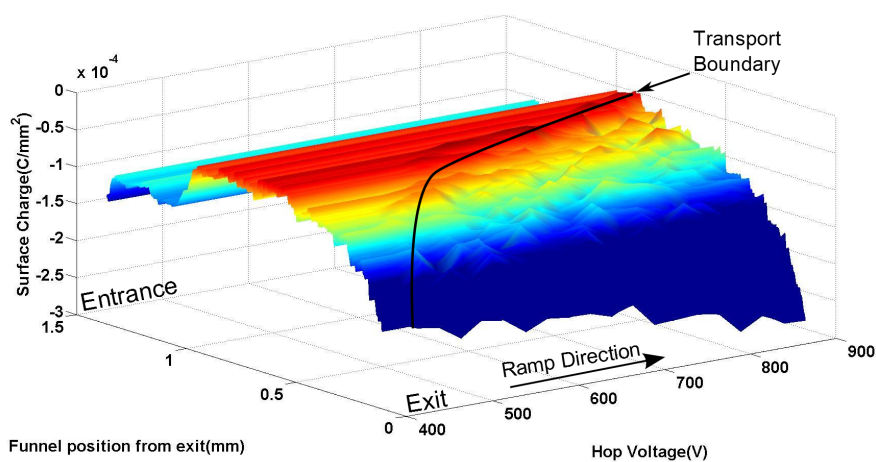


Figure 4.29: Surface charge density along the funnel wall vs. the hop voltage during the ramp-back-up for Case 3 (70 eV first crossover).

#### 4.5.5 Simulation Summary

The results of the simulation can be summarized as follows:

- Electrons emitted onto the hop bottom shift the I-V curve to the right.
- Metal on the hop bottom collects electrons emitted to the hop bottom and prevents the I-V curve shift to the right.
- The I-V curve is dominated by the percentage of the wall that allows secondary electron transport.
- Hopping transport occurs only on portions of the hop funnel that meet these criteria:
  - The potential of the region of wall must allow primary electrons to collide with an energy greater than the first crossover.
  - A sufficient electric field must be present to pull the secondary electrons toward the funnel exit so that the electrons gain energy above the first crossover before they collide with the funnel wall.
- The size of the charge sink region determines the shape of the ramp-down curve.
- The sudden loss (gain) of electron transport in a region is followed by a sudden negative (positive) charging of the wall. This charging is the main source of the hysteresis in the I-V curve.

#### 4.5.6 Simulation Comparison with Experiment

Many of the different I-V curve shapes found experimentally have been recreated by the simulations. However, the context to create the I-V curves in simulations

is different than found in the experiments. The knee during the ramp-down of Cases 1 and 2 shown in Figs. 4.7 and 4.18 are very similar to the ramp-down in the experimental results shown in Figs. 3.5, 3.11, and 3.12. The linear behavior shown in the ramp-up-first cases shown in Figs. 4.7, and 4.20 are very similar to the experimental results shown in Figs. 3.7a, 3.7b, and 3.10b. The linear behavior of the ramp-back-up cases shown in Figs. 4.17, 4.7, and 4.20 resemble the results found in 3.7c, 3.8c, and 3.9c. All these I-V curve shapes from simulations resemble the experiments, but the context in which they were created is different.

The reason for the particular I-V curve shape in the simulations does not necessarily explain the reason for the shapes experimentally, but they give some possible explanations. The initial conditions of the experimental setup are truly unknown because of the great deal of unknowns: secondary electron yield characteristics, funnel wall surface smoothness, cathode charging, and unwanted cathode emission, to name a few. These unknowns can drastically change the shape of the I-V curve. The simulation does not model these things, but has shown many different shapes of curves just by modeling the “ideal” hop funnel operation. By adding these experimental unknowns to the simulation model, even more simulated I-V curve shapes could be formed, which may be able to recreate the experimental results.

## CHAPTER 5

### CONCLUSIONS

Hysteresis is a fundamental characteristic of current transmission through hop funnels. All the experiments and simulations presented in this thesis confirm this. The general shape of the I-V curve, however, cannot be characterized from the experiments performed alone. The hop funnel transport mechanism is extremely sensitive to slight changes in the experimental setup. The integrity of the funnel wall, slight changes in the electron source optics, and any slight external force will alter the I-V characteristics. This sensitivity makes it very difficult to replicate the results.

The reason behind the inconsistency is currently unknown. Given the same exact initial conditions, the I-V curves are very consistent except for a slight evolution of the curve. This result is promising because this shows that the hysteresis mechanism is consistent. Something in the initial setup is causing the shift in the I-V curves. The setup as a whole has hysteresis in its own right, but determining the features of the curve that are caused by the funnel itself is difficult.

In order to characterize hop funnels experimentally, the experimental setup needs to be consistent. To achieve this consistency, many aspects of the setup proposed in this thesis should be reworked. Given the circumstances, the pixel addressing used to pinpoint the point of emission, the placement of the hop funnel, and the hop electrode for the 90° funnel were all applied by hand. All of this work by hand should

be automated. The screen printing of the electrodes used on the  $60^\circ$  hop funnels was a big step in this direction. New  $90^\circ$  funnels should be created with this process. The integrity of the hop funnel samples must also be consistent by storing the samples in a clean environment. Heating the sample may also protect the integrity of the samples and remove contaminants.

The simulations performed here allow a look into the transport mechanism in hop funnels alone. As was found by Hendriks et al. [8], the transport mechanism in the funnel depends on the first unity-gain crossover of the secondary electron yield of the material and the electric field. Two conditions are needed to support electron transport: (i) the energies of the primary electrons must be greater than the first crossover point when they collide with the wall, and (ii) a sufficient electric field must be present to pull the secondary electrons up the funnel and gain energy greater than the first crossover before they collide with the funnel.

The simulations also give some insight into the hysteresis mechanism. The sudden loss or gain of electron transport in the region is followed by a sudden negative or positive charging of the wall, respectively. Once electron transport starts in the region, it becomes easier to sustain. Once electron transport stops, it becomes harder to initiate again. This is the main source of the hysteresis.

The  $70\text{ eV}$  first crossover ramping procedure shows this hysteresis mechanism having little effect. The large charge sink region left by the ramp-up dominates the behavior of the I-V curves thereafter. The  $70\text{ eV}$  first crossover case should be rerun but by ramping up to a higher hop voltage to reduce this charge sink region to see if the results are similar to the  $40\text{ eV}$  first crossover results. Also, the  $40\text{ eV}$  first crossover case should be rerun, but ramping up the hop voltage to a lower level to see if this shows similar results to the  $70\text{ eV}$  case shown in this thesis.

Surface roughness of the funnel wall is something that should be characterized. The levels of transmission during the ramp-up shown in Fig. 3.5 could be explained by a rough funnel wall surface. SEM images should be taken of the cross-section of the funnel used in the experiment to look for a ridge in the surface. Also, simulations should be performed with a ridge in the surface of the funnel wall to attempt to recreate the transmission levels.

The use of silver paste may also be a source of hysteresis. Ions in silver have the tendency to “move” with an applied electric field. The silver can form dendrites that can travel along surfaces up to  $200\ \mu\text{m}$  on time scales on the order of  $\text{ms}$  [27]. This mechanism corresponds to a possible movement of silver of over 10% the length of the funnel wall during one ramp of the hop electrode. Even if this is a source of hysteresis, it is most likely not the sole source of hysteresis as shown by simulations. Different metals should be used to see what the effect of the silver paste truly is.

The simulation software has proven to be a good model of the hysteresis mechanism, but many assumptions were made. The secondary emission yield and the emission direction is not random nor does the model include electron backscatter. Adding these mechanisms will allow a more accurate I-V curve. The strongly varying surface charge along the walls is also undesirable. Preventing this mechanism is unrealistic because it would require too many electron rays, but taking a moving average on each iteration or after each simulation would smooth out these extreme fluctuations in surface charge density.

To simulate an entire I-V curve, the simulations take about a week and require the user to manually start the next voltage step. These simulations used Lorentz 2E version 8, which is a serial code and is not able to automate the necessary surface charge post-processing needed. A new version now exists, version 9, and it is a parallel

code and may be able to automate the entire ramping procedure. By switching to the new version, many different ramping situations can be tested in a short amount of time.

## Bibliography

- [1] Robert J. Barker et al. *Modern Microwave and Millimeter-Wave Power Electronics*. Wiley, 2005.
- [2] I. Brodie and P.R. Schwoebel. “Vacuum microelectronic devices [and prolog]”. In: *Proceedings of the IEEE* 82.7 (1994), pp. 1006–1034. ISSN: 0018-9219. DOI: 10.1109/5.293159.
- [3] C. A. Spindt et al. “Field emitter array development for microwave applications. II”. In: vol. 16. 2. Kyongju (Korea): AVS, 1998, pp. 758–761. DOI: 10.1116/1.589898. URL: <http://link.aip.org/link/?JVB/16/758/1>.
- [4] R.A. Tuck et al. “The pFED - a viable route to large field emission displays”. In: *Vacuum Nanoelectronics Conference, 2005. IVNC 2005. Technical Digest of the 18th International*. 2005, pp. 80–81. DOI: 10.1109/IVNC.2005.1619494.
- [5] Liu Min et al. “Transverse energy distribution analysis in a field emission element with an insulator funnel”. In: *Nuclear Instruments and Methods in Physics Research Section B: Beam Interactions with Materials and Atoms* 234.3 (2005), pp. 210–218. ISSN: 0168-583X. DOI: 10.1016/j.nimb.2005.01.120. URL: <http://www.sciencedirect.com/science/article/pii/S0168583X05000029>.
- [6] C. Lester, J. Browning, and L. Matthews. “Electron-Hop-Funnel Measurements and Comparison With the Lorentz-2E Simulation”. In: *Plasma Science, IEEE*

- Transactions on* 39.1 (2011), pp. 555–561. ISSN: 0093-3813. DOI: 10.1109/TPS.2010.2087775.
- [7] B. H. W. Hendriks et al. “Dynamical behavior of electron hop transport over insulating surfaces”. In: *Journal of Applied Physics* 85.3 (1999), pp. 1848–1856. ISSN: 0021-8979. DOI: 10.1063/1.369309.
- [8] B.H.W. Hendriks et al. “Modes in electron-hopping transport over insulators sustained by secondary electron emission”. In: *J. Phys. D: Appl. Phys.* 30.8 (1997), pp. 1252–1264. DOI: 10.1088/0022-3727/30/8/016.
- [9] *Integrated Software*. <http://www.integratedsoft.com/>.
- [10] R. H. Fowler and L. Nordheim. “Electron Emission in Intense Electric Fields”. In: *Proceedings of the Royal Society of London* 119.781 (1928), pp. 173–181. DOI: 10.1098/rspa.1928.0091.
- [11] Dorota Temple. “Recent progress in field emitter array development for high performance applications”. In: *Materials Science and Engineering: R: Reports* 24.5 (1999), pp. 185–239. ISSN: 0927-796X. DOI: 10.1016/S0927-796X(98)00014-X. URL: <http://www.sciencedirect.com/science/article/pii/S0927796X9800014X>.
- [12] W. Zhu et al. “Very large current density from carbon nanotube field emitters”. In: *Electron Devices Meeting, 1999. IEDM Technical Digest. International*. 1999, pp. 705–708. DOI: 10.1109/IEDM.1999.824249.
- [13] K Kitamura et al. “Fabrication of vertically aligned ultrafine ZnO nanorods using metal-organic vapor phase epitaxy with a two-temperature growth method”. In: *Nanotechnology* 19.17 (2008), p. 175305. URL: <http://stacks.iop.org/0957-4484/19/i=17/a=175305>.

- [14] M. A. Guillorn et al. "Operation of a gated field emitter using an individual carbon nanofiber cathode". In: *Applied Physics Letters* 79.21 (2001), pp. 3506–3508. DOI: 10.1063/1.1419038. URL: <http://link.aip.org/link/?APL/79/3506/1>.
- [15] J. D. Levine et al. "Field emission from microtip test arrays using resistor stabilization". In: *Journal of Vacuum Science Technology B: Microelectronics and Nanometer Structures* 13.2 (1995), pp. 474–477. ISSN: 1071-1023. DOI: 10.1116/1.588336.
- [16] Babu R. Chalamala et al. "Oxidation of Molybdenum Thin Films and its Impact on Molybdenum Field Emitter Arrays". In: *MRS Proceedings* 13.2 (2001), p. 685. ISSN: 1071-1023. DOI: doi:10.1557/PROC-685-D14.2.1.
- [17] *Electron Microscopy*. <http://www.vcbio.science.ru.nl/en/fesem/eds/>.
- [18] E. M. Baroody. "A Theory of Secondary Electron Emission from Metals". In: *Phys. Rev.* 78 (6 1950), pp. 780–787. DOI: 10.1103/PhysRev.78.780. URL: <http://link.aps.org/doi/10.1103/PhysRev.78.780>.
- [19] Robert G. Lye and A. J. Dekker. "Theory of Secondary Emission". In: *Phys. Rev.* 107 (4 1957), pp. 977–981. DOI: 10.1103/PhysRev.107.977. URL: <http://link.aps.org/doi/10.1103/PhysRev.107.977>.
- [20] Elise Rene Boerwinkle Adamson. "Secondary Electron Emission Coefficient From Lexan: The Low Energy Crossover". PhD thesis. Texas Tech University, 1993.
- [21] X. Meyza et al. "Secondary electron emission and self-consistent charge transport and storage in bulk insulators: Application to alumina". In: *Journal of*

- Applied Physics* 94.8 (2003), pp. 5384–5392. DOI: 10.1063/1.1613807. URL: <http://link.aip.org/link/?JAP/94/5384/1>.
- [22] R. F. Willis and D. K. Skinner. “Secondary Electron Emission Yield Behaviour of Polymers”. In: *Solid State Communications* 13.6 (1973), pp. 685–688.
- [23] J.R.M. Vaughan. “A new formula for secondary emission yield”. In: *Electron Devices, IEEE Transactions on* 36.9 (1989), pp. 1963–1967. ISSN: 0018-9383. DOI: 10.1109/16.34278.
- [24] Lei Wei et al. “Characteristic of the cold cathode with secondary electron emission”. In: *Vacuum Electron Sources Conference, 2004. Proceedings. IVESC 2004. The 5th International*. 2004, pp. 52–54. DOI: 10.1109/IVESC.2004.1413954.
- [25] Xiaobing Zhang et al. “Analysis of the transverse energy distribution of hopping electrons through a glass funnel”. In: *Applied Surface Science* 251.1-4 (2005), pp. 182–190. ISSN: 0169-4332. DOI: 10.1016/j.apsusc.2005.03.189. URL: <http://www.sciencedirect.com/science/article/pii/S016943320500526X>.
- [26] *DuPont*. <http://www2.dupont.com/>.
- [27] S. Yang, J. Wu, and A. Christou. “Initial stage of silver electrochemical migration degradation”. In: *Microelectronics Reliability* 46.9-11 (2006), pp. 1915–1921. ISSN: 0026-2714. DOI: 10.1016/j.microrel.2006.07.080. URL: <http://www.sciencedirect.com/science/article/pii/S0026271406002174>.